



National Library  
of Canada

Bibliothèque nationale  
du Canada

Canadian Theses Service

Service des thèses canadiennes

Ottawa, Canada  
K1A 0N4

## NOTICE

The quality of this microform is heavily dependent upon the quality of the original thesis submitted for microfilming. Every effort has been made to ensure the highest quality of reproduction possible.

If pages are missing, contact the university which granted the degree.

Some pages may have indistinct print especially if the original pages were typed with a poor typewriter ribbon or if the university sent us an inferior photocopy.

Reproduction in full or in part of this microform is governed by the Canadian Copyright Act, R.S.C. 1970, c. C-30, and subsequent amendments.

## AVIS

La qualité de cette microforme dépend grandement de la qualité de la thèse soumise au microfilmage. Nous avons tout fait pour assurer une qualité supérieure de reproduction.

S'il manque des pages, veuillez communiquer avec l'université qui a conféré le grade.

La qualité d'impression de certaines pages peut laisser à désirer, surtout si les pages originales ont été dactylographiées à l'aide d'un ruban usé ou si l'université nous a fait parvenir une photocopie de qualité inférieure.

La reproduction, même partielle, de cette microforme est soumise à la Loi canadienne sur le droit d'auteur, SRC 1970, c. C-30, et ses amendements subséquents.

**Illite/smectite diagenesis in the Beaufort-Mackenzie Basin, Arctic Canada**

by

**Jaehong Ko**

Department of Geological Sciences  
McGill University, Montreal  
Quebec, Canada

A thesis submitted to the Faculty of Graduate Studies and Research  
in partial fulfillment of the requirements for  
the degree of Doctor of Philosophy.

© 1992, J.Ko



National Library  
of Canada

Bibliothèque nationale  
du Canada

Canadian Theses Service    Service des thèses canadiennes

Ottawa, Canada  
K1A 0N4

The author has granted an irrevocable non-exclusive licence allowing the National Library of Canada to reproduce, loan, distribute or sell copies of his/her thesis by any means and in any form or format, making this thesis available to interested persons.

The author retains ownership of the copyright in his/her thesis. Neither the thesis nor substantial extracts from it may be printed or otherwise reproduced without his/her permission.

L'auteur a accordé une licence irrévocable et non exclusive permettant à la Bibliothèque nationale du Canada de reproduire, prêter, distribuer ou vendre des copies de sa thèse de quelque manière et sous quelque forme que ce soit pour mettre des exemplaires de cette thèse à la disposition des personnes intéressées.

L'auteur conserve la propriété du droit d'auteur qui protège sa thèse. Ni la thèse ni des extraits substantiels de celle-ci ne doivent être imprimés ou autrement reproduits sans son autorisation.

ISBN 0-315-74836-2

Canada

## ABSTRACT

Illitization in the Beaufort-Mackenzie Basin is characterized by random, a mixture of random and ordered, R1-ordered, and P>1-ordered illite/smectite (I/S). Proportions of I-layers increase with depth, while the dominant I/S type changes in that order. Illitization in offshore wells is generally more advanced than onshore because of higher geothermal gradients. Illitization in geopressure zones and sandy intervals appears to be faster than under normally pressured conditions and in shales, respectively, due to higher water/particle ratios. Hydrocarbons generally occur above and in the interval of random I/S, but rarely below the depth where ordered I/S is found.

Layer formulae of S- and I-layers are estimated to be  $[Al_{1.57}Fe_{.19}Mg_{.31}Ti_{.07}] [Si_{3.84}Al_{.16}]O_{10}(OH)_2$  and  $[Al_{1.84}Mg_{.16}] [Si_{3.33}Al_{.67}]O_{10}(OH)_2$ , respectively. The increase in concentrations of  $K_2O$ , Rb and rare earth elements (REE), the decrease in octahedral elements (Mg, Ti, Sc, Zn, Zr), and the increase in tetrahedral elements (Al, Be, V) can be attributed to the conversion of S-layers to I-layers with increasing depth. The REE appear to be mobilized during illitization.  $\delta^{18}O$  values range from 2.91 to 15.72 ‰ (SMOW), and increase with depth, contrasting to the trends observed in the Gulf Coast and elsewhere. This probably is related to the rapid increase in  $\delta^{18}O$  of pore waters with depth.

## SOMMAIRE

L'illitisation dans le bassin de Beaufort-Mackenzie est caractérisée par de l'I/S désordonnée, un mélange d'I/S désordonnée et ordonnée, de l'I/S ordonnée R1 et encore R>1. La proportion de couches I augmente en profondeur pendant que le type dominant d'I/S change selon la séquence énoncée précédemment. A cause de gradients géothermiques plus élevés, l'illitisation est généralement plus avancée dans les puits les plus éloignés des côtes. L'illitisation semble procéder plus rapidement en zones soumises à des pressions anormalement élevées et en zones sableuses qu'en zones sous pression normale et en zones argileuses, respectivement, à cause d'un rapport eau:solide plus élevé. Les hydrocarbures se trouvent généralement au-dessus de et dans la zone de l'I/S désordonnée, mais rarement au-dessous des profondeurs où de l'I/S ordonnée est observée.

Les formules des couches des type S et I sont estimées respectivement à  $[Al_{1.57}Fe_{.19}Mg_{.31}Ti_{.07}][Si_{3.84}Al_{.16}]O_{10}(OH)_2$  et  $[Al_{1.84}Mg_{.16}][Si_{3.33}Al_{.67}]O_{10}(OH)_2$ . L'augmentation des concentrations en  $K_2O$ , Rb et en terres rares, le déclin des éléments octaédriques (Mg, Ti, Sc, Zn, Zr) et l'augmentation des éléments tétraédriques (Al, Be, V) peuvent être attribués à la conversion de couches de type S au type I durant l'enfouissement. Les terres rares semblent être remobilisées pendant l'illitisation. Les valeurs de  $\delta^{18}O$  varient de 2.91 à 15.72 ‰ (SMOW), et augmentent en profondeur, à l'inverse de la situation observée dans le Gulf Coast et ailleurs. Cette différence est probablement due à l'augmentation rapide du  $\delta^{18}O$  de l'eau interstitielle avec la profondeur d'enfouissement.

## TABLE OF CONTENTS

ABSTRACT	ii
SOMMAIRE	iii
TABLE OF CONTENTS	iv
LIST OF ILLUSTRATIONS	viii
Tables	viii
Figures	viii
ACKNOWLEDGEMENTS	xi
CHAPTER I. INTRODUCTION	I-1
GEOLOGIC SETTING	I-2
Sequences, Stratigraphy and Sedimentology	I-7
Geothermal Gradients, Geopressure, Formation Water	
Chemistry and Sandstone Diagenesis	I-13
MATERIALS AND METHODS	I-17
CHAPTER II. CRITICAL REVIEW OF CURRENT DEVELOPMENTS IN ILLITE/SMECTITE DIAGENESIS	II-1
GRADUAL VS. EPISODIC PROCESS	II-1
MARKOVIAN CRYSTALLITES VS. FUNDAMENTAL PARTICLES	II-6
LAYER CHARGE VS. POTASSIUM	II-12
SINGLE PHASE SOLID SOLUTION VS. TWO PHASES	II-16
TRANSFORMATION VS. NEOFORMATION	II-21
CHAPTER III. I/S MINERALOGY	III-1

X-RAY DIFFRACTION CHARACTERISTICS OF <math>< .1 \mu</math>	
FRACTIONS	III-1
I/S Mineralogy	III-5
Estimation of I/S Composition	III-7
DISCUSSION	III-12
Peak Broadness and Intensity	III-12
Abnormal Glycol Behavior	III-14
Discrete Illite or Elementary Illite Particle	III-15
Mixture of Random and Ordered I/S	III-16
Implications of X-Ray Diffraction Patterns of K-Saturated	
Samples	III-16
CHAPTER IV. BASINAL TRENDS	IV-1
RESULTS AND INTERPRETATIONS	IV-1
B.A.-Shell-IOE Reindeer D-27	IV-1
<i>I/S diagenesis</i>	IV-4
<i>Interpretation</i>	IV-6
<i>Layer charge development</i>	IV-9
IOE Taglu C-42	IV-11
<i>I/S diagenesis</i>	IV-13
IOE Taglu G-33	IV-15
Wells in the vicinity of Reindeer and Taglu	IV-16
Offshore Wells	IV-23

DISCUSSION	IV-29
Mixture of Random and Ordered I/S	IV-29
Basinal Trends	IV-30
Effects of Geopressure and Lithology on I/S diagenesis	IV-31
Temperature and I/S Diagenesis	IV-34
Hydrocarbons and I/S Diagenesis	IV-35
CHAPTER V. GEOCHEMISTRY AND OXYGEN ISOTOPES	V-1
EXPERIMENTAL METHODS	V-1
RESULTS	V-2
Geochemistry	V-2
<i>Major elements</i>	V-8
<i>Trace elements</i>	V-9
<i>Rare earth elements</i>	V-11
<i>Structural formulae</i>	V-13
Oxygen Isotopes	V-17
INTERPRETATION AND DISCUSSION	V-20
Geochemistry	V-20
Oxygen Isotopes	V-25
CHAPTER VI. CONCLUSIONS, CONTRIBUTIONS TO KNOWLEDGE, AND SUGGESTIONS FOR FUTURE RESEARCH	VI-1
<u>Contributions to Knowledge</u>	VI-5
<u>Suggestions for Future Research</u>	VI-7

REFERENCES	R-1
APPENDICES	A-1
Appendix I. Sample wells, depths and I/S composition	A-2
1) Reindeer D-27	A-2
2) Taglu C-42	A-5
3) Wells in the vicinity of Reindeer and Taglu	A-6
4) Offshore wells	A-8
Appendix II. Changes in I/S composition upon K-saturation	A-10
Appendix III. Stratigraphic data available for offshore wells	A-11
Appendix IV. Accuracy and precision of geochemical analysis	A-12
Appendix V. Geochemical data- major, trace and rare earth element concentrations	A-14
1) Major elements	A-14
2) Trace elements	A-15
3) Rare earth elements	A-16
Appendix VI. Correlation chart for 24 major, minor, trace and rare earth elements	A-17

## LIST OF ILLUSTRATIONS

### Tables

I-1. Well locations and sample distribution.	I-19
II-1. Behavior of I/S with differently charged component-layers in solutions of cations requiring high and low dehydration energy.	II-19
V-1. Structural formulae of I/S.	V-16
V-2. Oxygen isotopic composition of I/S and calculated $\delta^{18}\text{O}$ of pore water using I/S-water fractionation factors according to Savin and Lee (1988).	V-28

### Figures

I-1. Geographic location map and physiography.	I-3
I-2. Tectonic elements.	I-5
I-3. Structural elements.	I-6
I-4. Stratigraphic sequences and units.	I-8
I-5. Schematic NW-SE cross-section.	I-9
I-6. Isopach map of Late Cretaceous to Holocene strata.	I-10
I-7. Progradation of major deltaic sequences.	I-12
I-8. Distribution of growth faults and diapirs.	I-14
I-9. Geothermal gradient map.	I-15
I-10. Distribution of geopressure.	I-16
I-11. Location of wells used in this study.	I-18
II-1. Comparison of I/S according to Markovian crystallite and	

fundamental particle models.	II-7
<b>II-2.</b> The colloidal behavior of I/S in solution.	II-17
<b>II-3.</b> Phase diagrams based on the composition of relatively shallow ground waters.	II-22
<b>III-1.</b> X-ray diffraction patterns of typical Beaufort-Mackenzie clays (<1 $\mu$ fraction).	III-2
<b>III-2.</b> X-ray diffraction patterns of (a) air-dried, (b) glycolated, (c) heated at 400°C and (d,e) 550°C specimens.	III-4
<b>III-3.</b> Plot of 003/004 <sub>s</sub> peak parameters with respect to depth.	III-9
<b>III-4.</b> Deconvolution of a X-ray diffraction curve in the 3.3 Å region.	III-11
<b>III-5.</b> Effects of strain broadening for a 10 Å structure.	III-13
<b>III-6.</b> X-ray diffraction patterns showing the effect of K-saturation for various types of I/S.	III-18
<b>IV-1.</b> Plot of I-content (%I) in I/S with respect to depth, stratigraphy, lithology and geopressure for Reindeer D-27.	IV-3
<b>IV-2.</b> Comparison of four models proposed to interpret I/S burial curves of Reindeer D-27.	IV-7
<b>IV-3.</b> Plot of I-content versus depth for K-saturated specimens in comparison to Na-saturated specimens of Reindeer D-27.	IV-10
<b>IV-4.</b> Plot of I-content (%I) in I/S with respect to depth, stratigraphy, lithology and geopressure for Taglu C-42.	IV-12
<b>IV-5.</b> Plot of I-content (%I) in Na- and K-saturated I/S with depth,	

stratigraphy, lithology and geopressure for Taglu G-33.	IV-17
IV-6. Plots of I-content (%I) versus depth, stratigraphy, lithology and geopressure for wells in the vicinity of Reindeer and Taglu.	IV-19
IV-7. Plots of I-content (%I) versus depth for offshore wells.	IV-25
IV-8. Diagram showing the effect of geopressure on I/S diagenesis.	IV-33
IV-9. The relationship between positions of hydrocarbon occurrence and I/S diagenesis	IV-36
V-1. Major and trace element concentrations in <.1 $\mu$ fractions of the Reindeer D-27 well with respect to depth.	V-3
V-2. Plots of principal component analysis.	V-7
V-3. Scatter plots of positively correlated elements.	V-10
V-4. Distribution of rare earth elements.	V-12
V-5. (a) La and (b) Ce concentrations as function of depth.	V-14
V-6. Scatter plots of (a) La and (b) Ce concentrations with respect to Al <sub>2</sub> O <sub>3</sub> , Be, and V.	V-15
V-7. Depth plot of $\delta^{18}\text{O}$ values of I/S and calculated isotopic compositions of pore water according to Savin and Lee (1988).	V-18
V-8. Plots of cationic, octahedral, and tetrahedral charges with depth.	V-23
V-9. Plots of SiO <sub>2</sub> , Al <sub>2</sub> O <sub>3</sub> , MgO and TiO <sub>2</sub> concentrations in a formula unit with respect to I-contents.	V-24
V-10. Models depicting variable oxygen isotopic trends of I/S resulting from variations in $\delta^{18}\text{O}$ of pore water.	V-26
V-11. Interpretation of the isotopic composition of pore water.	V-29

## ACKNOWLEDGEMENTS

Financial assistance from Strategic and Operating grants by the Natural Sciences and Engineering Research Council of Canada, from the Petroleum Research Fund administered by the American Chemical Society, and Amoco Canada Petroleum Co. Ltd. through Dr. R. Hesse is gratefully acknowledged. I appreciate Dr. R. Hesse for allowing me to carry out the project independently. I benefited from his meticulous reviews while writing this thesis.

I wish to make special thanks to Dr. J. Dixon (Institute of Sedimentary and Petroleum Geology, Calgary) for his kind assistance with samples, maps, and information. Dr. W. Petruk (CANMET, Ottawa) is thanked for loaning and eventually selling us the high-speed centrifuge, without which I would have never finished this thesis. Dr. K. Govindajaru (C.R.P.G., France; for discounting on analytical services of preliminary testing samples), Ms. Celine Doule (Department of Medical Sciences, McGill; for freeze drying), Dr. Fred Longstaffe and Mr. Paul Middlestead (University of Western Ontario, London; for oxygen isotope analyses), Mr. Thinley Topgyal (E.R.C.B., Calgary; for washing samples), Dr. Sung Ho Youn (Gulf, Calgary), Dr. J. Paquette (Department of Geological Sciences, McGill; for translation of abstract) and numerous other people are gratefully acknowledged. Esso Resources Canada, Calgary, staff at the Arctic/Atlantic Division (Drs. Burns Cheadle, Bernard Collot) and Dr. Ron Dean (retired) are thanked for providing Taglu samples and having kept interests in my study. Reviews of Chapter II by Drs. A. Mucci, S. Wood and an anonymous colleague and Chapter V by T. Ahmedali in the Department of Geological Sciences at McGill University are very much

appreciated.

Finally, I wish to thank my wife, daughter, family and many personal friends for their patience and cheers.

## CHAPTER I. INTRODUCTION

The illitization of smectitic materials has been one of the most interesting subjects of clay mineralogical and diagenetic studies in the past two decades. The phenomenon has been recognized worldwide in burial diagenetic (e.g. Burst, 1969; Perry and Hower, 1970), hydrothermal (e.g. Inoue et al., 1987; Eberl et al., 1987), and contact-metamorphic environments (e.g. Nadeau and Reynolds, 1981), and experimentally duplicated in the laboratory (e.g. Eberl and Hower, 1976).

Smectite is converted to illite via mixed-layer minerals of illite/smectite (I/S). Clay-dewatering associated with the reaction appears to play an important role in primary migration of hydrocarbons, overpressure development and sandstone diagenesis. At the depth of hydrocarbon formation<sup>1</sup>, source rocks would have lost most of their porosity and pore water. Thus, one of the problems concerning deep hydrocarbon generation lies in identifying the flushing mechanism. For the U.S. Gulf Coast, it has been suggested that water released from interlayers of smectitic material may provide a boost necessary for primary migration of hydrocarbons generated in deep basins (Bruce, 1984). The volume of smectite-water appears large enough even to contribute to overpressure development (e.g. Magara, 1976).

The byproducts of I/S diagenesis that include quartz, kaolinite, chlorite and other minerals may precipitate in sandstones adjacent to shales and, thus, reduce permeability and porosity. On the other hand, organic acids produced during organic matter maturation

---

<sup>1</sup>Most oil and gas generation occurs in the temperature range from 80°C to 120°C. For a geothermal gradient of 30°C/km, this corresponds to 3-4 km of burial.

in shales and the release of these acids by smectite-water may enhance permeability through secondary porosity development.

The Beaufort-Mackenzie Basin which is one of the largest hydrocarbon habitats in Canada<sup>2</sup>, exhibits some similarities of structure, sedimentology and stratigraphy to the Gulf Coast, but also significant differences. It contains significant proportions of mixed-layer I/S in the clay-size fractions (Foscolos and Powell, 1982). Hydrocarbon occurrences are associated with the zone of abnormally high fluid pressure and related structures, growth faults and shale diapirs. In this respect, the Beaufort-Mackenzie Basin presents ample opportunities to examine and evaluate the concepts of I/S diagenesis developed mainly in the Gulf Coast.

## GEOLOGIC SETTING

The Beaufort-Mackenzie Basin is located in northwestern Canada. Geographically, it underlies the Yukon Coastal Plain, the present Mackenzie Delta, the Tuktoyaktuk Peninsula and adjacent offshore shelf and slope regions in Beaufort Sea (Fig. I-1). The area comprises approximately 155,000 km<sup>2</sup>. Structurally, the basin is bounded by the Northern Interior Platform to the southeast, the Cordilleran Orogen in the southwest, and the continental slope to the north (Young et al., 1976).

The major tectonic elements in the surroundings of the Beaufort-Mackenzie Basin include the Romanzof Uplift, the Rapid Depression, the Aklavik Arch Complex and the

---

<sup>2</sup>The Geological Survey of Canada estimates recoverable reserves of about 1.5-2.0 billion bbl of oil and 10.9-12.6 tcf of gas (Dixon et al., 1988).

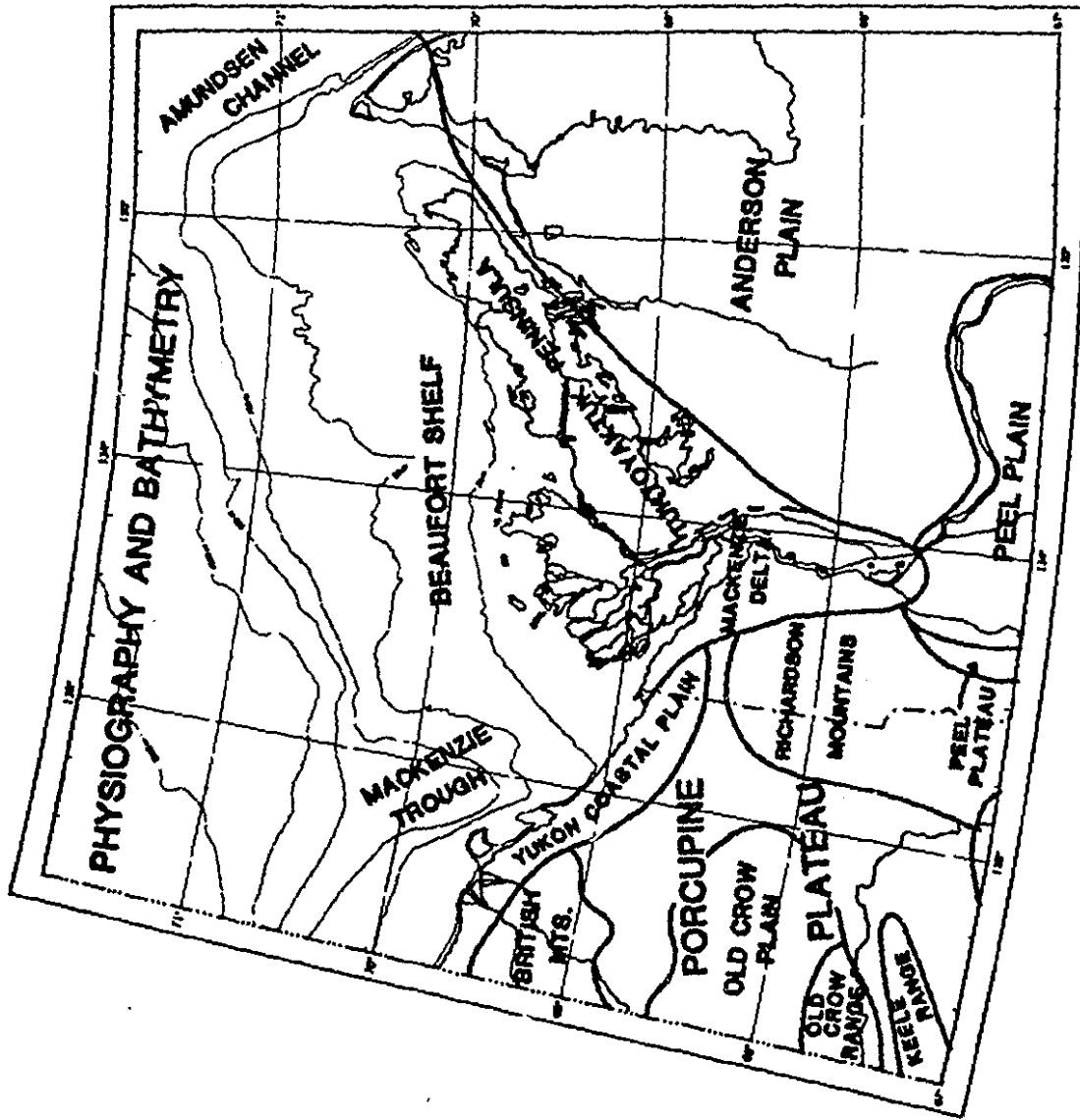


Figure I-1. Geographic location map and physiography (after Dixon et al., 1985).

Northern Interior Platform (Fig. I-2). The Romanzof Uplift consists of uplifted Proterozoic clastics and carbonates which are unconformably overlain by Paleozoic rocks. It developed principally during the Columbian Orogeny (Late Jurassic to Cretaceous) by a family of southeast-trending high-angle reverse faults (Young et al., 1976). The Rapid Depression is filled by Early Cretaceous flyschoid and Late Cretaceous to Tertiary molassoid rocks. The depression is interpreted to be the result of wrench tectonics created by the branching of a strike-slip fault that depressed the area at the restraining bend (*sensu* Crowell, 1974) in response to compressive stresses. The Aklavik Arch Complex consists of northeast-trending structural highs and lows formed by complex folding and faulting. It has a prolonged tectonic history extending from Proterozoic to Tertiary, during which times the various components of the complex were intermittently and independently active (Yorath and Norris, 1975). The Interior Platform is basically the Canadian Shield covered by thin veneers of Paleozoic and Mesozoic sediments.

The principal structural elements in the region are strike-slip faults: Tintina, Kaltag-Porcupine and Richardson (Fig. I-3). For the Richardson Fault, the present movement is predominantly vertical. The Tintina Fault is one of the major linear features in the Cordillera. It is collinear with the Northern and Southern Rocky Mountain Trenches. Together, these fault systems have a combined length of about 2,500 km. The Richardson Fault Array extends offshore and is connected with the Cape Kellett Fault Zone near Banks Island (Norris and Yorath, 1981). Orthogonal salient and recess patterns that formed together with their southern extension, the Plateau Fault, suggest that these faults may have developed from inherited structural features related to rift-transform controlled

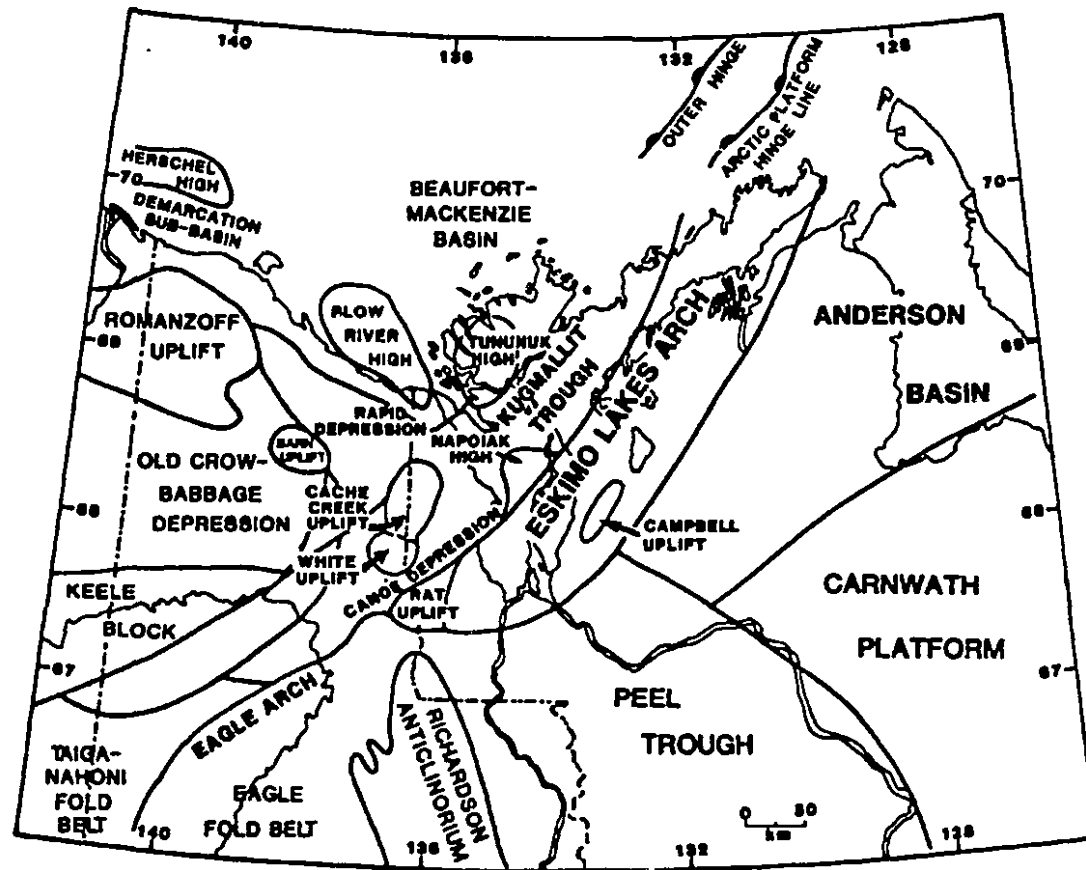


Figure I-2. Tectonic elements (after Dixon et al., 1985). Aklavik Arch- Eskimo Lakes Arch, Campbell Uplift, Kugmallit Trough, Canoe Depression, Cache Creek Uplift, White Uplift, Napoiak High, Tununuk High. Interior Platform- Anderson Basin, Carnwath Platform, Peel Trough.

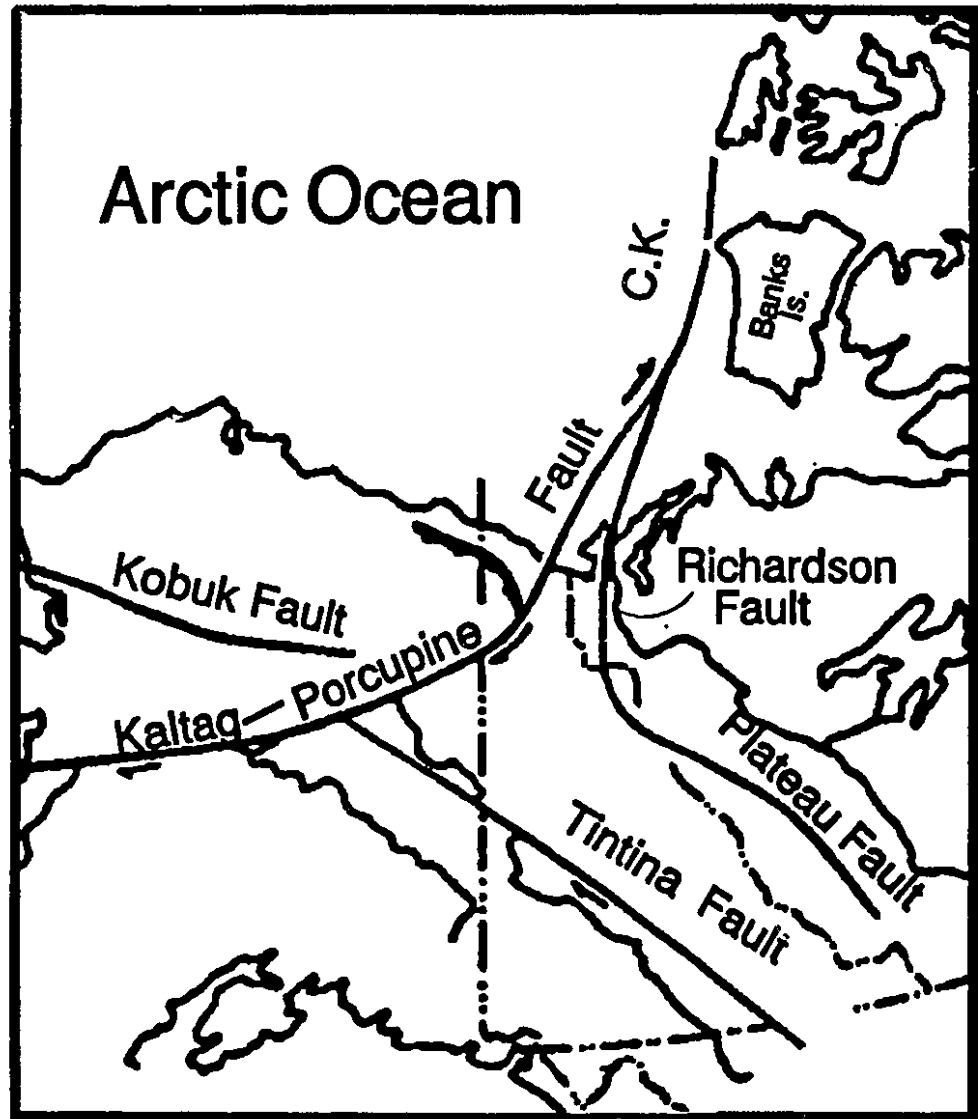


Figure I-3. Structural elements (after Norris and Yorath, 1981). C.K. - Cape Kellet Fault.

I tectonics of Proterozoic sea-floor spreading. The Kaltag-Porcupine Fault is the major Laramide structural element that separates the Tintina Fault and its offset equivalent, the Kobuk Fault. The Kaltag-Porcupine Fault braids into splays of the Rapid Fault Array as it turns sharply northward at the southern tip of the Rapid Depression.

### **Sequences, Stratigraphy and Sedimentology**

The post-Cretaceous part of the Beaufort-Mackenzie Basin consists of thick progradational deltaic sequences of various ages. The basic structure, stratigraphy, sedimentology and organic geochemistry of these partly onshore and partly offshore deltaic sequences are fairly well known from extensive geophysical surveys, drill-holes and subsequent studies (e.g. Dixon et al., 1985). Stratigraphic and sequence names used in this thesis follow Dietrich et al. (1985) (Fig. I-4).

The sequences include, from oldest to youngest, the Fish River, Reindeer, Richards, Kugmallit, Akpak-Mackenzie Bay, and Iperk sequences (Fig. I-5). The individual sequences contain fluvio-deltaic (delta plain), delta front, prodelta mud and basinal turbidite facies. Each sequence represents time periods of about 5 to 20 Ma. The maximum thickness of the sequences varies from a few hundred metres to several kilometres, with the total thickness exceeding 10 km at the depocentre (Fig. I-6).

The **Fish River Sequence** represents the first deltaic cycle deposited in the Beaufort-Mackenzie Basin. It consists of latest Cretaceous to Early Paleocene shale-dominated prodeltaic shelf and slope sediments of the Tent Island Formation, and fluvio-deltaic sandstones of the Moose Channel Formation. The stratigraphic extent of sequences as

AGE		SEQUENCE Dietrich, Dixon, and McNeil (1985)	FORMATION Young and McNeil (1984)
QUAT.	Pleist. Hol.	SHALLOW BAY	Recent deposits
	Pleist. Glac.	Glacial deposits	HERSCHEL IS.
TERTIARY	Plio.	IPERK	NUKTAK
	Miocene	AKPAK	
		MACKENZIE	MACKENZIE BAY
	Oligocene	KUGMALLIT	KUGMALLIT
		? KOPANOAR	
	Eocene	RICHARDS	RICHARDS
		REINDEER	REINDEER
	Paleocene	FISH RIVER	FISH RIVER GP. MOOSE CHANNEL
			TENT ISLAND
	CRET.		

Figure I-4. Stratigraphic sequences and units (after Dietrich et al., 1985; Dixon et al., 1985).

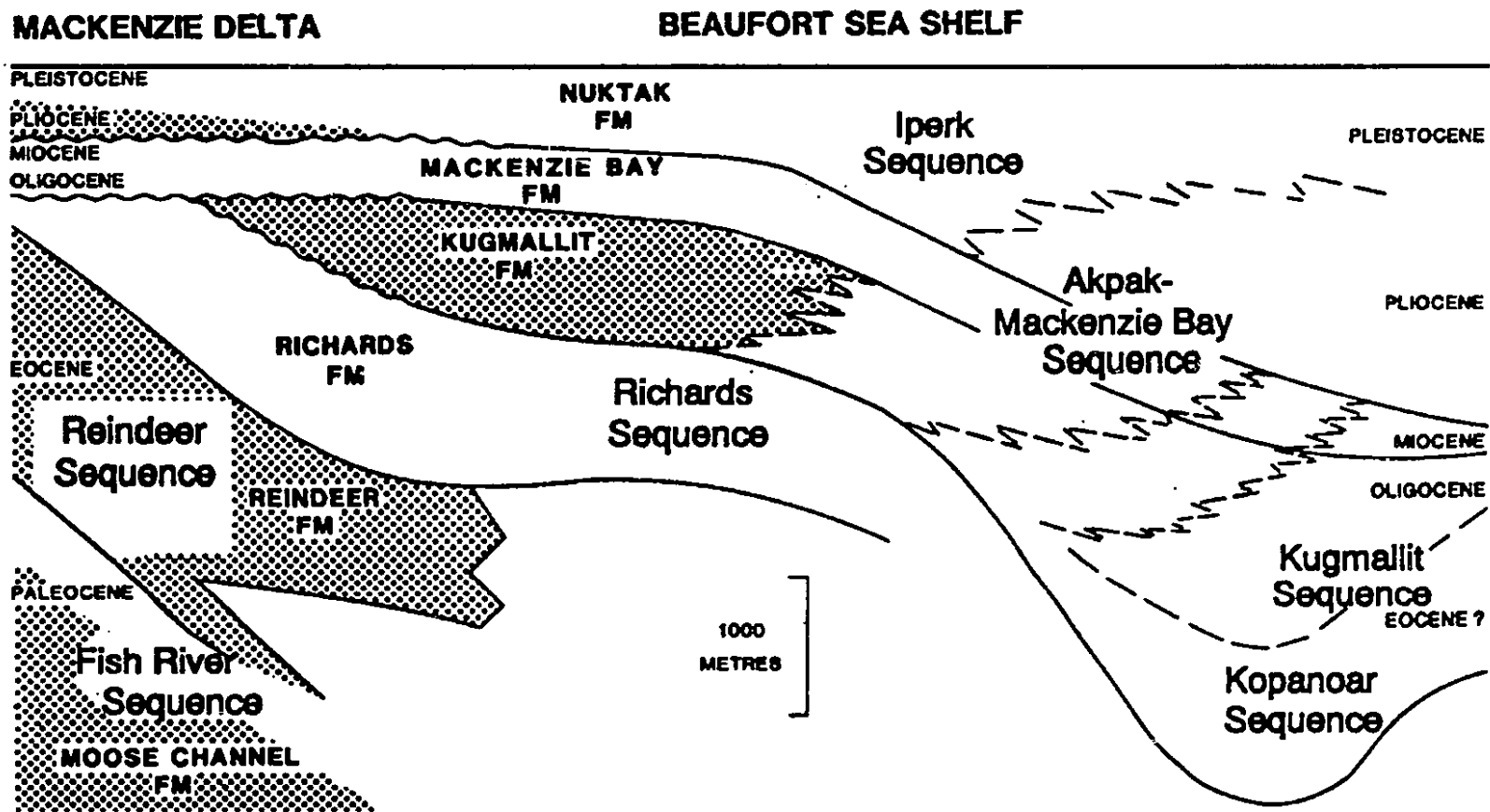


Figure I-5. Schematic NW-SE cross-section (after McNeil, 1985).

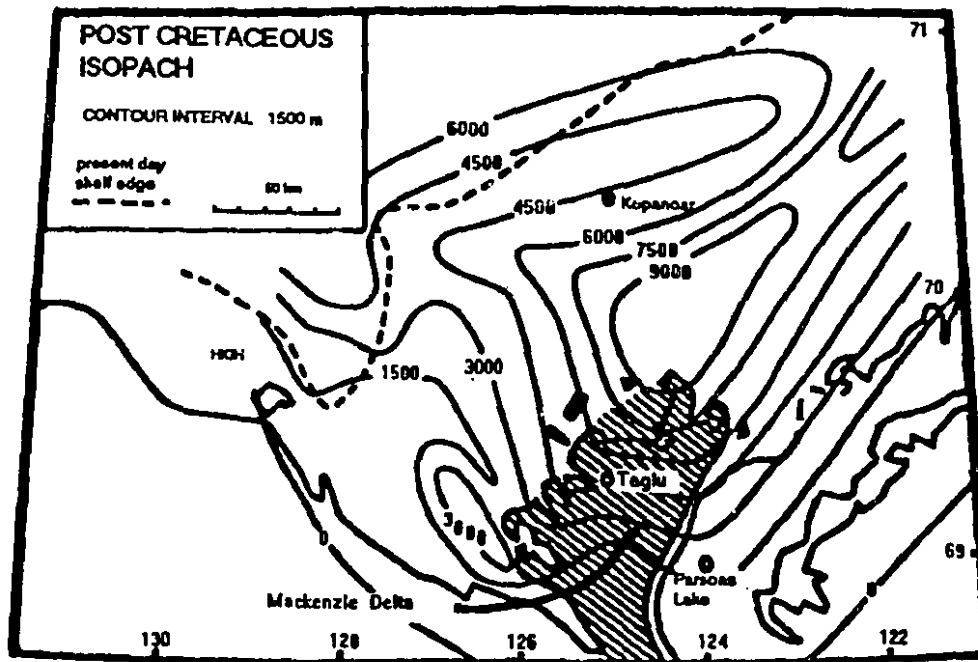


Figure I-6. Isopach map of Late Cretaceous to Holocene strata (after Willumsen and Cote, 1982).

shown in Figure I-7 may be debatable in detail (cf. Willumsen and Cote, 1982), but these subjects are beyond the scope of this thesis.

The Late Paleocene to Early Eocene delta of the **Reindeer Sequence** had its depocentre near the Taglu gas field. The thick delta plain/delta front sandy units of the Reindeer Formation have been one of the major exploration targets in the basin. The Reindeer Sequence is overlain conformably by the Late Eocene to Early Oligocene **Richards Sequence**, a thick succession of organic matter-rich marine shale that is considered a potential hydrocarbon source (Snowdon and Brooks, 1985). The landward equivalent of the sequence is not preserved because of extensive Late Eocene erosion.

The Oligocene **Kugmallit Sequence** is the thickest deltaic unit in the basin with a maximum thickness of up to 3 km near the depocentre off Pullen Island. The sequence contains numerous prodelta to delta front/delta plain coarsening-upward cycles, and thick turbiditic sand units (Kopanoar Sequence). The latter provides the reservoirs for offshore hydrocarbons.

The **Mackenzie Bay-Akpaq Sequence** consists of mudstones and siltstones (Mackenzie Bay Formation) of Late Oligocene to Middle Miocene age. In the subsurface, the sequence is characterized by large-scale clinofolds readily identifiable on seismic profiles. The limited regional extent of the sequence is due to pre-Iperk (Late Miocene) erosion.

The thick clastic wedge of the **Iperk Sequence** was formed by northwesterly prograding, Late Miocene to Pleistocene deltas. It rests unconformably on older sequences and is overlain by Late Pleistocene to Holocene glacial and recent delta

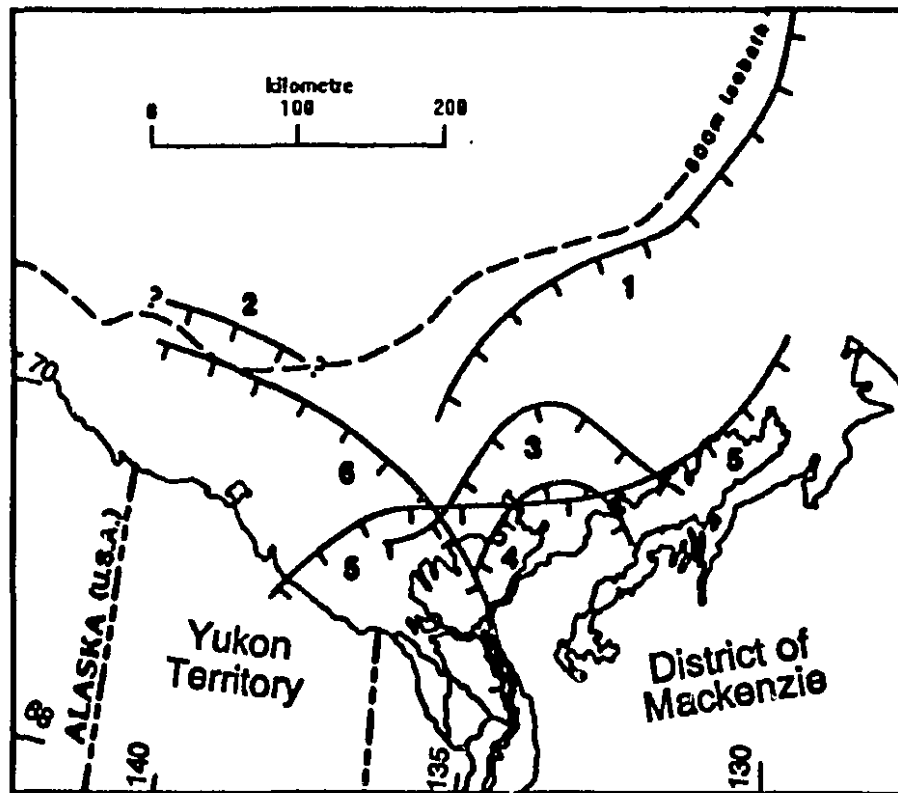


Figure I-7. Progradation of major deltaic sequences (after Dixon and Dietrich, 1990). 1- Iperk. 2- Mackenzie Bay. 3- Kugmallit. 4- Richards. 5- Reindeer. 6- Fish River.

deposits (Shallow Bay Sequence).

Structural styles within the Tertiary sediments are dominated by syndepositional growth faults, folds, and shale diapirs (Fig. I-8). Growth faults and folds appear to have developed under the influence of both external (tectonic) and internal (gravitational) forces (Hemingson and Carew, 1984). Diapirs are predominant in the western part of the basin. Their development is probably related to eastward migration of depocentres through time. As a heavier sandy mass progrades towards the east, loading upon finer-grained sediments in the west would be relieved. This would result in diapir development mainly in the western part of the basin (cf. Daily, 1976).

#### **Geothermal Gradients, Geopressure, Formation Water Chemistry and Sandstone Diagenesis**

Geothermal gradients on land are generally within the range for normal continental crust, between 20 to 30 °C/km (Judge and Bawden, 1987). High values (>30 °C/km) encountered basinwards are surprising because of thick, Tertiary sedimentary successions present offshore (Fig. I-9). These relatively high geothermal gradients suggest a thinner crust in the shelf region or a heat source to the north.

Hydrocarbon occurrence in the basin was related to the distribution of geopressure by Hemingson and Carew (1984) and Hitchon et al. (1990). The top of the geopressure zone appears to shallow basinwards (Fig. I-10). Thus, the sequences in which geopressure is encountered become progressively younger in a basinward direction.

Formation waters of the basin show relatively low salinities compared to other basins (e.g. Alberta Basin). Hitchon et al. (1990) proposed the influx of meteoric waters as a



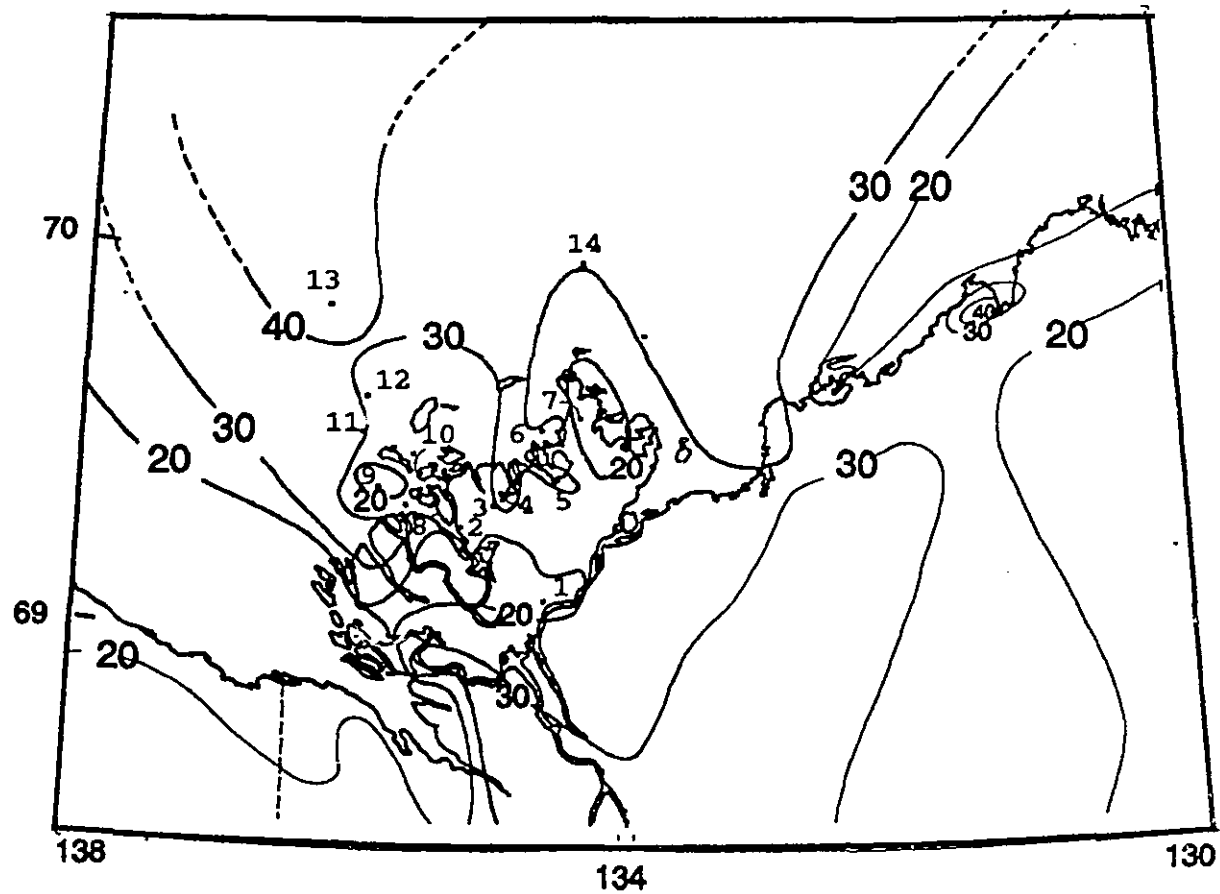


Figure I-9. Geothermal gradient map (after Judge and Bawden, 1987). 1-Reindeer D-27. 2-Kumak E-58. 3-Taglu C-42. 4-Taglu G-33. 5-Mallik A-06. 6-Unark L-24A. 7-Ivik J-26. 8-Niglintgak M-19. 9-Adgo C-15. 10-Garry P-04. 11-Netserk B-44. 12-Netserk F-40. 13-Tarsiut N-44. 14-Issungnak 20-61.

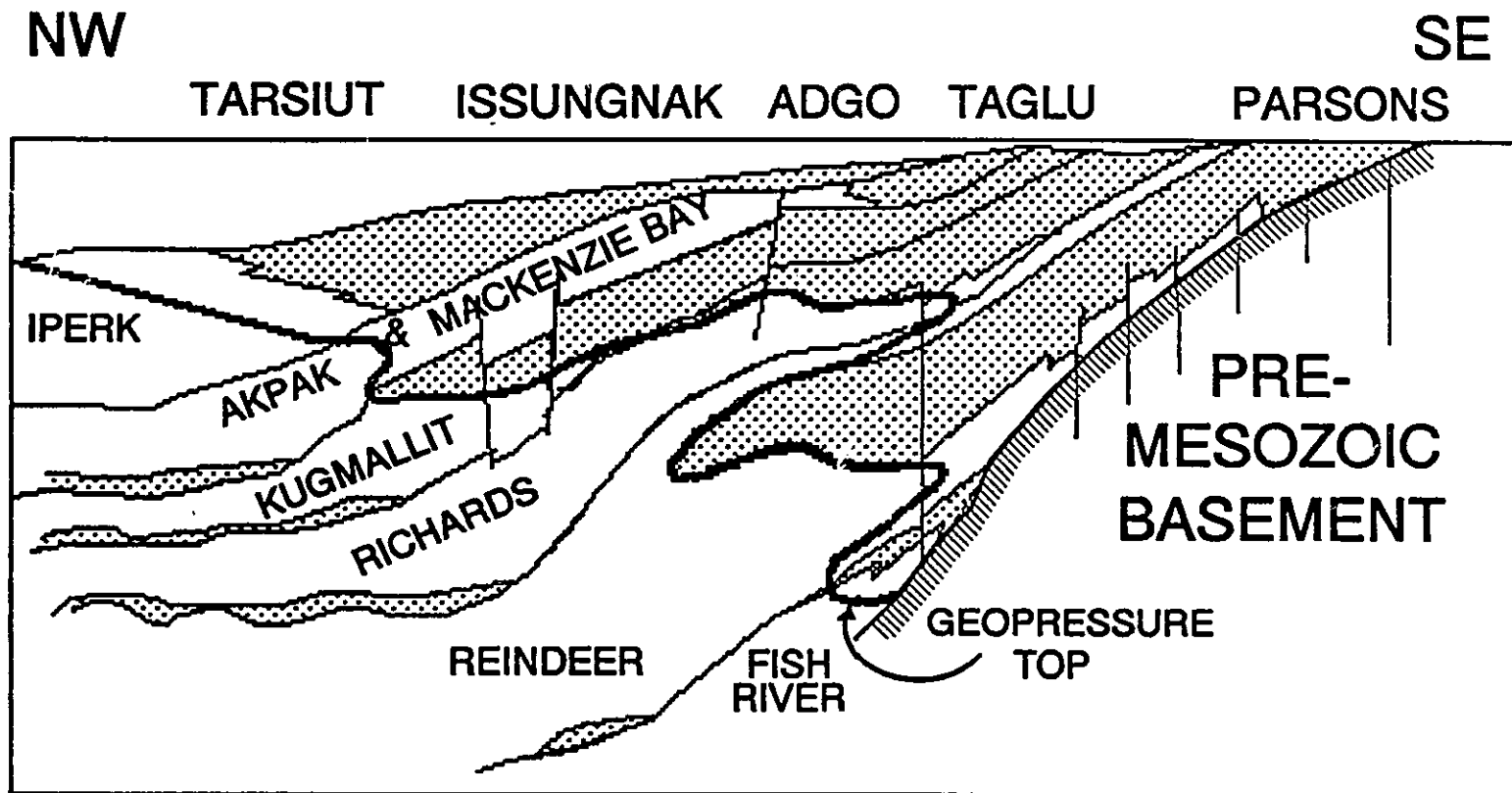


Figure I-10. Distribution of geopressure (after Hemingson and Carew, 1984).

possible cause. Most salinity data fall in the range of 6000 to 35000 mg/l and show unusually high concentrations of bicarbonate (up to about 5000 mg/l).

Petrography and diagenesis of sandstones have been studied by Schmidt (1987). The framework grain composition indicates a recycled orogenic provenance (sensu Dickinson and Suczek, 1979). Cements and replacive minerals include various carbonates, quartz, kaolinite, chlorite, pyrite and leucoxene. Porosity ranges from 3 to 43 % and averages 17 %. Most porosity (about 85 % of the total) was interpreted to be of secondary origin (Schmidt, 1987).

## MATERIALS AND METHODS

Twenty-two wells were chosen to establish the basin-wide variations in I/S mineralogy based on geographic distribution, hydrocarbon occurrence and the depth range of available samples (Fig. I-11). For most wells, the following data were available through variable open and in-house publications from government, industry and research institutes: bio- and lithostratigraphy, structure, geothermal gradients, hydraulic regime and depths of hydrocarbon occurrence.

A total of 215 samples (110 core samples, 105 drill cuttings) were selected for detailed mineralogical analyses (Table I-1). Drill-cuttings were collected from every sample interval in individual wells, and combined by weight with appropriate intervals in order to obtain a sufficient amount of fine-grained fractions. Drill-cutting samples from intermediate depths in offshore wells and shallow depths in onshore wells showed signs of contamination by drilling mud, even after repeated washing, and were not included in

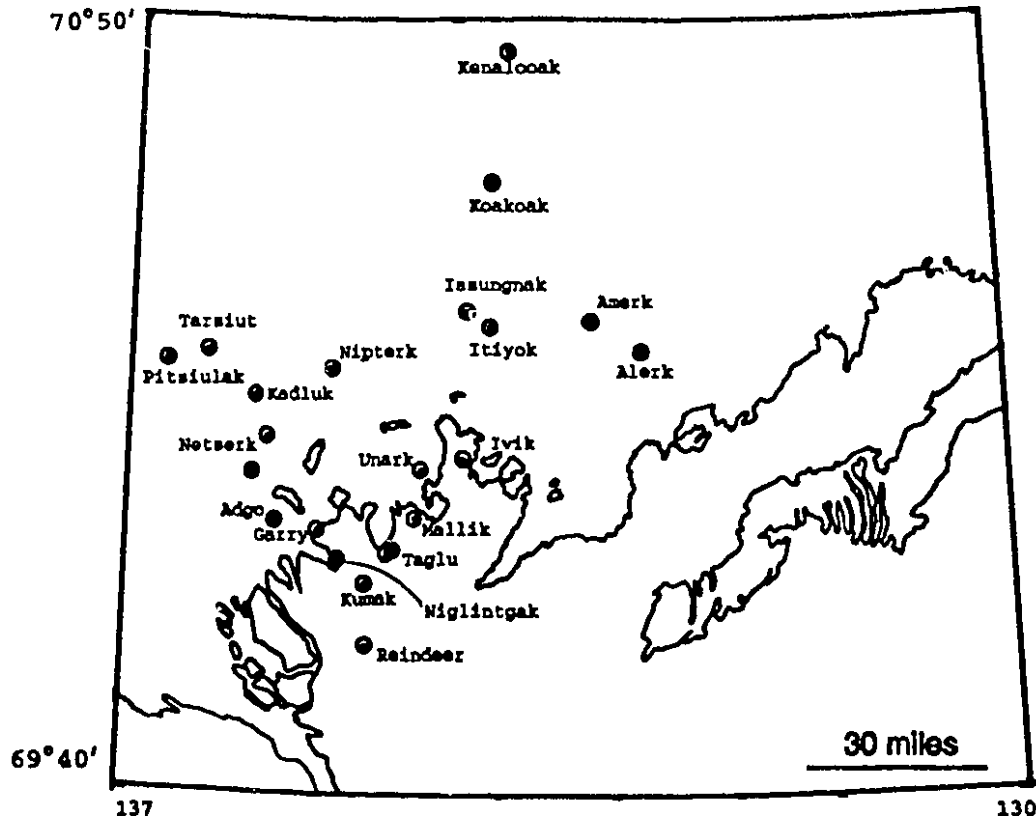


Figure I-11. Location of wells used in this study.

Table I-1. Well locations and sample distribution.

Well Name	Location		Drill Cuttings	Cores	Total
	Latitude	Longitude			
Reindeer D-27	69°06'05"	134°36'54"	66	18	84
Taglu C-42	69°21'03"	134°56'35"	24	5	29
Taglu G-33	69°22'17"	134°53'36"	-	12	12
Kumak E-58	69°17'29"	135°14'55"	-	5	5
Niglintgak M-19	69°18'49"	135°19'26"	-	6	6
Garry P-04	69°23'46"	135°30'19"	-	6	6
Adgo C-15	69°24'13"	135°49'03"	-	4	4
Mallik A-06	69°25'01"	134°30'16"	-	9	9
Ivik J-26	69°35'42"	134°20'38"	-	6	6
Unark L-24A	69°33'30"	134°37'02"	-	4	4
Netserk B-44	69°33'03"	135°55'58"	-	2	2
Netserk F-40	69°39'23"	135°54'21"	-	1	1
Kadluk O-07	69°46'48"	136°01'17"	-	4	4
Nipterk L-19	69°48'38"	135°19'53"	-	6	6
Tarsiut N-44	69°53'49"	136°11'39"	-	4	4
Pitsiulak A-05	69°54'14"	136°45'35"	-	1	1
Issungnak 2O-61	70°01'00"	134°18'48"	-	4	4
Itiyok I-27	69°56'40"	134°05'19"	-	1	1
Alerk P-23	69°52'57"	132°50'22"	-	2	2
Amerk O-09	69°58'56"	133°30'53"	-	8	8
Koakoak O-22	70°21'59"	134°06'40"	4	2	6
Kenalooak J-94	70°43'44"	133°58'28"	11	-	11

Total      105      110      215

the study. Washed cuttings were screened through a 10 mesh sieve for primary removal of cavings, and from the sieved material only shale chips were hand-picked.

Drill-cutting and crushed core samples of about 50 g were shaken for about 8 hours, and soaked in Na-acetate solution (pH 6) for one night to remove carbonates and soluble salts. Organic matter was removed using 30 % H<sub>2</sub>O<sub>2</sub> following Jackson (1969). Samples were then Na-saturated, and excess salts were removed by repeated washing and dialysis until no chloride was detected with AgNO<sub>3</sub>. For better dispersion, 10 % Na-metaphosphate (calgon) solution was added to the suspension (20 ml calgon/350 ml suspension). To maximize the amount of fine fractions, suspensions were ultrasonified briefly before size fractionation. Centrifugation according to Stokes' law was used to obtain a <.1 μ fraction which is the optimum size fraction for the Beaufort-Mackenzie material, i.e. this fraction consists chiefly of I/S clays. Suspensions of the <.1 μ fraction were freeze-dried to avoid artifacts of oven-drying on I/S clays caused by heating.

Slides of oriented particles were prepared following the membrane-filter transfer method (Moore and Reynolds, 1989; modified after Drever, 1973). Each slide was made from 100 mg of dried powder. Air-dried slides were kept in a desiccator (~0 % relative humidity) until X-ray diffraction in order to obtain a "single-layer" state for interlayer water in expandable layers of I/S. Glycol treatment was done by solvation in a desiccator containing ethylene glycol at the bottom. Samples were kept at 60 °C for 3 nights which appear to be an adequate period to obtain a constant and maximum glycol-layer thickness for Beaufort-Mackenzie I/S. Prior to X-ray diffraction, these samples were transferred to an air-tight box chamber containing a beaker with ethylene glycol.

I

Some selected samples were heat-treated at 400 and 550 °C for an hour to ensure proper identification of components in mixed-layer clays, and the distinction between kaolinite and chlorite (see Fig. III-2). About 60 samples from three wells (Reindeer D-27, Taglu C-42, Taglu G-33) were K-saturated to estimate the proportion of high-charge expandable-layers that collapse to form illite-like layers. K-saturation was done by keeping samples of the <1 μ fraction in 1 N KCl solution overnight, followed by washing with a fresh solution. Desalination was done by washing once with distilled water followed by dialysis to avoid any loss of ultra-fine particles. For K-saturated samples about 20 mg of dried powder were used for slide preparation, because K-saturated clays were highly flocculated resulting in greater sample thickness compared to Na-saturated samples prepared from the same amount of material.

X-ray diffraction was conducted with a Siemens D-500 X-ray diffractometer equipped with a graphite diffracted-beam monochromator. The X-ray source was CuK $\alpha$  radiation generated at 40 kV and 20 mA. The slit conditions were 1° for the divergent slit and .15° for the receiving slit. An automated data collection system (DACO-MP) was used for step-scans usually carried out between 2 to 35 °2 $\theta$  at 0.01 °2 $\theta$  step size and 1s counting time, unless stated otherwise.

## CHAPTER II. CRITICAL REVIEW OF CURRENT DEVELOPMENTS IN ILLITE/SMECTITE DIAGENESIS

From the short outline in Chapter I, it is evident that I/S diagenesis is of major geologic and economic importance. It has been intensely studied using a wide variety of mineralogical and geochemical techniques (for references, see discussion). However, the impression one may get at first that it is a well understood process does not stand up under close scrutiny. Even the identity of I/S itself has been questioned (Nadeau et al., 1984b). The most controversial issues of the current debate are:

- (i) Is illitization a gradual or episodic process?
- (ii) Does I/S consist of Markovian crystallites or fundamental particles?
- (iii) Does illitization stop when potassium is depleted?
- (iv) Is I/S a single-phase solid solution or does it consist of two or more phases?
- (v) Does illitization involve a transformation process or neoformation?

### GRADUAL VS. EPISODIC PROCESS

Geologists interested in burial diagenesis of argillaceous sediments are accustomed to the notion that clay-mineralogical reactions in the subsurface are slow, continuous reactions that span considerable temperature and depth ranges. The smectite-to-illite reaction has served as the key example for this point of view. I/S clays with gradually increasing proportions of I-layers occur with increasing burial depths corresponding to the temperature range from 60 to 160°C. The gradual nature of the illitization process has been demonstrated by numerous studies including X-ray diffraction, geochemistry (e.g. Hower et al., 1976), K-Ar dating (e.g. Aronson and Hower, 1976), and O- and H-isotopic

work (e.g. Yeh and Savin, 1977; Yeh, 1980).

This conventional view has been challenged by Morton (1985) who suggested that the smectite-to-illite reaction is rather a rapid, instantaneous event, based on Rb/Sr isotopic analyses of claystones from the Oligocene Frio Formation in the Texas Gulf Coast. "The interpretation of the S/I Rb/Sr data as a true isochron challenges the standard interpretation of Gulf Coast clay diagenesis. If 'episodic' diagenesis has truly occurred, the possible role of clay diagenesis and diagenesis in general on petroleum generation and migration in Gulf Coast style sediments will need to be reevaluated" (Eslinger and Pevear, 1988). Whether or not Morton's hypothesis is correct, his results have been reproduced in several drill holes in the Gulf Coast (Ohr et al., 1991; Mack et al., 1990).

Morton's proposed episodic diagenesis, which would have affected a 2 km thick sediment column virtually at once, would have to have started (i) at a subsurface depth of about 1 to 1.5 km, (ii) at subsurface temperatures of  $<50^{\circ}\text{C}$ , and (iii) only 0.5 to 7 Ma after deposition. The minimum age of 0.5 Ma would suggest unreasonably high sedimentation rates of up to 6 km/Ma.

The feasibility of instantaneity in a geologic time frame can be assessed by kinetic considerations. Eberl and Hower's (1976) data indicate that at  $50^{\circ}\text{C}$ , pure smectite may be changed to a 20 % expandable I/S in about 0.6 Ma, which is geologically instantaneous. However, as these authors pointed out, the question is whether the kinetics of a relatively simple system under the chosen experimental conditions are applicable to the complex natural system. Later studies suggested that the rate of illitization also depends on solution chemistry, composition of the starting material and many factors

other than temperature, and that the reaction may not be first order (Roberson and Lahann, 1981; Howard and Roy, 1985; Whitney and Northrop, 1988). The presence of cations with high dehydration energy-  $Mg^{2+}$ ,  $Ca^{2+}$  and  $Na^+$ - in solution significantly slows the reaction [For a cation of given charge, the lower the dehydration energy (e.g. K, Rb, Cs), the faster the reaction rate]. Whether the illitization reaction is first or higher order is not clear. Data available from Roberson and Lahann (1981, Figs. 4, 5) and Whitney and Northrop (1988) suggest that the reaction rate in the composition range of ordered I/S is very different from that in the range of random I/S. For a natural contact-metamorphic environment, Pytte and Reynolds (1989) suggested that the reaction may be sixth order (fifth order with respect to smectite). Their empirical time-temperature relation predicts that it would take 750 Ma at 50°C for 100 % smectite to convert to a 20 % expandable I/S. However, by raising the temperature, geologic instantaneity (~1 Ma) can be achieved at 125°C. These kinetic considerations provide certain, though broad constraints in terms of time and temperature for the illitization process in geologic environments.

The Rb-Sr dating method is considered next. The Rb-Sr isochron method assumes a) a constant  $^{87}Sr/^{86}Sr$  ratio in the geologic system of interest at the onset of the event and b) closure of the system with respect to Rb and Sr during and after the event. In sedimentary systems, a prerequisite for constant  $^{87}Sr/^{86}Sr$  ratios of a solid phase (e.g. I/S) is the isotopic homogeneity of Sr in solution. Sea water is probably the only solution that shows a relatively uniform Sr isotopic composition over extended time-periods due to the long residence time of Sr in the ocean compared to the mixing time of the ocean (Burke

et al., 1982).

The Sr isotopic composition of meteoric waters (surface and ground waters) varies considerably, and depends on ages and rock types of the drainage basin and the aquifer. The global average of surface waters is 0.7119 based on river data (Palmer and Edmond, 1989). Ground waters show Sr isotopic compositions similar to those of surface waters (Stueber et al., 1975). For a given aquifer, the  $^{87}\text{Sr}/^{86}\text{Sr}$  ratio of the water is equal to or near the value of the host rock, especially for carbonate aquifers (Starinsky et al., 1980).

Formation waters show a wide range of  $^{87}\text{Sr}/^{86}\text{Sr}$  ratios from 0.7061 to 0.7341 (Russell et al., 1988; Nakano et al., 1989). The  $^{87}\text{Sr}/^{86}\text{Sr}$  ratio of formation waters varies laterally and with depth in a given basin. It depends on isotopic compositions of the original water and host rocks, and the degree of water/rock interaction. In general, high ratios are attributed to the contribution from Rb,K-bearing minerals (K-feldspar and micas) and low ratios to Sr,Ca-bearing phases including marine carbonates, evaporites and plagioclase. The Sr isotopic composition of the formation water can generally be described as:

$$(^{87}\text{Sr}/^{86}\text{Sr})_p = X(^{87}\text{Sr}/^{86}\text{Sr})_o + \sum Y(^{87}\text{Sr}/^{86}\text{Sr})_{\text{Sr}} + \sum Z(^{87}\text{Sr}/^{86}\text{Sr})_{\text{Rb}} \quad (1)$$

where subscripts denote p - present water, o - original water, Sr -Sr-bearing solids and Rb - Rb-bearing solids, and X, Y and Z represent fractions contributed by the corresponding reservoirs. If sea water is the original water,  $(^{87}\text{Sr}/^{86}\text{Sr})_o$  is assessed from the well established curve of sea water  $^{87}\text{Sr}/^{86}\text{Sr}$  through time, and X equals  $\sim 8$  ppm/total dissolved Sr. For meteoric waters, the first term will be, in general, negligible due to the low Sr concentration ( $<1$  ppm) in fresh water.

Sea water is, as mentioned, the only water mass of homogeneous isotopic composition.

Thus, it is possible that I/S clays equilibrated with sea water may provide an isochron. However, Sr in I/S is exchangeable, especially so in less evolved I/S which is characterized by the high proportion of expandable layers. Sr on basal faces and in exchange interlayer-sites of I/S is readily equilibrated with surrounding waters and shows the same  $^{87}\text{Sr}/^{86}\text{Sr}$  ratio as the water last encountered (Schultz et al., 1989; Mack et al., 1990).

The Sr heterogeneity of formation waters, basin-wide or in-depth, is a rule rather than an exception (Stueber et al., 1984; Morton and Land, 1987; Russell et al., 1988). Therefore, isochrons obtained for I/S clays over a depth range of several kilometres require an alternative explanation that disregards the necessary prerequisite, i.e. the isotopic homogeneity of the environmental Sr. According to Zheng (1989), theoretically an isochron can be generated if a positive correlation exists between  $^{87}\text{Sr}/^{86}\text{Sr}$  and  $^{87}\text{Rb}$ . A suite of coeval samples can yield a straight line on the isochron diagram, if the condition  $^{87}\text{Sr}/^{86}\text{Sr} = a + b^{87}\text{Rb}$  is met (where a and b are constants and  $b > 0$ ). It should be noted that the correlation between  $^{87}\text{Sr}/^{86}\text{Sr}$  and  $^{87}\text{Rb}$  need not be strict. A fair correlation is generally enough.

In basins where the isotopic composition of the formation water depends primarily on either Sr- or Rb-bearing phases, the previous equation (1) is simplified to

$$(^{87}\text{Sr}/^{86}\text{Sr})_p = X(^{87}\text{Sr}/^{86}\text{Sr})_o + Y(^{87}\text{Sr}/^{86}\text{Sr})_{\text{Sr}} \quad (2) \text{ where the Sr,Ca-bearing phase is}$$

predominant;

$$(^{87}\text{Sr}/^{86}\text{Sr})_p = X(^{87}\text{Sr}/^{86}\text{Sr})_o + Z(^{87}\text{Sr}/^{86}\text{Sr})_{\text{Rb}} \quad (3) \text{ where the Rb,K-bearing phase is}$$

predominant;

where X equals (1-Y) or (1-Z) and  $(^{87}\text{Sr}/^{86}\text{Sr})_o$ ,  $(^{87}\text{Sr}/^{86}\text{Sr})_{\text{Sr}}$  and  $(^{87}\text{Sr}/^{86}\text{Sr})_{\text{Rb}}$  can be constants. There will then be a linear relationship between the  $^{87}\text{Sr}/^{86}\text{Sr}$  ratio of the formation water and Sr concentrations, because the equations (2) and (3) become

$$(^{87}\text{Sr}/^{86}\text{Sr})_p = (^{87}\text{Sr}/^{86}\text{Sr})_o + Y[(^{87}\text{Sr}/^{86}\text{Sr})_{\text{Sr}} - (^{87}\text{Sr}/^{86}\text{Sr})_o] \quad (4)$$

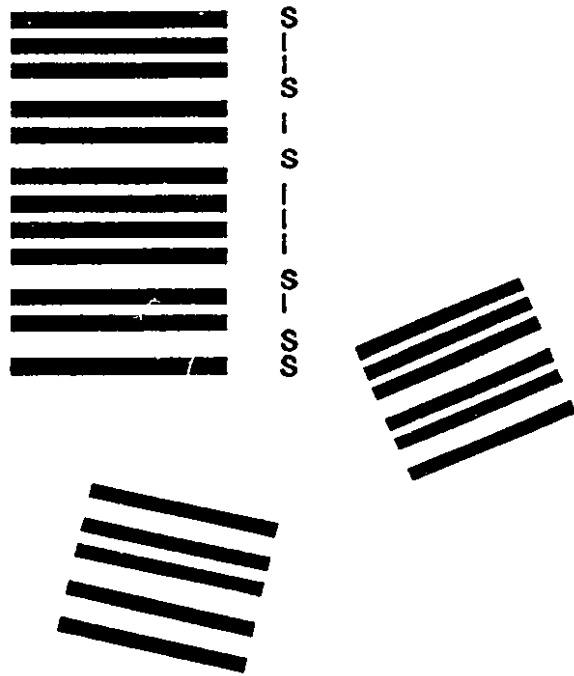
$$(^{87}\text{Sr}/^{86}\text{Sr})_p = (^{87}\text{Sr}/^{86}\text{Sr})_o + Z[(^{87}\text{Sr}/^{86}\text{Sr})_{\text{Rb}} - (^{87}\text{Sr}/^{86}\text{Sr})_o] \quad (5)$$

respectively, where  $(^{87}\text{Sr}/^{86}\text{Sr})_{\text{Sr}}$  and  $(^{87}\text{Sr}/^{86}\text{Sr})_{\text{Rb}}$  may represent the isotopic composition of the whole rock. The linearity may extend for elements other than Sr derived from solid phases, if congruent solution is assumed. In sedimentary basins, it appears that either carbonates or clastics are predominant. The contemporary occurrence of both is uncommon in large basins. In most basins where the illitization reaction is active, Sr is probably derived from K-feldspar, micaceous clays and/or I/S itself. Therefore, the latter linear equation (5) can be applied for such basins. If I/S clays were in equilibrium with this formation water, they would produce a quasi-isochron. Unlike Morton's hypothesis, which requires a large volume of an isotopically homogeneous water mass and a relatively instantaneous reaction for I/S diagenesis, the hypothesis considered here simply requires a water mass in which Rb,K-bearing phases predominate the Rb-Sr systematics.

### MARKOVIAN CRYSTALLITES VS. FUNDAMENTAL PARTICLES

I/S clays have been known to consist of randomly or regularly interstratified smectite and illite layers (Fig. II-1a). They are identified by non-integer series of reflections and line broadening in X-ray diffraction. Computer simulation of X-ray diffraction patterns for I/S clays indicates that the X-ray coherent domain size varies but, in general, falls in the

a) Markovian crystallites



b) Fundamental particles

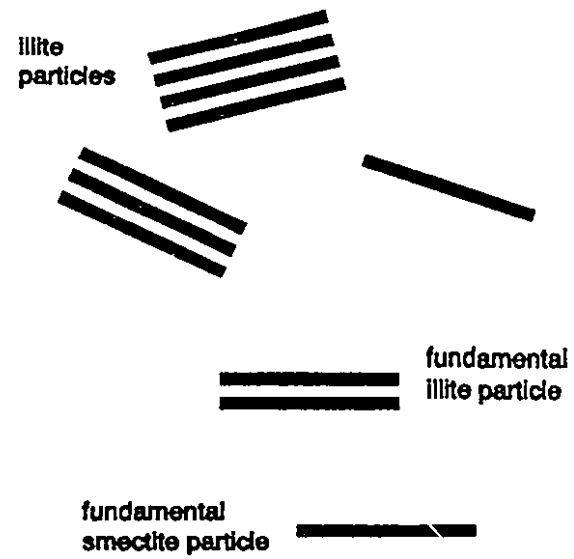


Figure II-1. Comparison of I/S according to Markovian crystallite and fundamental particle models.

range of 5-15 layers (Reynolds and Hower, 1970). Markovian crystallites, also known as MacEwan crystallites, are defined by proportions of component layers and junction probabilities within the sequence. The junction probability describes the probability of finding a certain layer type that follows a specified layer type or sequence in an arbitrary, but defined direction (MacEwan, 1956). The probability varies from 0 to 1 and is used to measure the degree of randomness, ordering and segregation in stacking sequences of mixed-layer clays.

The basic assumption that mixed-layer clays are the entity in which component layers are intimately mixed to form a fixed sequence has been challenged by Nadeau et al. (1984a-c). Based on transmission electron microscopic (TEM) thickness measurements of finely dispersed mixed-layer clays, Nadeau et al. suggested that clays yielding X-ray diffraction patterns of mixed-layer nature are physical mixtures of 'fundamental particles' (Fig. II-2b). A fundamental smectite-particle is a single 2:1 silicate layer 10 Å thick, whereas a fundamental illite-particle consists of two such layers, 20 Å thick, coordinated by interlayer K<sup>+</sup>. The interfaces between these particles are capable of adsorbing water or organic molecules, thus, mimicking the presence of smectite layers defined according to the Markovian crystallite model. According to Nadeau et al., random mixed-layering of I/S is an artifact that results from mixing of fundamental smectite- and fundamental illite-particles. Clays made up exclusively of fundamental illite-particles produce X-ray traces of an ordered I/S mixed-layer mineral. The fundamental particle concept implies that illite and smectite exist separate from one another rather than united epitaxially in a sequence as assumed previously. In the scheme, illitization is simply a process of

crystal growth, for which material is derived from dissolution of smectite minerals and, later, thin illite particles. Later studies (e.g. Inoue et al., 1987) confirmed the observations of Nadeau et al. that particles are 1-5 unit cells thick, significantly thinner than those predicted by the Markovian crystallite model and shown in lattice-fringe images (e.g. Vali and Köster, 1986).

The two models seem to be incompatible. However, assuming that they are describing the same phenomenon, it is clear that the problem stems from whether I/S crystallites are separable across smectite layers, which has not been questioned by advocates of the Markovian model. Similarly, followers of the fundamental particle hypothesis did not consider that fundamental illite- and smectite-particles could, in fact, be derived from crystallites where they form neighbors. Altaner and Bethke (1988) provided the basis to bridge the two seemingly contradictory models. These authors constructed theoretical crystallites according to the Markov model and investigated the fundamental particle content in crystallites. Their results show that the size distribution of particles which can be dissociated across smectite layers in crystallites is in good agreement with the distributions of fundamental particles observed in TEM.

Parting of I/S crystallites into elementary particles (sensu Altaner and Bethke 1988) upon dispersion is probably analogous to the behavior of smectite. Fast cryofixation of dilute smectite suspensions indicates that free particles of a single 2:1 silicate layer dominate the population, for which the average thickness was estimated to be about 3 unit cells (Vali and Bachmann, 1988).

Smectite consists of a negatively-charged 2:1 silicate layer, water and exchangeable

cations. Water molecules are linked to the oxygen surfaces of the tetrahedral sheets by hydrogen bonds. Exchangeable cations are either associated with silicate layers in a more or less regular manner filling in the "hexagonal" cavities of the tetrahedral sheets, or with water layers to form hydration complexes depending on the valency and hydration energy of cations. In smectite, silicate layers are held together by van-der-Waals forces and, to a lesser extent, the electrostatic force between hydrated cations and negatively charged layers. Short range dissociation (about 4-5 layers of water) between silicate layers is attributed to hydration of interlayer cations, hydration of the layer surface itself, or both. As the separation distance increases, electric double-layer repulsion becomes an important force between silicate layers.

It is well known that colloid particles develop an electric double-layer upon dispersion in a liquid (Derjaguin-Landau-Verwey-Overbeek or DLVO theory; for clay colloid chemistry, see van Olphen, 1977). The DLVO theory provides a key insight into why and how I/S clays dissociate into fundamental (or elementary) particles and these particles associate into crystallites with crystallographic continuity. However, it is rather poorly appreciated in clay-mineralogical studies. A brief discussion of colloid chemistry will help to clarify the confusion regarding the identity and behavior of I/S clays.

The electric double-layer consists of the particle charge and a layer of counter-ions of equivalent, but opposite charge which accumulate in the liquid near the particle surface. The counter ions which are attracted by the charged surface form an atmosphere in which ion concentration gradually decreases with increasing distance from the particle surface. The electric potential is obtained from the distribution of ions and the surface charge of

the particle. The distribution of ions follows the Schulze-Hardy rule: the higher the electrolyte concentration and the higher the valence of the ions, the thinner the diffuse double-layer. When two colloidal particles approach each other in suspension, there will be repulsion between them resulting from interaction of their diffuse counter-ion atmospheres. Work is required to bring the particles from infinite separation to proximity. This is provided by the van-der-Waals attraction which counteracts the electrostatic repulsive force between the double layers. When the van-der-Waals force overcomes the electrostatic repulsive force, the particles will associate.

In smectite, the association may be face-to-face, face-to-edge, and edge-to-edge due to broken bonds present at the edges of silicate layers. Double-layers forming at the edges of tetrahedral and octahedral sheets appear mostly positive, but can be negative depending on pH. The mode of association is determined by the sum of the van-der-Waals force, the double-layer repulsion and the electrostatic attraction between the oppositely charged edge and face double-layers. In the presence of a small quantity of peptizing anions or alkalis that neutralize or reverse the edge charge, the edge-to-edge and edge-to-face associations are eliminated. In this way the suspension is stabilized, deflocculated, or peptized. In a flocculated suspension, settling produces a loose, voluminous particle aggregation showing a card-house structure. A stable suspension forms a dense, closely packed sediment dominated by face-to-face associations. When dried, faces come closer and the van-der-Waals force increases drastically, following an inverse power function of distance. As dehydration continues, layers, water molecules and cations position to conform to a low-energy configuration. The spacing is the result

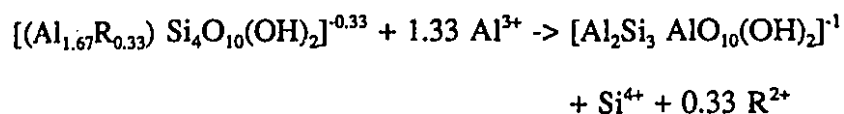
of a delicate balance among three basic forces- the van-der-Waals force, the electrostatic force between silicate layers and cations, and the force involved in the dehydration or hydration of cations.

The concept of colloid chemistry that works on smectite is probably applicable to I/S clays. A careful TEM study combining ion-milling (Lee et al., 1985) and alkylammonium methods (Vali and Hesse, 1990) will reveal if I/S clays really exist as an entity in which I- and S-layers are intimately mixed maintaining crystallographic continuity, or if mixed-layering is an artifact of interparticle diffraction between thin particles. The ion-milling technique allows direct observation of the in-place structural state of I/S clays that may be disturbed or destroyed by the normal preparation technique involving dispersion. The alkylammonium method developed by Vali and Hesse (1990) would facilitate the identification of expandable layers without sacrificing the advantage of ion-milling, although variable spacings due to different layer charges and the presence of expandable illite (Vali et al., 1991) would complicate the problem. The existence of expandable illite that does not expand upon glycol or glycerol solvation has been known since alkylammonium was adopted in layer-charge studies of clay minerals; however, its significance has not yet been widely appreciated. Further characterization of expandable illite and better understanding of the mechanisms for the alkylammonium-exchange reaction are needed.

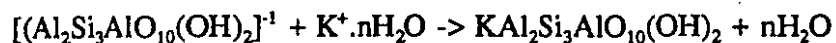
### **LAYER CHARGE VS. POTASSIUM**

Illitization of smectitic material requires development of high layer-charge and fixation

of potassium. Thus, the reaction proceeds in at least two steps:



and



in which R represents divalent cations. The two reactions may not be simultaneous or interdependent. Rather, the layer charge may develop independently and, since potassium is readily available through the dissolution of K-bearing minerals and owing to its low dehydration energy, illite is probably an accidental end-product.

A similar view was first presented by Howard (1981) who identified high-charge expandable layers in I/S that are capable of fixing potassium into the interlayer position. Foscolos and Kodama (1974) reported the presence of high-charge expandable layers which they termed vermiculite. Bell (1986) showed lattice-fringe images of such layers (termed K-deficient illite) with alkylammonium treatment. Bell interpreted the high layer-charges as residual, resulting from weathering processes which remove potassium in illite leaving behind skeletal silicate layers. Nevertheless, in many cases, high-charge expandable layers appear to be the result of diagenesis (see discussion of oxygen isotopes and geochemistry of I/S in Chapter V).

Howard and Roy (1985) conducted hydrothermal experiments with Na-saturated smectite in K-deficient solutions and reported that smectite showed little change in X-ray character after a relatively long period of time at high temperatures. Upon potassium saturation, this smectite revealed up to 40 % layers that developed charges high enough

to form illite-like layers. These authors also reported an activation energy of <3.5 kcal/mole for the layer-charge developing reaction. This value is surprisingly low compared to activation energies obtained for the illitization reaction on the order of 20 to 30 kcal/mole (Eberl and Hower, 1976; Roberson and Lahann, 1981; Pytte and Reynolds, 1989). The low activation energy would indicate that layer-charge development does not involve the breaking of Si-O and Al-O bonds. Neither would the reaction be surface-controlled. Surface-controlled reactions that depend on the catalytic activity of surfaces or surface defects, typically, have activation energies in the range of 10-20 kcal/mole (Lasaga, 1981). The low values fall in the range of diffusion-controlled reactions in fluid media. If the low activation energies are truly representative of the reaction, it could be said that  $Al^{3+}$  and  $Si^{4+}$  ions enter or leave the oxygen net of the tetrahedral sheet as freely as they move in the fluid. However, a realistic explanation for the low activation energy would be that the reaction is a kind of chemisorption process, i.e., adsorption of  $Al^{3+}$  from a solution into the tetrahedral sheet. A charge increase due to  $Al^{3+}$  adsorption would be compensated by dissolution of some  $Si^{4+}$ -filled tetrahedra or incorporation of  $O^{2-}$  and  $OH^-$  at the edges of tetrahedral and octahedral sheets.

The potassium-fixation reaction is assumed to be diffusion-controlled as well (cf. Sawhney, 1966). Clays having significant exchange capacity exhibit selectivity for cations with low dehydration energy such as  $K^+$ ,  $NH_4^+$ ,  $Rb^+$  and  $Cs^+$  (Sawhney, 1972). Once these ions are introduced into the interlayer position where the electrostatic force between the silicate layer and the cation is greater than the cation hydration energy, the layer collapses to become an illite-like layer. Since diffusion-controlled reactions do not

require high energies, the resulting activation energy for the overall reaction combining layer-charge development and potassium fixation is expected to be far less than those obtained from laboratory illitization experiments, or estimated for reactions occurring in the natural environment. The later section on *transformation vs. neoformation* attempts to solve this dilemma.

Layer charges of expandable layers in I/S clays need more attention and, if studied in detail, would hint at how the illitization reaction progresses. A general practice has been to assume that expandable layers are low-charge smectite and that high-charge smectite- or vermiculite-layers are of negligible importance. In reality, there may be a wide range of layer charges distributed in expandable layers (Velde and Brusewitz, 1986). Unfortunately, the misconception that vermiculite maintains its spacing in the diffraction pattern after ethylene glycol solvation as it does after glycerol treatment has led to oversight of the possible third component. Vermiculite forms double-layer complexes with ethylene glycol and gives spacings of 16.2 Å in contrast to glycerol complexes that normally give spacings of about 14.3 Å (Brindley, 1966). If the same applies to dioctahedral vermiculite- or high-charge smectite-layers in I/S clays, it would be difficult to recognize their presence.

The alkylammonium method is, as mentioned, best suited to investigate the layer-charge development in I/S clays. Other methods, such as conventional cation exchange capacity or chemical formulae established from chemical analyses, may provide the total or averaged layer charge. However, they do not convey information on the distribution of charges. The alkylammonium method has been successfully applied to identify the

charge heterogeneity and to treat the charge distribution in smectite and more or less regularly interstratified I/S minerals (Lagaly and Weiss, 1975; Lagaly, 1979). For I/S mixed-layer clays, problems are more complicated, since component layers contributing X-ray scatter are of varied types. Broadly, there are three components: non-expanding illite, expandable illite that does not expand with ethylene glycol or water but with alkylammonium, and glycol-expandable layers that may show a whole spectrum of layer charges. Currently, computer programs to deal with multi-component mixed-layers of this complexity are not available, but are essential for the study of layer-charge development in I/S clays.

#### SINGLE-PHASE SOLID SOLUTION VS. TWO PHASES

Mixed-layer clays have been conceived as single-phase solid solution of end-member clays forming mixed-layers. However, some doubts exist whether mixed-layer I/S is a phase because of its unpredictable behavior in solution. A phase is defined as part of a system which is chemically and physically uniform throughout. The phase concept is phenomenological, and thus operates on a macroscopic scale, not at the level of the unit cell (Zen, 1962). The identity of I/S distinct from illite or smectite can be established by its X-ray diffraction characteristics and lattice fringe images. The internal structural state of I/S is described by proportions of component layers and sequences with suitable statistical parameters. Confusion arises when I/S clays are dispersed in water. I/S may remain intact or dissociate into component layers (Fig. II-2). Dissociation is expected where the attractive force, either van-der-Waals, electrostatic or both, becomes less than

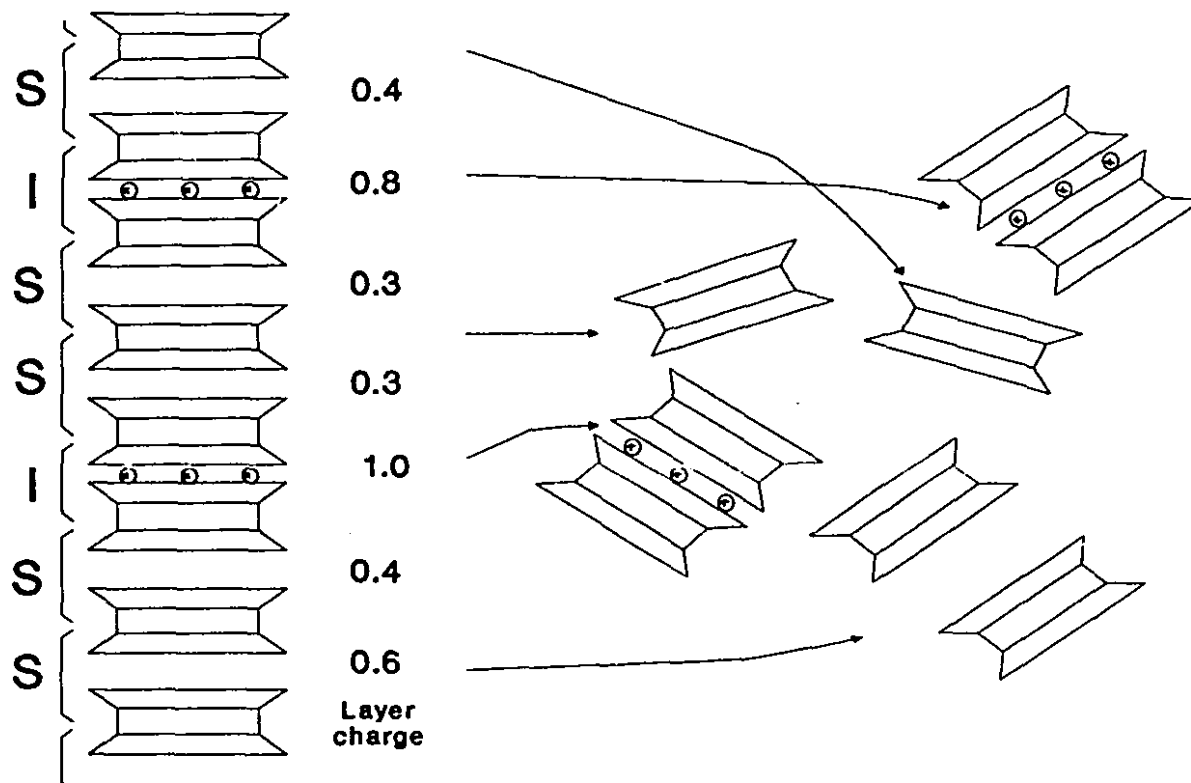
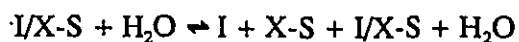


Figure II-2. The colloidal behavior of I/S in solution.

the double-layer repulsive force as discussed in the section on *Markovian crystallites vs. fundamental particles*. The composition of a colloidal solution of I/S in water can be described as:



where X is an exchange cation. Note that the equation is not balanced. In this system, illite, smectite or I/S should be considered as a species. In other words, not all the species in solution are necessarily phases. The relative abundance of species is determined by chemical equilibria among the species. Special care should be taken to define a phase when it is involved in reaction with the environment, i.e. H<sub>2</sub>O. Table II-1 shows species that may be present in a colloidal solution of I/S according to the DLVO theory and literature. I/S with low-charge expandable layers will dissociate across interfaces between expandable layers and may behave like two phases, depending on the proportions of component layers and the degree of order.

For high-charge expandable layers, expansion is limited and complete dissociation will not occur (cf. vermiculite; Norrish and Ransell-Colom, 1963). High-charge layers will collapse in solutions containing cations with low dehydration energy to form illite-like layers. Thus, I/S with high-charge expandable layers will behave as a single phase I/S or I depending on the dehydration characteristics of exchange cations. In the case that both low- and high-charge expandable layers are present in I/S, single- to triple-phase behavior is possible.

Experimental studies of phase equilibria at low temperatures have been carried out to monitor the composition of aqueous solutions that are in equilibrium with solid phases

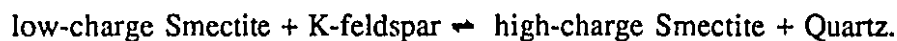
Table II-1. Behavior of I/S with differently charged component-layers in solutions of cations requiring high and low dehydration energy.

Layer charge  I/S type  Dehydration energy	Low Charge		Mixture of Low and High Charge		High Charge	
	random I/S	ordered I/S	random I/S	ordered I/S	random I/S	ordered I/S
High	I, S	I	I, S, I/S	I/S, I	I/S	I/S
Low	I, S	I	I, S	I	I	I

therein. The system  $K_2O-Al_2O_3-SiO_2-H_2O$  is commonly used to depict phase relations involving I/S clays. I/S forms a compositional continuum with illite and smectite end-members in numerous plots of geochemical data (Hower and Mowatt, 1966; Aagaard and Helgeson, 1983; Meunier and Velde, 1989), indicating a solid-solution character. However, I/S clays in solution show multiphase behavior (e.g. Sass et al., 1987; Aja et al., 1991), because they dissociate in a liquid as discussed on the basis of colloid chemistry. I/S clays of fixed composition usually define several univariant lines and invariant points on the phase diagram including kaolinite, muscovite, microcline, Al-hydroxides, illite and smectite. It is interesting to note that data points delineating the univariance between illite and smectite are scarce or close to the invariant point. If I/S clays consist of two or more phases, why is there not a clear-cut alignment of data points on the inferred phase boundary between illite and smectite, as they do with other mineral phases. The various values determined for K in the formula unit of phases (?) from the experiments may simply reflect layer charges that developed preferentially in the material for thermodynamic reasons. In nature, illitic material with a certain layer-charge is predominant, such as smectite (-0.4), vermiculite (-0.6), illite (~0.8), and muscovite or biotite (1). This observation suggests that the layer structures of these charges are relatively stable in free energy terms. Layer charges in-between are found in mixed-layer clays. However, it is possible that mixed-layer clays, in fact, consist mainly of component layers having structures of the above four minerals. The apparent layer-charge of mixed-layer clays may result from the various combination of these component layers.

Water compositions of the natural system (of Stanley and Benson, 1979) used as

evidence for solid solution of I/S by Aagaard and Helgeson (1983) have been reinterpreted in terms of a phase boundary between illite and smectite (Garrels, 1984) (Fig. II-3). However, a line can be better drawn through the data points parallel to the vertical axis of  $\log a_{\text{K}}/a_{\text{H}^+}$ , which could be a silica-saturation line (Fig. II-3c). It is more likely that the line may approximate an assemblage boundary for reactions that are insensitive to potassium concentration such as:



At high aqueous silica concentrations, equilibrium favors the reactants, whereas at low silica concentrations the products are favored.

### TRANSFORMATION VS. NEOFORMATION

Transformation does not involve break-down of the whole structure (e.g.  $\alpha$ -to- $\beta$  quartz transition), whereas neoformation is carried out through complete dissolution of the precursor phase and reprecipitation as a new form. Neither of these reaction mechanisms alone seems to account fully for the illitization process. The illitization reaction displays aspects of both transformation and neoformation. Chemical reactions- layer-charge development and potassium fixation- may not require large-scale bond-breaking of the pre-existing structure, as discussed above in the section of *layer charge vs. potassium*, based on considerations of the activation energy. However, illitization involves structural adjustment of I/S that attained at a certain composition. The structural changes accompanying the S-to-I reaction proceed in several steps:

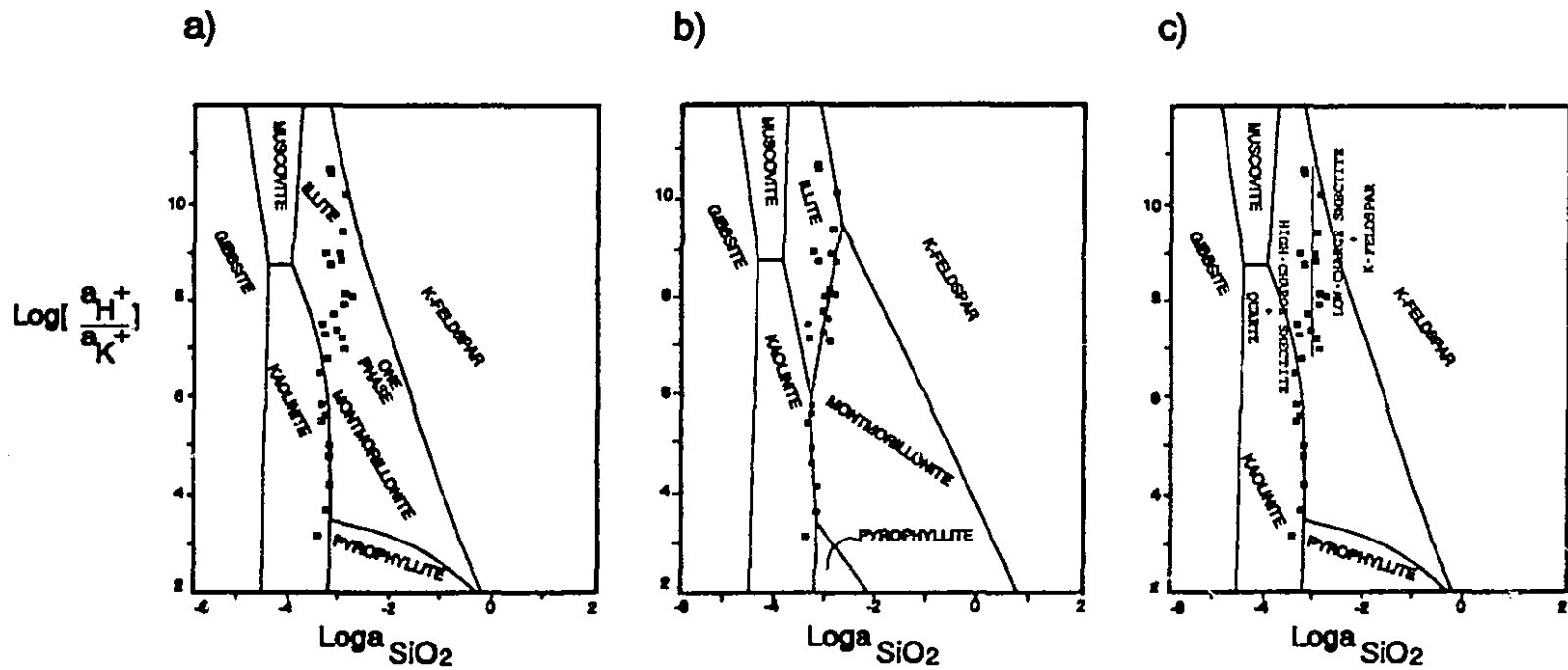


Figure II-3. Phase diagrams based on the composition of relatively shallow ground waters (after Garrels, 1984).  
 a) solid solution model. b) two phase model. c) new interpretation of water composition involving reaction assemblages (A solid solution for I/S is assumed).



mixture will simply be the sum of the free energies of the chemical species present in the mixture, since  $\Delta G_{\text{mix}} = 0$ . For a solid solution, the free energy can be greater than, less than or equal to the free energy of a mechanical mixture in which the relative ratios of components are the same as in a solid solution.

The entropy of mixing,  $\Delta S_{\text{mix}}$ , consists of a statistical term,  $W$ , describing the number of possible different arrangements by the components in the system, and Boltzmann's constant,  $k$  ( $=1.3806 \times 10^{-23} \text{JK}^{-1}$ ),

$$S = k \cdot \ln W.$$

For a two-component system, the number of different arrangements over the  $N$  sites becomes

$$W = N! / (xN)! [(1-x)N]!$$

where  $x$  and  $(1-x)$  represent fractions filled by the components. The logarithm of  $W$  is always positive (because  $W > 1$ ) and so is the entropy. It is also expected that the entropy of an ordered structure is small owing to the fact that the number of ordered arrangements is much smaller than the number of random arrangements.

Returning to the free energy, since temperature on an absolute scale is positive, the entropy term,  $T\Delta S_{\text{mix}}$ , always tends to decrease the free energy. Thus, it is paradoxical that in the diagenesis of I/S clays, with increasing temperature, they tend to assume ordered instead of random arrangements since  $\Delta S_{\text{ordered}} < \Delta S_{\text{random}}$ . To counter an increase of the free energy due to ordering,  $\Delta H_{\text{mix,ordered}} - \Delta H_{\text{mix,random}}$  must be negative. In other words, the ordering reaction must be exothermic. The enthalpy of mixing can be rationalized in terms of the energy of interaction among component units. In I/S clays

there are three pairs, I-I, I-S and S-S, to be considered. Phenomenologically speaking, ordering appears to take place to avoid the S-S association rather than to increase the I-S association. There is a tendency to achieve the maximum separation between S's, as seen in long-range ordered mixed-layer I/S. This probably is related to the surface free energy. The interlayer of the smectite layer is a solid-liquid interface where the surface energy dominates the free energy term. The effective reduction of surface free energy, hence, of the overall free energy is accomplished by the arrangement of layers, as observed in nature, with maximum distance between smectite layers in the stacking sequence of I/S. Even if the reaction is exothermic, it would be sluggish, since the activation energy is expected to be relatively high; i.e. the total activation energy on the order of 20-30 kcal minus 3.5 kcal. The reaction requires transport of material on a macroscopic scale and, therefore, should involve dissolution.

Steps III and IV probably follow the easier reaction path. The chemical reaction, i.e. layer charge development and potassium fixation, is kinetically favored, because it does not require a large activation energy. However, at these stages, the energy barrier for dissolution may not exist due to elevated temperatures. The local development of layer charges within the structure may not be strictly a transformation. The random formation of I-layers in IS(R1) ordered mixed-layers would result in an odd number of I's between S's, i.e. a sequence dominated by SIS and SIIIS. This may explain the rare occurrence of IIS (R2) ordering in a mixture. If neoformation is operating in the composition range of  $35 \pm 5\%$  expandable layers, IIS (R2) ordering will be dominant since it is the configuration for maximum separation of S's. However, it appears that when the random

development of I-layers in R1-ordered I/S reaches a certain point, the free energy may take over to regulate the locations of charge development and I-layer formation to reduce the surface energy. The morphology of elementary particles of long-range ordered I/S and 1Md illite is similar to those of short-range ordered I/S except for thickness (Inoue et al., 1987). The points discussed so far are supported by observations of the behavior of I/S clays upon K-saturation in the Beaufort-Mackenzie Basin (see Fig. III-6). Random mixed-layer I/S does not form ordered I/S by simple introduction of potassium into high-charge expandable layers. R1-ordered I/S becomes R>1 ordered. R>1-ordered I/S shows little change in the degree of ordering, but produces discrete peaks corresponding to illite.

Ostwald ripening is an alternative mechanism introduced to interpret structural changes of I/S (Inoue et al., 1988; Eberl and Srodon, 1988; Eberl et al., 1990). The mechanism may explain lateral growth of I/S clays. However, it is probably not responsible for the increase in layer thickness. Ostwald ripening is a process of crystal growth by which small particles dissolve due to high surface free energy, while large particles grow as matter is transferred from the former to the latter through dissolution and reprecipitation (Baronnet, 1984). In general, clay minerals including I/S appear to be stabilized in terms of size by lateral growth rather than along the C-axis, as evidenced by face development and spacings ( $c^0 > a^0, b^0$ ) [cf. Bravais' law, Periodic bonding theory]. The effect of layer thickness on size would be negligible considering the dimensions of length and width. The statistical thickness distribution of elementary particles (sensu Altaner and Bethke, 1988) of I/S clays can be mistaken as a profile characteristic of Ostwald ripening, since processes causing the change from short-range through long-range ordering of I/S to I resemble crystal growth by coalescence.

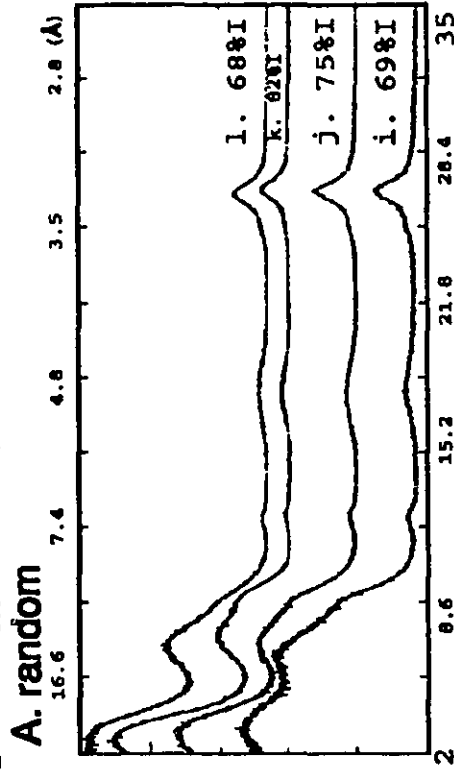
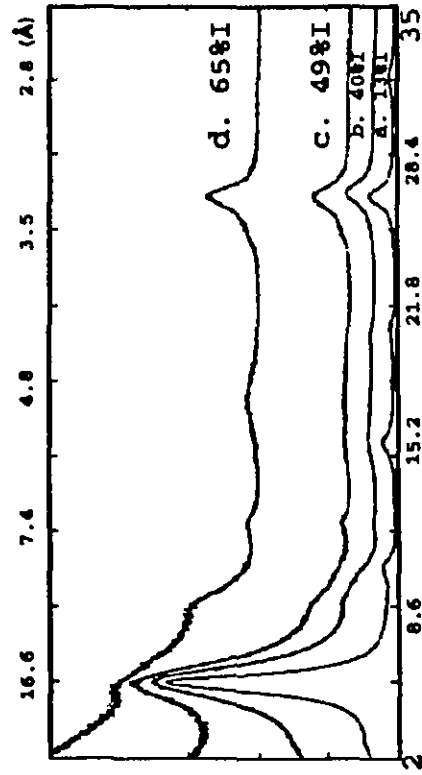
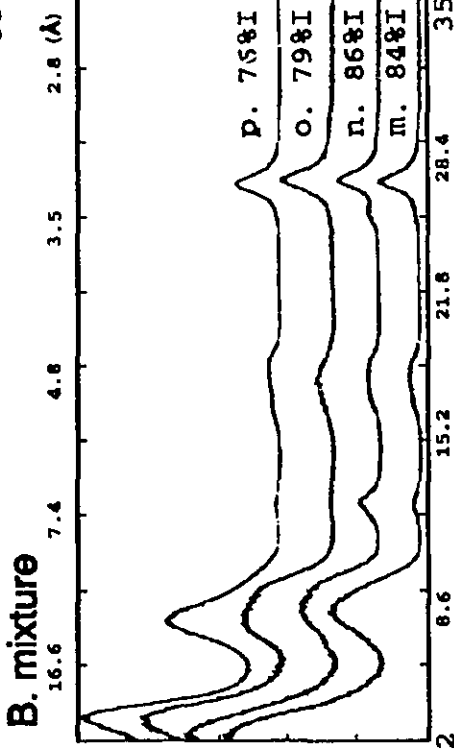
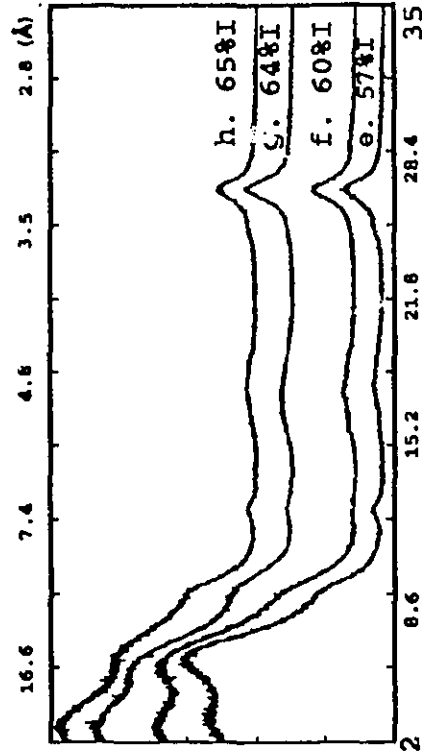
## CHAPTER III. I/S MINERALOGY

The degree of illitization is measured by expandability, i.e., the proportion of the expandable component in I/S, which is often depth- and thus temperature-dependent. Its possible use as a thermal indicator has attracted the attention of the petroleum industry. However, applications have never exploited the full potential due to the fact that too many factors are involved in compositional variations of I/S, including formation water chemistry, porosity and permeability of strata, nature of the starting material, kinetics, etc. A more serious problem is the precision in estimating I/S composition. The complicated nature of X-ray diffraction patterns of I/S and the omnipresence of discrete illite lead to errors on the order of 20 %. This chapter describes the mineralogy of I/S mixed-layer clays from the Beaufort-Mackenzie Basin and provides a new method which can be used in estimating the I-content, especially for I/S with poorly-defined peak positions and weak intensities.

### X-RAY DIFFRACTION CHARACTERISTICS OF $<1 \mu$ FRACTIONS

Figure III-1 shows typical X-ray diffraction patterns of Beaufort-Mackenzie samples. The  $7 \text{ \AA}$  peak and its  $\{00l\}$  series correspond to kaolinite except for some deep samples of Reindeer D-27 which contain chlorite (Fig. III-2). Variable amounts of discrete illite are always present, interfering with I/S reflections. Peaks of illite that are often broad due to fine particle-size occur as a shoulder or asymmetry on the high-angle side of low-angle reflections of I/S (001) and a small hump at  $5 \text{ \AA}$  (002). The (003) peak of illite is not separable from the  $(003)_{10}/(005)_{17}$  peak of I/S (subscripts denote the basal spacings).

**Figure III-1.** X-ray diffraction patterns of typical Beaufort-Mackenzie clays (<1  $\mu$  fraction). Glycolated. A. Random I/S. B. Mixture of random and ordered I/S. C. R1-ordered I/S. D. R>1-ordered I/S. (a - Taglu C-42 8468, b - Ivik J-26 10213, c - Taglu G-33 8279, d - Taglu G-33 5376, e - Reindeer D-27 6850-6800, f - Mallik A-06 9266, g - Taglu C-32 10430, h - Reindeer D-27 8250-8200, i - Reindeer D-27 8650-8600, j - Reindeer D-27 9250-9200, k - Reindeer D-27 9650-9600, l - Taglu C-42 13800-13700, m - Reindeer D-27 11443, n - Reindeer D-27 12650-12600, o - Taglu C-42 15800-15700 ft, p - Amerk O-09 4866 m). For Description, see text.



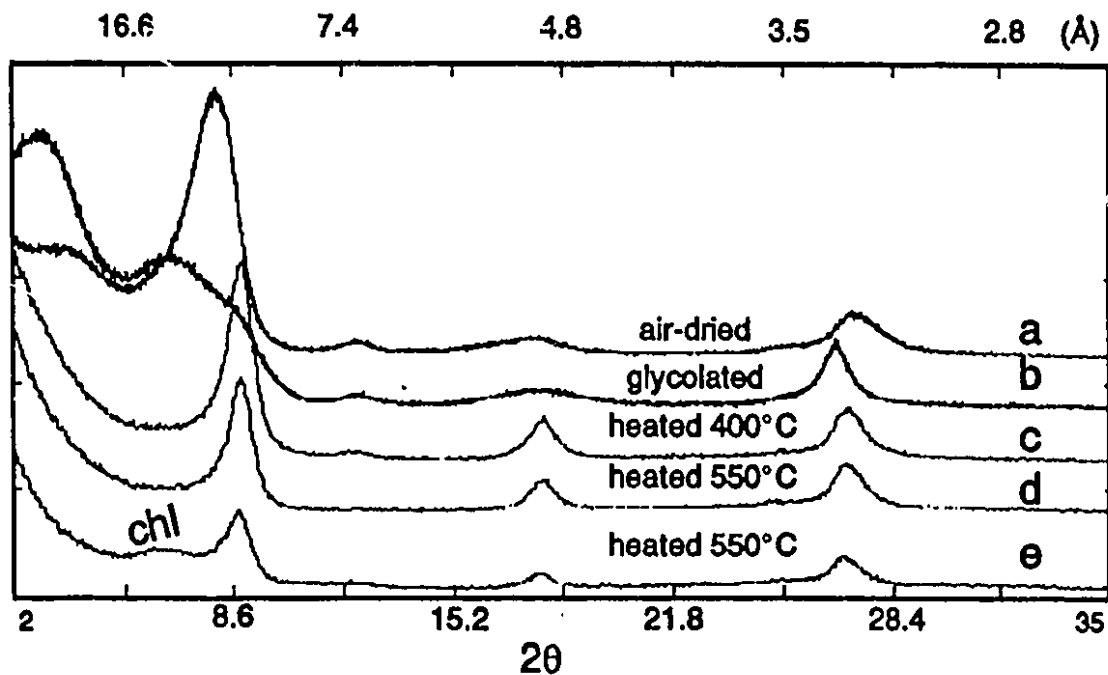


Figure III-2. X-ray diffraction patterns of (a) air-dried, (b) glycolated, (c) heated at 400°C and (d,e) 550°C specimens.  $<.1 \mu$  fractions (a-d: Reindeer D-27 9200-9250, e: 11100-11150 ft). Collapse to 10 Å after heating indicates that mixed-layers consist of 2:1 layer-silicates, i.e. illite and smectite. 7 Å-series reflections disappear after heating at 550°C (d), indicating they correspond to kaolinite. Chlorite in Reindeer deep sample (e) persists after heating at 550°C.

I/S clays are characterized by broad reflections. The full width at half-maximum intensity (f.w.h.m.) for low-angle reflections ranges from 1 to 2 °2θ for less evolved I/S with low I-content (e.g. Fig. III-1a, b). A close approximation of the f.w.h.m. can be obtained for particle thicknesses varying between 2 to about 8 layers, using the computer program Newmod2 of Reynolds (1985). However, with increasing I-content, peaks between 17 and 10 Å become so broad that the f.w.h.m. can not be simulated with the Newmod2 program.

### **I/S Mineralogy**

X-ray patterns of Beaufort-Mackenzie I/S can be grouped into 4 categories: random, a mixture of random and ordered, R1-ordered, and R>1-ordered I/S. **Random mixed-layer I/S** is characterized by the peak appearing at about 5.2 °2θ [(001)<sub>10</sub>/(001)<sub>17</sub>]. With increasing proportions of I-layers, saddle/peak ratios of the (001)<sub>10</sub>/(001)<sub>17</sub> peak decrease (c.f. Rettke, 1981; Inoue et al., 1989). With increasing degree of illitization, the intensity of higher-order peaks decreases. At about 40 %I, the precise position of higher-order peaks, especially (002)<sub>10</sub>/(003)<sub>17</sub>, cannot be determined. With increasing I-layer content in I/S, the intensity of discrete illite peaks also increases as shown by increasing shoulder heights on the first order peak [(001)<sub>10</sub>/(001)<sub>17</sub>] of I/S at about 10 Å (Fig. III-1A).

A mixture of random and ordered I/S is identified by two peaks, one at very low angles (<4.2°2θ), indicative of a superlattice structure, and the other between 17 to 15 Å (Fig. III-1B). The second peak for ordered I/S usually occurs at less than 14.5 Å (Bethke et al., 1986). Previously, a mixture of random and ordered I/S has been identified in

hydrothermal experiments (Whitney and Northrop, 1988). Contamination by drilling mud is highly unlikely, because samples were well consolidated. Note that two of the diffractograms shown in Figure III-1B (f and g) were obtained from core material. This mixture of random and ordered I/S was identified in about 30 core and drill-cutting samples. The relative abundance of ordered I/S in the mixture increased with depth (see Chapter IV). Intensities of the  $(001)_{27}$  peak increase while those of  $(001)_{10}/(001)_{17}$  decrease (Fig. III-1B). Compositions of random I/S in the mixture range from about 55 to 65 %I based on saddle/peak ratios of the  $(001)_{10}/(001)_{17}$  peak. Compositions of ordered I/S are probably similar to those of coexisting random I/S, though they were difficult to estimate due to the weak intensity of peaks at about  $16^\circ 2\theta$  [ $(002)_{10}/(003)_{17}$ ] and the presence of discrete illite.

**R1-ordered I/S** shows two distinct peaks at low angles,  $(001)_{27}$  and  $(001)_{10}/(002)_{27}$  (Fig. III-1C). R1-ordering is defined by peak positions of  $(001)_{10}/(002)_{27}$  that vary from 14.5 to 12.8 Å (Hower, 1981; Bethke et al., 1986). In general, with increasing proportions of I-layers,  $(001)_{27}$  shifts towards lower angles while  $(001)_{10}/(002)_{27}$  shifts towards higher angles. Positions of other peaks,  $(002)_{10}/(005)_{27}$  and  $(003)_{10}/(008)_{27}$ , were usually not measurable, either due to weak intensities or proximity to discrete illite peaks. Resolution, even with the profile-fitting program FIT, was rarely possible. Deconvolution of peaks in the 5 Å region (cf. Eberl et al., 1987) did not provide reliable results to estimate composition. Deconvolution results appear inconsistent among samples with similar XRD patterns, and thus of similar composition. In many cases, the results did not bear any physical meaning, i.e. intensity, peak positions and the f.w.h.m. do not reflect

the nature and relative abundance of phases present. Air-dried samples displayed better-defined and resolvable peaks. Compositions of R1-ordered I/S based on peaks of air-dried samples range from 65 to 80 %I. I/S of 65-70 %I is characterized by a relatively high saddle at about 17 Å (Fig. III-1i), probably due to the imperfection of ordering, i.e. the presence of smectite-to-smectite junctions (S.S). The difference between the  $2\theta$  angles (differential  $2\theta$ ) between  $(001)_{27}$  and  $(001)_{10}/(002)_{27}$  is usually less than 3.5°. I/S of about 75 %I shows well-defined peaks of  $(001)_{27}$  and  $(001)_{10}/(002)_{27}$  (Fig. III-1j), and the differential  $2\theta$  between the two peaks ranges from 3.5 to 4.0°. Position of the  $(001)_{27}$  peak varies between 29 and 34 Å, while that of the  $(001)_{10}/(002)_{27}$  peak between 14 and 13 Å. As the I-layer content of I/S approaches 80 %I, the  $(001)_{27}$  peak disappears. Nevertheless, the convexity of X-ray traces near  $2^\circ 2\theta$  indicates the presence of a superlattice structure of increased spacing (e.g. R3).

**R>1-ordered I/S** usually shows a single peak at d-values  $<12.8$  Å (Fig. III-1D). Peak positions suggest Reichweite values greater than 1, but less than 3. Most R>1-ordered I/S is found in deep samples (see Chapter IV). Compositions based on peaks of I/S-1 water (denoting a single interlayer-water) cluster at 84-88 %I. Some samples show values as high as 92 %I. This estimate is, however, at best, a guess owing to the high concentration of chlorite in these samples. Chlorite seems to weaken the overall intensity of I/S peaks and, thus, lower the efficiency of deconvolution in the 3.3 Å region.

### Estimation of I/S Composition

Conventional methods to estimate the composition of I/S use peak positions or differential

2 $\theta$  values on glycolated samples (Reynolds and Hower, 1970; Reynolds, 1980; Srodon, 1980, 1984; Watanabe, 1981). These methods, however, were not applicable for most Beaufort-Mackenzie samples due to the weak intensity of the important peaks, especially (002)<sub>v</sub>/(003)<sub>s</sub>.

For random I/S and most of the samples with a mixture of random and ordered I/S, saddle/peak ratios of the (001)<sub>10</sub>/(001)<sub>17</sub> peak were used to estimate composition. A working curve similar to Inoue et al. (1989; modified after Rettke, 1981) was constructed based on patterns generated by the Newmod2 program. In calculating the patterns, default parameters given by the program were used because many parameters can not be determined with certainty. Compositions obtained by conventional methods generally agree with those estimated from saddle/peak ratios. An error range of 10-15 % was estimated for the method according to Inoue et al. (1989).

For ordered I/S, the addition of another variable, i.e. the degree of ordering, complicates the relationship between composition and peak parameters, i.e. peak position, intensity, f.w.h.m., differential 2 $\theta$  values and saddle/peak ratios. For Beaufort-Mackenzie samples, three well-defined peaks were always detected, regardless of interference by discrete illite peaks. These include the peak between 17 and 10 Å on glycolated samples, and the peaks at 12.5-10 Å and at 3.3-3.1 Å on air-dried samples. The peak between 17 and 10 Å on glycolated samples was used to define the degree of ordering in terms of Reichweite value (Bethke et al., 1986). Peaks on air-dried samples, especially the higher-order peak between 3.3 and 3.1 Å, show depth-related variations (Fig. III-3). Parameters of the peak, i.e. position and the f.w.h.m., change systematically with depth. Peak

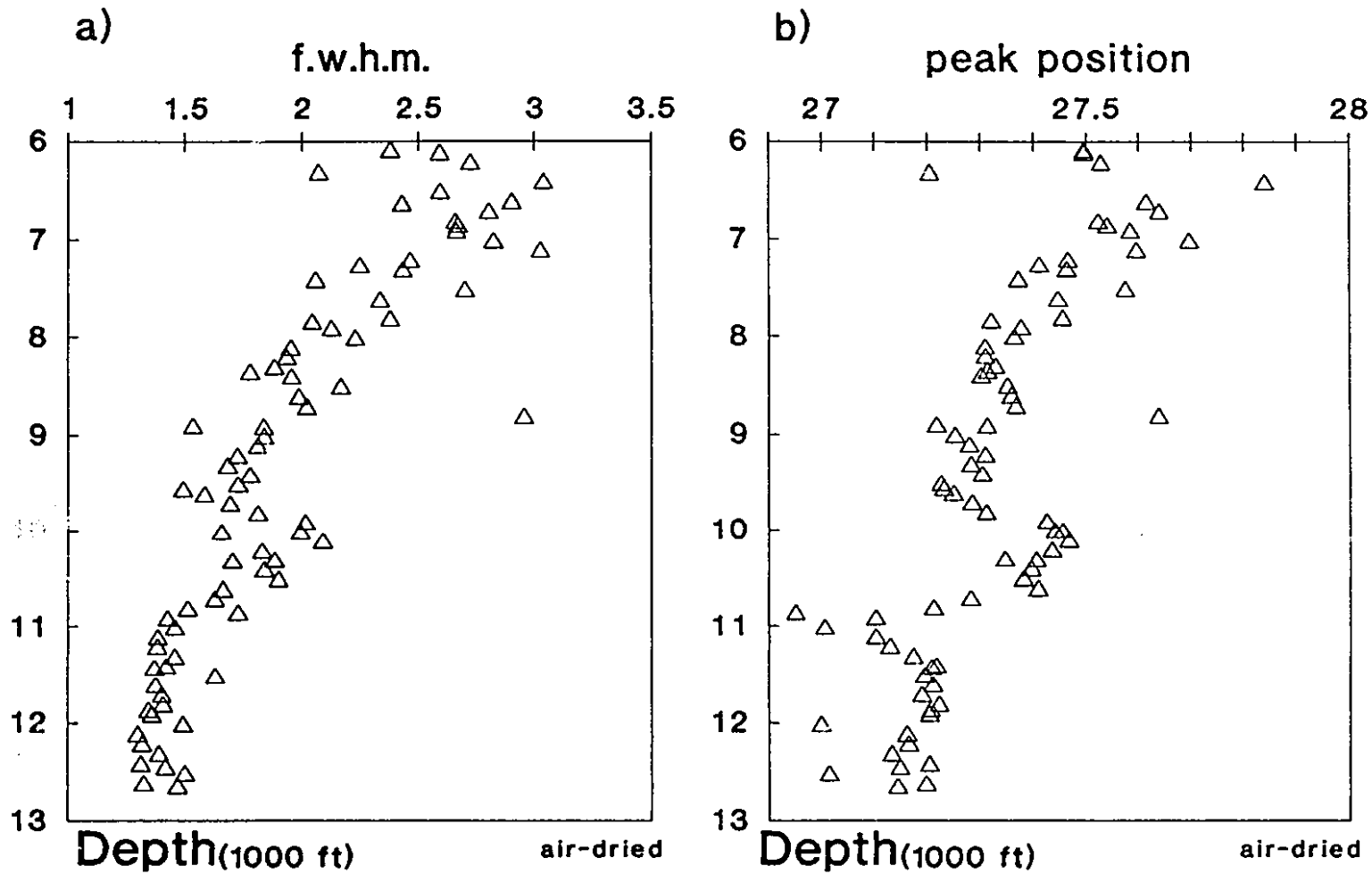


Figure III-3. Plot of  $003/004_s$  peak parameters with respect to depth. Air-dried. Reindeer D-27.  
 a) f.w.h.m. b) peak position (both in  $2\theta$ ). For data, see Appendix I.

positions move towards  $26.8^\circ 2\theta$  ( $3.3 \text{ \AA}$ ) and the f.w.h.m. decreases with increasing depths of burial. The f.w.h.m. ranges from  $>2$  for random, 2-1.5 for R1-ordered, and  $<1.5$  for  $R>1$ -ordered I/S. The peak position suggests a single-layer state of interlayer-water for most expandable layers in I/S. In estimating the composition of ordered I/S, peaks in the  $3.3 \text{ \AA}$  region were deconvoluted based on a three-peak model for patterns with f.w.h.m. $>1.5$ , or a two-peak model for f.w.h.m. $<1.5$  (Fig. III-4; see also Appendix I). The peak at  $3.5 \text{ \AA}$  corresponds to kaolinite and/or chlorite, that at  $3.3 \text{ \AA}$  to illite, and that at  $<3.3 \text{ \AA}$  to I/S. At a f.w.h.m. of  $<1.5$ , intensities of the deconvoluted peak using a three peak model are inconsistent with the relative abundance of phases present. This is due to the proximity of peak positions of illite and I/S.

Compositions of R1-ordered I/S based on the  $(003)_{10}/(007)_{22.5}$  peak of I/S-1 water range from 65 to 80 %I. Although compositions generally fall within the known range for R1-ordered I/S, the estimates appear to be higher than those expected from glycolated samples based on low-angle peaks. Compositions estimated on glycolated samples with a better-defined  $(002)_{10}/(005)_{27}$  peak are usually lower by about 5 %I than those obtained from air-dried samples.

The composition of  $R>1$ -ordered I/S was also estimated by deconvoluting peaks in the  $3.3 \text{ \AA}$  region on air-dried samples. A two-peak model was used because a relatively small f.w.h.m. does not permit resolution of peaks belonging to illite and I/S with high I-layer content. Patterns of glycolated  $R>1$ -ordered I/S show little differences between samples, especially for deep samples from Reindeer D-27. For most Beaufort-Mackenzie samples, compositions fall in the narrow range between 84 and 88 %I. Compositions obtained

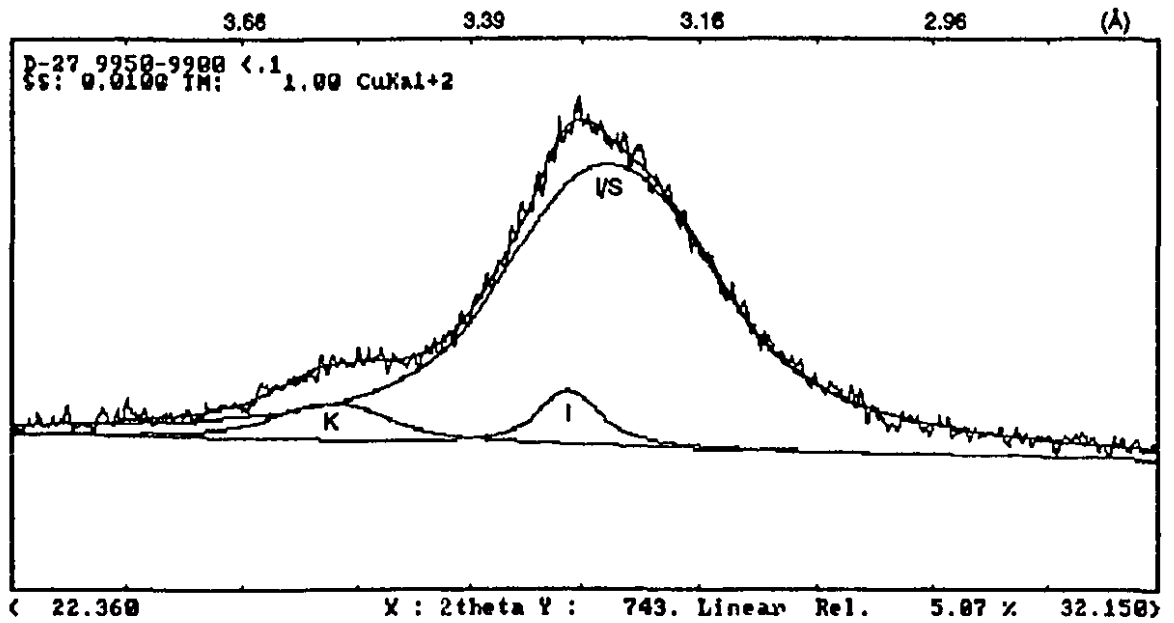


Figure III-4. Deconvolution of a X-ray diffraction curve in the 3.3 Å region. Air-dried. A smooth curve on the diffraction pattern is the sum of three curves corresponding to I/S, kaolinite (K) and illite (I). Pseudo-Voigt function is used.

from glycolated samples with better-defined peaks in the 5 Å region, though deconvolution results were less consistent, seem to agree with compositions estimated from peaks of I/S-1 water.

## DISCUSSION

### Peak Broadness and Intensity

The abnormal broadness and weak intensities of I/S peaks are attributed to turbostratic effects and {001} stacking defects (Reynolds, 1989) and, most likely, to varying thicknesses of glycol layers. Srodon (1980) showed that the thickness of smectite-glycol complexes can vary from 16.5 to 17.3 Å. The same thickness variation may be characteristic of smectite-layers in I/S. The effect of varying glycol-layer thickness within a sequence of individual particles is probably similar to that of strain-broadening (Warren and Averbach, 1950). In strain-broadening, displacement of the lattice (lattice strain) may be infinitesimal; however, the effect can be very profound on diffraction patterns (Reynolds, 1989). Figure III-5 shows the results of strain broadening for 10 Å structures with a mean displacement of adjacent unit-cells from 0 to 2 Å. Broadening increases and intensity decreases with increasing 2θ angles. Eventually, at a large displacement (e.g. 2 Å), all high-angle peaks disappear and only a first-order peak that represents the unit-cell itself may be seen. Differences in glycol-layer thickness are analogous to the displacement of adjacent unit cells in strain broadening. The glycol-layer thickness depends on layer charges and types of interlayer cations. For instance, vermiculite forms double-layer complexes with ethylene glycol and gives spacings of 16.2 Å (Brindley,

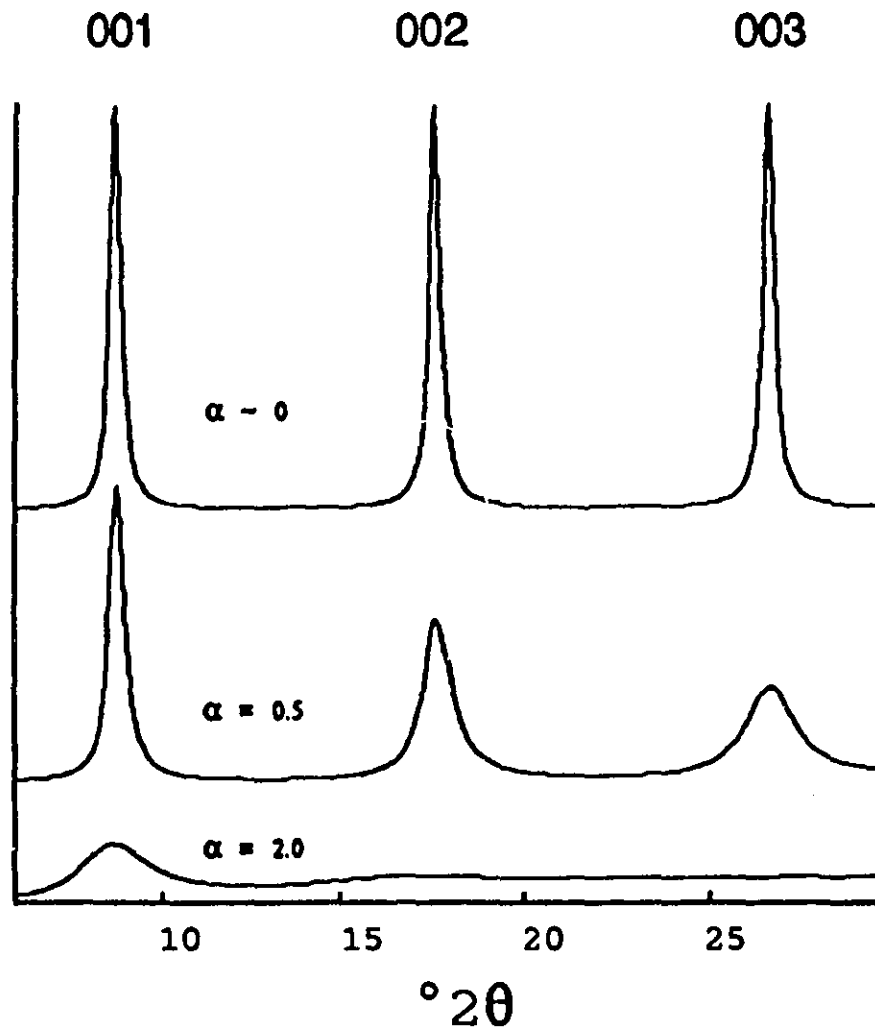


Figure III-5. Effects of strain broadening for a 10 Å structure (after Reynolds, 1989).  $\alpha$  - mean displacement between adjacent layers in Å.

1966). In mixed-layer I/S, expandable layers display a wide range of layer charges (Lagaly, 1979; Howard, 1981; Vali et al., 1991). Although most expandable layers are expected to form double glycol-layers, spacings may vary from 16.2 to  $>17 \text{ \AA}$  depending on layer charge.

### Abnormal Glycol Behavior

In the Beaufort-Mackenzie Basin, some high-charge expandable layers appear to form single-layer complexes with glycol. The overall XRD patterns of I/S can be reasonably assessed on the basis of a two-component mixed-layer model,  $10 \text{ \AA}$  and  $17 \text{ \AA}$ ; however, the presence of the third component, i.e. a single-layer complex ( $14 \text{ \AA}$ ), is identified in the  $2\theta$  region where positions of the  $14 \text{ \AA}$ -series lie between those of the  $17 \text{ \AA}$ - and  $10 \text{ \AA}$ -series [e.g.  $(001)_{14}$ ,  $(003)_{14}$ ]. The peak between  $17$  and  $10 \text{ \AA}$  is broader than that which can be obtained with Newmod2 based on a two-component model. The peak in the  $5 \text{ \AA}$  region does not show an appreciable effect of glycolation between  $5.7 \text{ \AA}$  [ $(003)_{17}$ ] and  $5 \text{ \AA}$  [ $(002)_{10}$ ]. Normally, the glycolation effect on I/S is more pronounced on the lower-angle side of  $5 \text{ \AA}$  than on the higher-angle side because of the proximity of the third order peak  $(003)$  of  $17 \text{ \AA}$  to the second order peak  $(002)$  of  $10 \text{ \AA}$  compared to  $(004)$  of  $17 \text{ \AA}$ . However, for most Beaufort-Mackenzie samples, the glycol effect is reversed. This abnormal behavior is attributed to the effects of the  $14 \text{ \AA}$ -component. For K-saturated samples, the glycol effect appears normal, i.e. a stronger  $(002)_{10}/(003)_{17}$  and a weaker  $(002)_{10}/(004)_{17}$  peak (see Fig. III-6). The  $14 \text{ \AA}$ -component collapsed to form illite-like layers upon K-saturation and, thus, no longer existed. In general, K-saturated samples

showed better-defined reflections at the low-angle side of 5 Å.

### Discrete Illite or Elementary Illite Particle

Most discrete illite is probably an artifact of dispersion (discussion based on geochemistry, see Chapter V). I/S crystallites are expected to dissociate into thin illite- and smectite-particles in a liquid according to the DLVO theory (for detailed discussion, see Chapter II). Some illite particles may not associate back into I/S upon drying. Therefore, dissociation of I/S would increase the illite population, and thus contribute to the intensity of discrete illite peaks. As shown in Fig. III-1A, the shoulder heights on the first order peak of random I/S at about 10 Å increase, as the intensity of (001)<sub>17</sub> decreases. The increased intensity of the illite peaks is not due to newly-formed illite that may precipitate with increasing degree of diagenesis. Rather, the increase is due to the increased number of potential illite-particles in I/S, as I-contents increase. No systematic change in intensities of the illite peak was observed in the composition range of ordered I/S. In general, the intensity of the illite peaks is similar to or even less than the intensity of those associated with random I/S. If illite was diagenetically formed, a more intense 10 Å peak is expected in samples containing ordered I/S. As mentioned earlier, however, this is not the case.

The next question is, if illite has an elementary particle origin (sensu Altaner and Bethke, 1988), why is there less illite in some samples containing ordered I/S than in those with random I/S. Ordered I/S contains more potential illite-particles owing to its higher I-content. This could be due to a greater proportion of high-charge layers that may

have developed in expandable layers of ordered I/S than in random I/S. In general, I/S crystallites dissociate into elementary particles at cleaves of low-charge layers. High layer-charge would prevent dissociation.

### **Mixture of Random and Ordered I/S**

A mixture of random and ordered I/S has rarely been identified in diagenetic studies. In fact, the mixture should not exist according to Nadeau et al. (1984a) who showed that the physical mixture of smectite and R1-ordered I/S (rectorite) would produce X-ray diffraction patterns corresponding to random I/S. The mixture of random and ordered I/S is widespread in the Beaufort-Mackenzie Basin. In Reindeer D-27, it is identified in a transitional interval, about 500 m thick, between random and R1-ordered I/S (see Chapter IV). The existence of a mixture of random and ordered I/S suggests that the reaction for the transition from random to ordered structures, i.e. ordering, is not instantaneous. The mixture probably represents a metastable state in the ordering reaction. In slow reactions (for rationale, see Chapter II), metastable co-existence of reactants and products is not unusual.

### **Implications of X-Ray Diffraction Patterns of K-Saturated Samples**

K-saturation experiments indicate that expandable layers in I/S consist of low- and high-charge smectite-layers. Expandable layers with high charge collapse to form illite-like layers upon K-saturation. With sodium as an interlayer cation, these layers formed 1- or 2-layer glycol-complexes depending on layer charge (see discussion above).

Upon K-saturation, the intensity of the  $(001)_{17}$  peak of random I/S decreases compared to Na-saturated samples, suggesting that the proportion of I-layers increased (Fig. III-6B a). A mixture of random and ordered I/S, upon K-saturation, lost the peaks representing random I/S (Fig. III-6B b). Random I/S in the mixture may have already acquired an ordered layer-structure, i.e. a structure of alternating expandable layers with high- and low-charge.

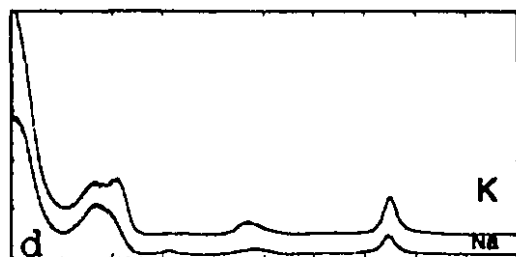
For ordered I/S, K-saturation alters the composition as well as the degree of ordering. R1-ordered I/S showed a gain of about 5-10 %I (see Chapter IV). In addition, some I/S particles appeared to have transformed into illite. In general, peaks representing illite, especially  $(001)$ , are more prominent than those in Na-saturated samples. The response of the  $(001)_{10}/(002)_{27}$  peak that defines the nature of ordering is more complicated. In most cases, it moves towards higher angles (Fig. III-6A a,b), suggesting that the degree of ordering is improved. In some cases, the peak is broader and has an almost flat top (Fig. III-6B c), indicating that K-saturated samples consist of I/S mixed-layers displaying various degrees of ordering from R1 to R3.

R>1-ordered I/S of Reindeer D-27 shows little change in XRD patterns upon K-saturation except for producing more prominent peaks corresponding to illite (Fig. III-6A c,d). On the other hand, K-saturated R>1-ordered I/S of Taglu C-42 displays a pattern similar to R1-ordered I/S (Fig. III-6B d). The  $(001)_{10}/(002)_{27}$  peak and the equivalent peak of R>1-ordered I/S shift towards lower angles. Unlike Reindeer samples, K-saturation altered the nature of ordering in Taglu C-42.

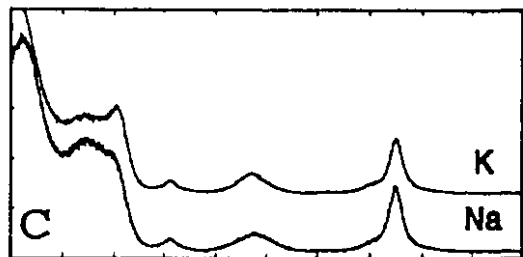
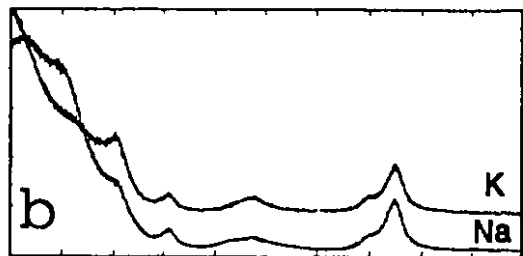
Upon simple K-saturation, the proportion of I-layers in random I/S increased, while

Figure III-6. X-ray diffraction patterns showing the effect of K-saturation for various types of I/S. A) Reindeer D-27 [a - 8375, b - 10329, c - 11443, d - 12462 ft]. B) Taglu C-42 [a - 9738, b - 11508, c - 13000-12950, d - 16030-16000 ft]. For explanation, see text.

**A)** 16.8 7.4 4.8 3.5 2.8 (Å)



**B)** 16.8 7.4 4.8 3.5 2.8 (Å)



higher-order I/S as well as illite developed from R1-ordered I/S, by transforming high-charge expandable-layers into I-layers. This suggests that the illitization reaction can be transformational for random or ordered I/S. Random I/S in the composition range of < ~60 %I may share a common structure, whereas long-range ordered I/S and probably also illite may develop from the R1-structure acquired as a result of ordering.

The development of I-layers in crystallites of R1-ordered I/S would result in odd numbers of I's between smectite-layers (see also Chapter II). Reichweite values greater than 1, but less than 3 for R>1-ordered I/S determined from X-ray diffraction patterns, are probably due to mixed stacking of R1- and R3-structures in the crystallite.

## CHAPTER IV. BASINAL TRENDS

The mineralogy of I/S mixed-layer clays from the Beaufort-Mackenzie Basin has been dealt with in Chapter III. Four different types of I/S were characterized on the basis of X-ray diffraction patterns of air-dried, glycolated, K-saturated and heat-treated  $<1 \mu$  fractions. These include random, a mixture of random and ordered I/S, R1-ordered, and R>1-ordered varieties. A method which can be used in estimating the I-content, especially for I/S with poorly-defined peak positions and weak intensities, has been devised.

K-saturation experiments provided insight into reaction mechanisms of illitization and layer-charge development in I/S. High-charge expandable layers in I/S crystallites collapse to form illite-like layers, i.e. high-charge layers transform to illite-like layers upon simple K-saturation. This implies that an increase in I-contents, regardless of whether it is random or ordered I/S, may involve transformation. Neof ormation probably operates while ordering of random I/S takes place.

In this chapter, the basinal trends of I/S diagenesis in the Beaufort-Mackenzie Basin are discussed, based on variations in composition and ordering, and their relationship to other geologic variables such as temperature, fluid pressure, lithology, stratigraphy, hydrocarbon occurrence and depositional environments.

### RESULTS AND INTERPRETATIONS

**B.A.-Shell-IOE Reindeer D-27 (lat.  $69^{\circ}06'05''$ N, Long.  $134^{\circ}36'54''$ W)**

Reindeer D-27 was the first exploratory well in the Beaufort-Mackenzie Basin (spudded

in 1965). It penetrated a total depth of 12668 ft (3861.2 m). Coring was carried out in intervals of about 600 ft, so that each interval represents about 5 % of the total drill depth. A bottom-hole temperature of 78.9°C was reported. Although the well was classed as dry and abandoned, an overflow of gassy mud to the surface was reported at 6856 to 6858 ft (2089.7-2090.3 m). Discovery was made at Reindeer F-36 located about 2 km south of Reindeer D-27. The well comprises Lower Cretaceous (Albian) shale and Tertiary deltaic successions that include the Fish River, Reindeer, Richards, Kugmallit and Iperk sequences (Fig. IV-1). The Fish River Sequence consists mainly of prodeltaic shales. The Reindeer Sequence contains relatively homogeneous prodeltaic shale and overlying delta front/delta plain sandy sediment, the facies boundary of which is placed at about 6200 ft (1890 m). The younger sequences (Kugmallit and Iperk) were not studied for the lack of samples.

Reindeer D-27 was selected as one of the major target wells to identify the burial trend of I/S in the Beaufort-Mackenzie Basin. A total of 84 samples (18 core samples, 66 drill cuttings) were studied. Reindeer D-27 has long cores covering a wide range of depths between 2907 and 12463 ft (886-3799 m). Well-consolidated drill cuttings were available from the relatively shallow depth of 6100 ft (1859 m) downwards. Mudrocks are the predominant lithology of the studied interval.

The mineralogy of the  $<1 \mu$  fraction is relatively simple. Besides mixed-layer I/S, discrete illite and kaolinite are always present (see Fig. III-1). Chlorite appears starting at 10800 ft (3292 m) depth (Appendix I), which corresponds to the stratigraphic top of the Albian. Although in drill-cutting samples chlorite persisted to the bottom of the hole,

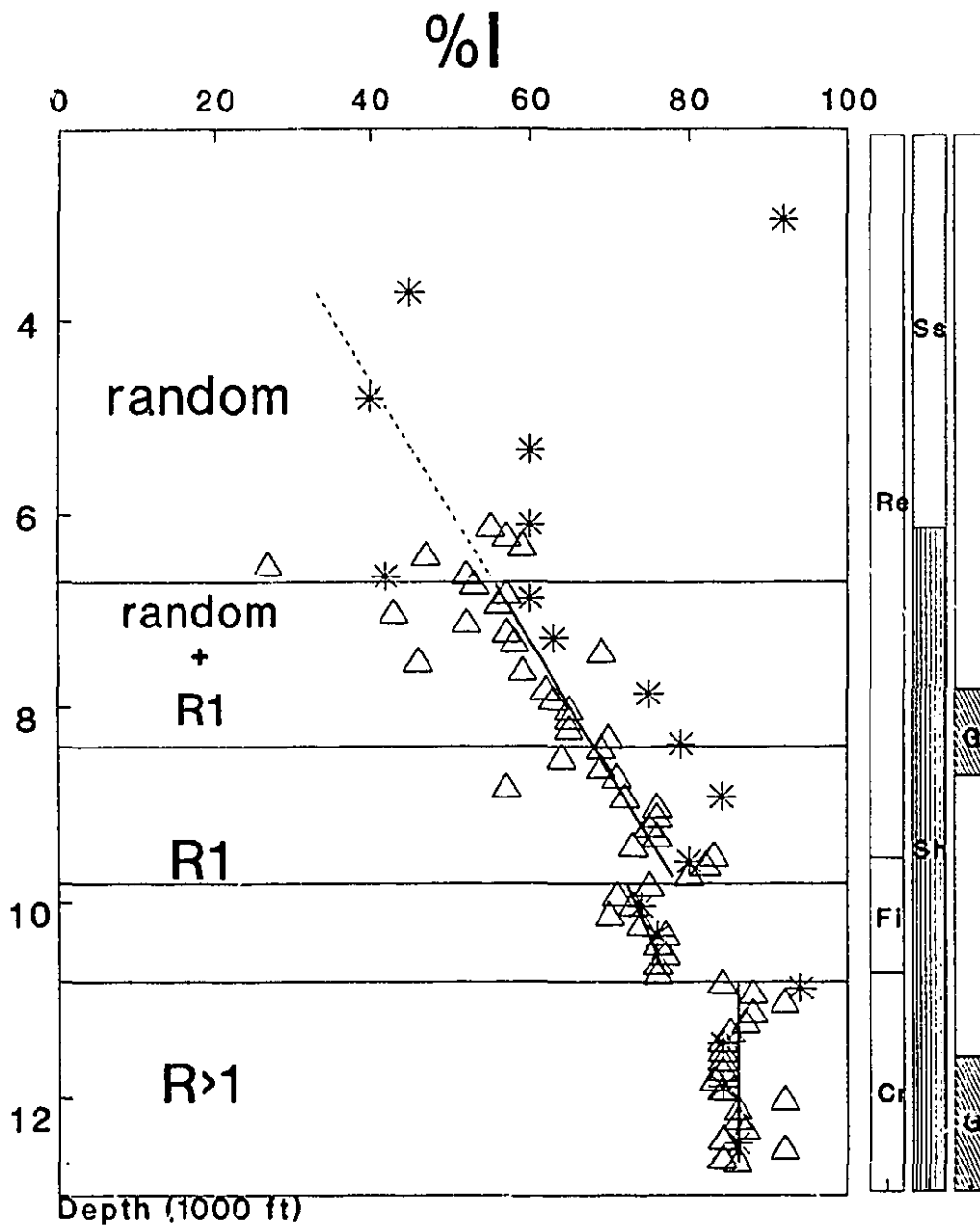


Figure IV-1. Plot of I-content (%I) in I/S with respect to depth, stratigraphy, lithology and geopressure for Reindeer D-27. \* - core, Δ - drill-cutting. Cr - Cretaceous, Fi - Fish River, Re - Reindeer. Sh - shale, Ss - sandstone. G - Geopressed.

the absence in core samples below 11443 ft (3488 m) suggests that chlorite is, in fact, restricted, at most, to an interval about 600 ft thick (10800-11443 ft). The presence of chlorite in deeper drill-cutting samples is due to the effect of cavings. Whether chlorite is of detrital or diagenetic origin is an interesting question which, however, was not pursued. It was noted that chlorite is an Fe-rich, di,tri-octahedral variety (see Appendix V; sample 10975).

### *I/S diagenesis*

I/S in Reindeer D-27 shows, as mentioned in Chapter III, a whole spectrum of X-ray diffraction patterns from random to R>1-ordered. Compositions range from 27 to 92 %I (Fig. IV-1). Random I/S, for which compositions vary from 27 to 60 %I, predominates at shallow depths above 6700 ft (2042 m). Between 6700 and 8350 ft (2042-2545 m), a mixture of random and R1-ordered I/S occurs, for which the relative abundance of ordered I/S increases with depth (see Fig. III-1B). Compositions of the mixture range from 52 to 70 %I. R1-ordered I/S is dominant in the interval between 8350 and 10750 ft (2545-3277 m), and contains between 69 and 80 %I. Below 10800 ft (3292 m), only R>1-ordered I/S with >80 %I is present.

Proportions of I-layers in I/S increase gradually with the depth (Fig. IV-1). The systematic trend displayed by more than 80 data points supports the validity of the methods used in estimating composition (see Chapter III). It is of interest to note that, though core samples follow the general trend, they contain I/S with higher percentages of I-layers than drill-cutting samples from similar depths. In drill-cutting samples, the I-

content of I/S was lowered due to cavings of diagenetically less evolved I/S from shallower depths.

In the interval of random I/S above 6700 ft (2042 m), no systematic trend was observed. However, there are indications which suggest that the illitization process has started. Collapse of expandable layers upon K-saturation is considerable in all samples except for that from 3700 ft (1128 m), i.e. some expandable layers in I/S have developed high enough layer-charge to form illite-like layers when  $K^+$  becomes available. The apparent lack of a trend in the interval of random I/S in Reindeer D-27 contrasts with other basins and some other wells in the Beaufort-Mackenzie Basin where the burial trend encompasses random I/S, like in the Gulf Coast, or is based solely on random I/S (e.g. in the Jeanne-d'Arc Basin on the Grand Banks offshore Newfoundland; Abid, 1991, personal communication).

The depth range between 6700 and 9800 ft (2042-2987 m) is characterized by linearly increasing I-contents with depth (1.15 %I/100 ft), and consists of the intervals representing a mixture of random and ordered I/S, and R1-ordered I/S.

A conspicuous discontinuity occurs between 9800 and 10800 ft (2987-3292 m), in an otherwise relatively simple trend. It was recognized in depth-plots of the various parameters obtained from X-ray diffraction patterns (see Fig. III-3) as well as of geochemical and isotope data. The interval is characterized by lower  $K_2O$  concentrations and lighter oxygen isotope ratios (see Chapter V), and displays its own I/S composition gradient (0.5 %I/100 ft) which is less than half of that for the stratigraphic section above. The top of the interval coincides with a local unconformity at 9880 ft (Chamney, 1973).

Below 10800 ft (3292 m), I/S composition changes relatively little with depth. The apparent variations in I-content may be an analytical artifact resulting from the effect of chlorite on deconvolution.

### *Interpretation*

The observed trends can be interpreted in four different ways (Fig. IV-2). The simplest interpretation is to relate the discontinuities at 9800 and 10800 ft to local and regional unconformities, respectively (Fig. IV-2a). In this case, the various trend changes across the unconformities are attributed to differences in composition, structure and chemistry of the starting I/S clays (cf. Roberson and Lahann, 1981).

The second hypothesis suggests continuation of a Tertiary trend into the Cretaceous (Fig. IV-2b). Unconformity, age or provenance did not affect systematic changes of I/S with increasing burial depth (e.g. Gulf Coast). I/S with lowered I-content between 9800 and 10800 ft is related to local variation in diagenetic factors such as temperature, pressure and pore water chemistry.

The third hypothesis proposes that Cretaceous I/S was illitized prior to deposition of most Tertiary sediments (Fig. IV-2c). The area had been a structural high in most of the Late Cretaceous forming an isolated northern extension of the Cache Creek Uplift which is a component of the Aklavik Arch Complex (Young et al., 1976). However, the presence of geopressure in the Cretaceous unit (Hitchon et al., 1990) suggests rapid sedimentation in Albian time, and that a considerable thickness may be missing due to erosion before deposition of the Tertiary deltaic sequences.

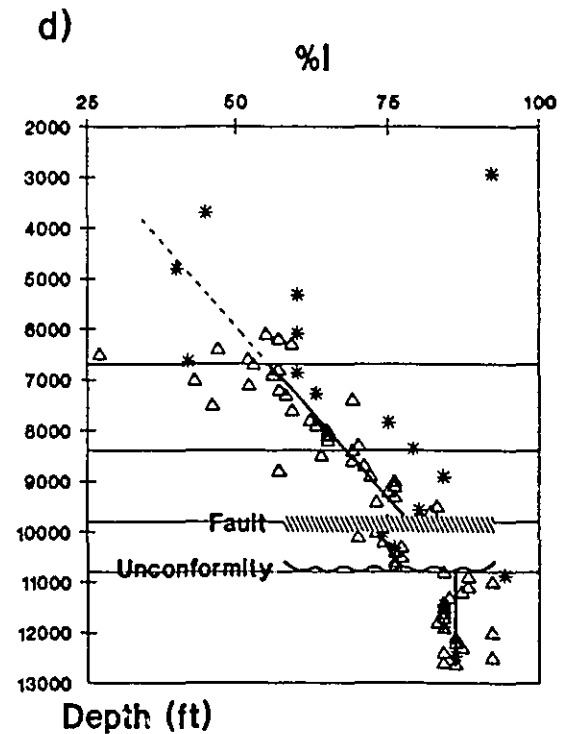
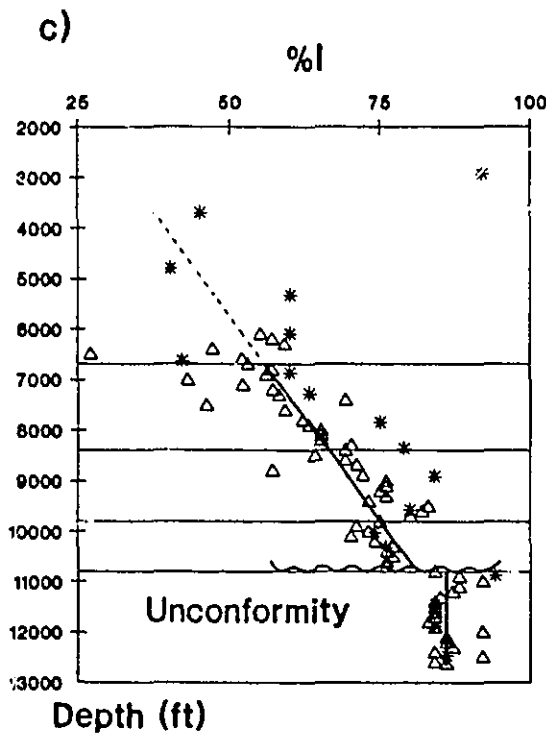
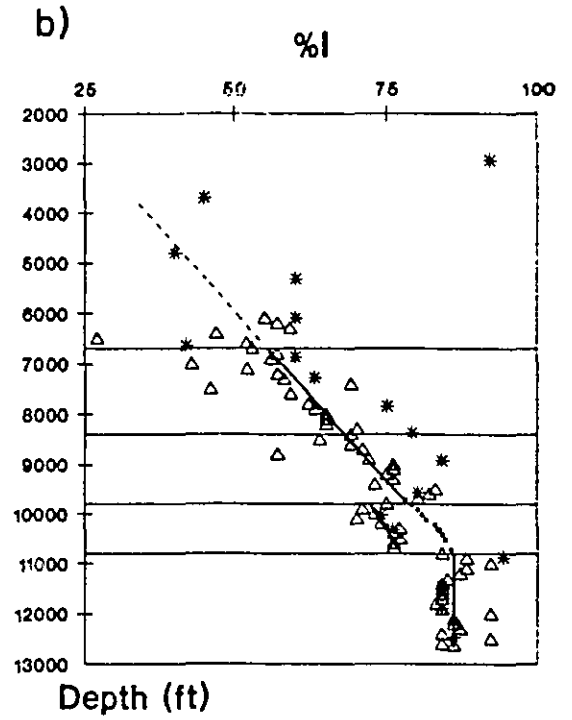
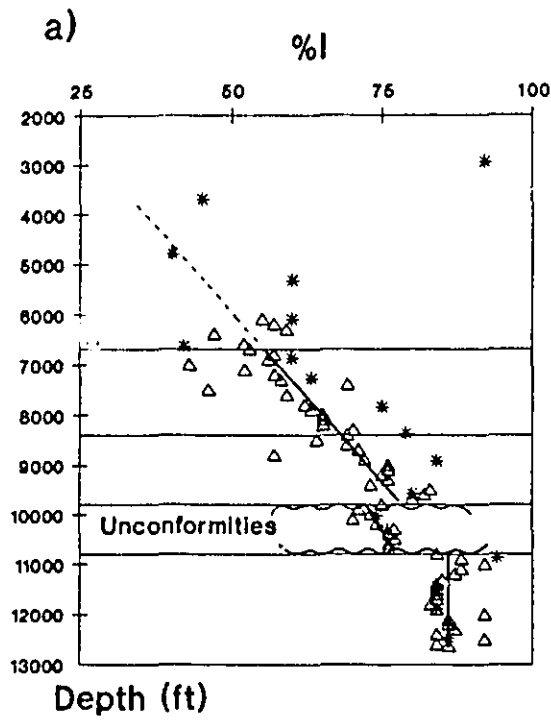


Figure IV-2. Comparison of four models proposed to interpret I/S burial curves of Reindeer D-27.

The fourth hypothesis uses a fault model to explain the compositional discontinuity of I/S (Fig. IV-2d). If a fault existed at all, it could have been a growth fault of listric type that is omnipresent in the basin. A fault at about 9800 ft would simplify the interpretation. Lowered I-contents and different compositional gradients might be due to local variation of diagenetic environments prior to fault movement.

Whether the Tertiary trend is continuous with the Cretaceous trend is difficult to determine from the data available. However, circumstantial evidence gathered in the course of this study suggests that the trends are probably not continuous. The oxygen-isotopic composition of I/S suggests that pore waters of Reindeer D-27 were stratified (see Chapter V). Thus, the chemistry of the pore waters which plays an important role in the illitization of I/S clays may have been significantly different for the Tertiary and Cretaceous sections. The mineralogy and chemical composition of Cretaceous samples are also markedly different from Tertiary samples (see Fig. V-2, 4), suggesting that the provenance of Cretaceous shales may not be the same as that of the Tertiary shales. It is likely that the starting compositions of I/S for the Tertiary and the Cretaceous were different. Therefore, the reaction rates that are considered sensitive to pore-water chemistry and compositions of the starting I/S (Roberson and Lahann, 1981), should have been dissimilar between the Cretaceous and Tertiary sections. The apparent continuity in trends is probably the result of a coincidence. As mentioned, the present compositions of Cretaceous I/S may have been attained through pre-Tertiary diagenesis prior to uplift and erosion.

The discontinuity within the Tertiary section is probably due to retarded illitization

between 9800 and 10800 ft. The mineralogical and geochemical compositions of I/S from the interval are not different from the section above (for geochemistry see Chapter V). The change in lithology, facies and probably age is very subtle at 9800 ft. The interval lies within the normally pressured zone, which is sandwiched between two geopressure zones above and below (Fig. IV-1). The retardation of illitization may be related to fluid pressure and water chemistry of the interval. The interval is characterized by isotopically light water (see Chapter V), suggesting that water/rock interaction was not as active as the sections above and below.

#### ***Layer charge development***

Some samples were K-saturated to identify the potential of I/S mixed-layers to form illite-like layers by collapse (Appendix II). These layers had layer-charges high enough to produce I-layers, but behaved as expandable layers because layer charges were not high enough to dehydrate interlayer cations other than  $K^+$ .

In Reindeer D-27, the proportion of I-layers in random I/S increased by 2 to 28 %I upon K-saturation (Fig. IV-3). K-saturated random I/S, except for the shallowest sample (3700 ft), showed a relatively uniform composition of about 65 %I. In other words, these random I/S clays are more or less identical in terms of layer charges. The lack of a trend based on apparent I/S compositions of Na-saturated samples in the interval of random I/S is deceiving. If potassium were available, these random I/S clays would display similar compositions.

R1-ordered I/S showed a gain of about 5-10 %I upon K-saturation, plus addition of

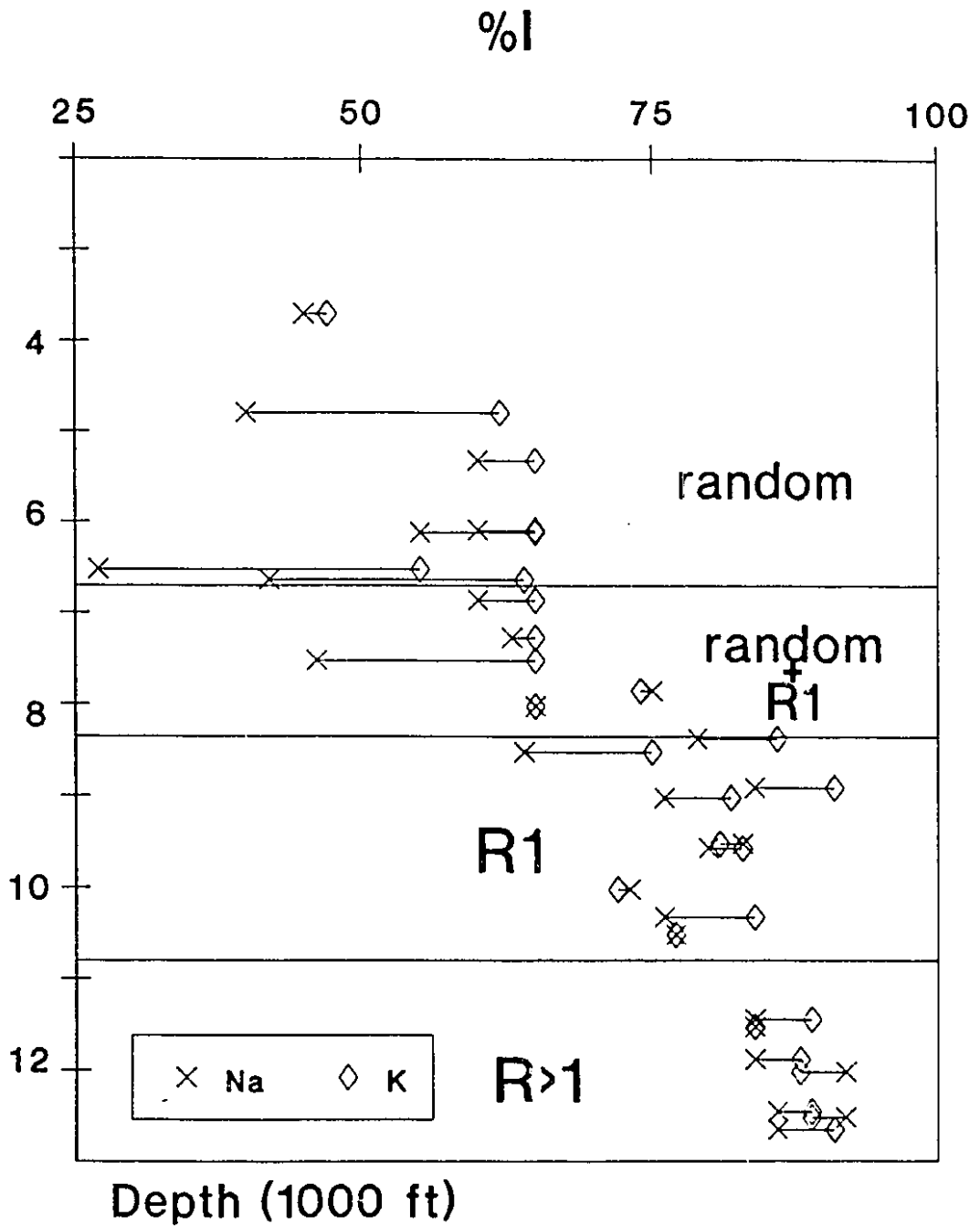


Figure IV-3. Plot of I-content versus depth for K-saturated specimens in comparison to Na-saturated specimens of Reindeer D-27. For data, see Appendix II.

illite. The peaks representing illite, especially (001), in K-saturated samples were more prominent than in Na-saturated samples (see Fig. III-6A). In general, the degree of ordering was improved. R>1-ordered I/S showed little change in the composition and the degree of ordering upon K-saturation; however, it also produced prominent peaks corresponding to illite (see Fig. III-6A c,d).

#### **IOE Taglu C-42 (lat. 69°21'03"N, long. 134°56'35")**

The Taglu C-42 well is located in the Taglu gas field where the first major discovery was made in the Beaufort-Mackenzie Basin. Recoverable reserve-estimates range upward of 3 Tcf (Bowerman and Coffman, 1975). The well penetrated a total depth of 16060 ft (4895.1 m). A bottom hole temperature of 121.1°C was reported. The stratigraphy comprises the Reindeer, Richards, Kugmallit and Iperk sequences, and Quaternary sediments (Fig. IV-4). However, the study is restricted primarily to the Reindeer Sequence, because samples from shallow depths showed signs of contamination by drilling-mud. Relatively well-consolidated drill-cutting samples were available below about 9000 ft (2743 m).

In contrast to Reindeer D-27, the studied interval of Taglu C-42 consists of thick sandstones and sandstone-shale alternations deposited in delta-front and shallow prodelta environments. The interval is geopressured from 8800 ft (2682 m) downwards (Hitchon et al., 1990). Fluid pressure in the Taglu field varies considerably within the geopressure zone and, internally, higher pressured zones exist (Hawkings and Hatlelid, 1975).

A total of 29 samples (5 core, 24 drill cuttings) were studied. Mineralogy of the <.1

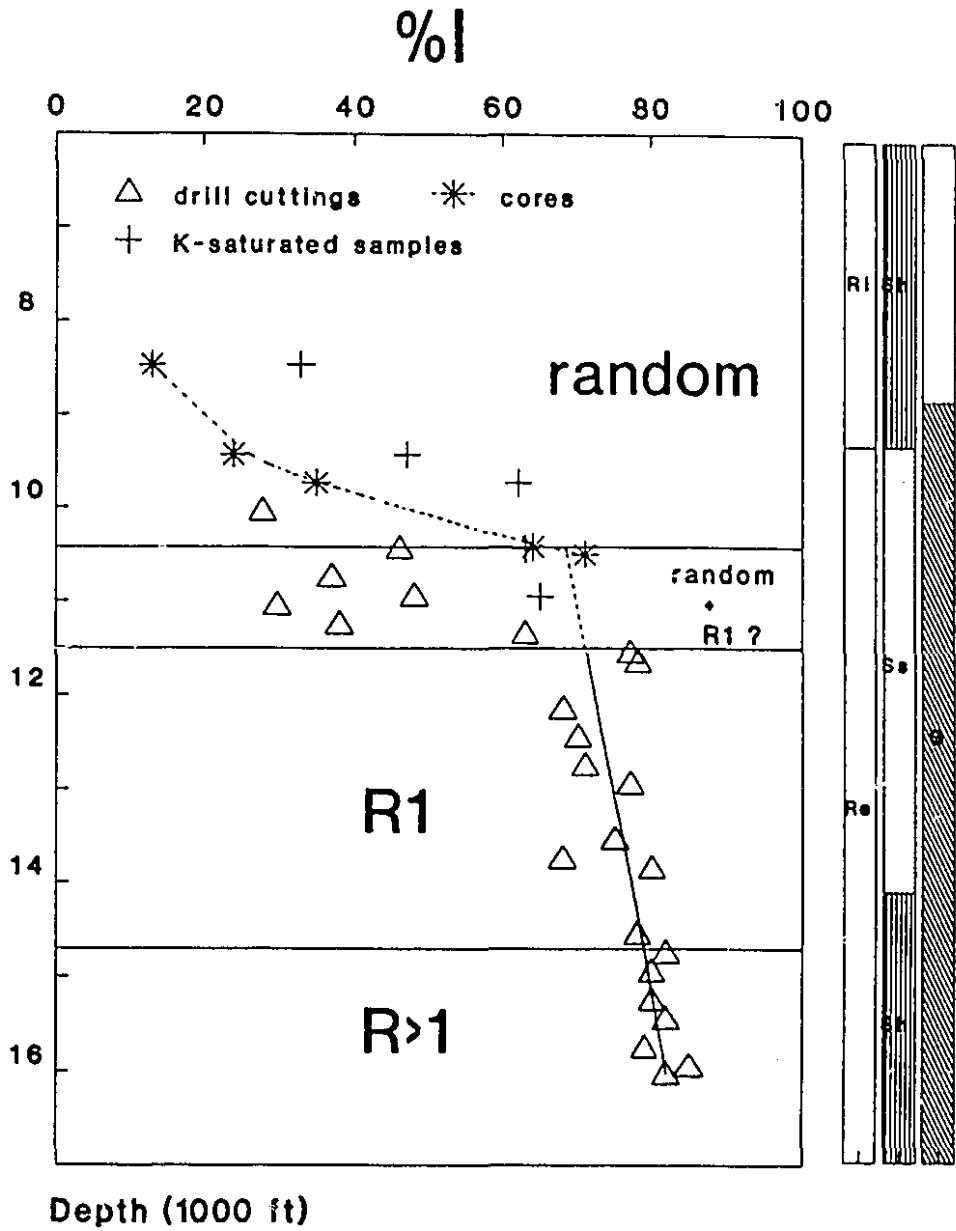


Figure IV-4. Plot of I-content (%I) in I/S with respect to depth, stratigraphy, lithology and geopressure for Taglu C-42. Ri - Richards. For other abbreviations in the columns, see Fig. IV-1.

$\mu$  fractions is similar to that of Tertiary samples of Reindeer D-27. I/S and illite constitute about 95 % and kaolinite makes up the rest. Compared to Tertiary samples of Reindeer D-27, the relative abundance of discrete illite is higher in Taglu C-42 (see Fig. III-1k).

### *I/S diagenesis*

Taglu C-42 contains the various types of I/S identified in Reindeer D-27, including random to R>1-ordered I/S. Compositions of Taglu I/S vary from 13 to 85 %I. The apparent change from random to R1-ordered I/S occurs at 11500 ft (3505 m), and from R1- to R>1-ordered I/S at 14700 ft (4481 m). The depths are surprisingly close to those where drill-bit sizes had been changed (11408 and 14791 ft). The possibility exists that the actual depths of structural changes in I/S may be shallower than the apparent depths, because cavings may have delayed detection of the first appearance of I/S with more advanced structures. A mixture of random and ordered I/S is found only in two core samples from about 10500 ft (3200 m). The absence of a mixture of random and ordered I/S in drill-cutting samples from the interval between 10500 and 11500 ft (3200-3505 m) does not necessarily imply that Taglu C-42 is devoid of the same kind of transition zone from random to ordered I/S observed in Reindeer D-27. The stratigraphic section between 10500 and 11500 ft (3200-3505 m) is dominated by sandstones, though some thin layers of mudrocks are present. Most shale chips in drill-cutting samples of this interval are probably derived from above where shale beds are more frequent and random I/S is predominant. However, at 8812 ft (2686 m) casing was set so that no material

I could be derived by caving from above that depth. The apparent I-content depends on the relative abundance of cavings and on the composition of I/S in the caved-in material.

K-saturation of Taglu samples produced results similar to Reindeer D-27 (see Fig. III-6B). In random I/S, the proportion of I-layers increased by 17-27 %I. K-saturated random I/S acquired about the maximum I-content for random I/S (62 %I) at 9738 ft (2968 m) [Fig. IV-4]. Above 9738 ft, compositions of K-saturated samples followed the trend of Na-saturated samples. A mixture of random and ordered I/S lost peaks representing random I/S. R1-ordered I/S showed broader and flattened peaks of  $(001)_{10}/(002)_{27}$ , but compositional changes were difficult to estimate due to a large increase of discrete illite that hindered precise determination of the position of the  $(002)_{10}/(005)_{27}$  peak. R1-ordered I/S of Taglu C-42 appears to contain more high-charge expandable layers ("potential illite-layers") than Reindeer samples. K-saturated R>1-ordered I/S displayed patterns similar to R1-ordered I/S, i.e. unlike Reindeer samples, K-saturation altered the nature of ordering. In Taglu C-42, the  $(001)_{10}/(002)_{27}$  peak and the equivalent peak for R>1-ordered I/S shifted towards lower angles (see Fig. III-6B d). This suggests that "potential illite-layers" may have developed preferentially in crystallites having long-range ordering. Upon K-saturation, these crystallites were transformed to illite, resulting in X-ray diffractions consisting of short-range ordered I/S and illite.

Illitization in Taglu C-42 is lagging behind Reindeer D-27. Ordered I/S emerges about 3000 ft deeper than in Reindeer D-27. The current geothermal gradient is much higher in Taglu C-42 than in Reindeer D-27 ( $\sim 4^{\circ}\text{C}/\text{km}$  higher based on bottom-hole temperatures). The advanced level of diagenesis in Reindeer D-27 is probably due to

deep burial prior to uplift to the present depth.

Illitization in Taglu C-42 for random I/S above 10500 ft has been about three times as fast as in Reindeer D-27 (2.9 %I/100 ft). However, once ordering was achieved, it slowed down to about 20 % (.2 %I/100 ft) of the rate in Reindeer D-27 (~1.1 %I/100 ft). An approximately 50 % increase in I-layers of I/S occurred in the 2000 ft thick interval of random I/S (8468-10508 ft; 2581-3203 m). Within this depth range, the temperature increases from 58° to 72°C (based on logged temperatures), and the stratigraphy changes at 9302 ft (2835 m) from delta-front sandstones of the Reindeer Sequence to prodeltaic shales of the Richards Sequence. Gas was recovered at 9440 (2877 m) and 9460 ft (2883 m), and oil at 10680 ft (3255 m) from drill-stem tests. The relationship of I/S diagenesis with temperature, stratigraphy, lithology and hydrocarbon occurrence will be discussed in a later section.

#### **IOE Taglu G-33 (lat. 69°22'17"N, long. 134°53'36"W)**

Taglu G-33 is the discovery well of the Taglu gas field. It is located about 6 km northeast of Taglu C-42. It penetrated a total depth of 9822 ft (2993.7 m). A bottom hole temperature of 70°C was reported. The stratigraphy of the well comprises the Reindeer, Richards, Kugmallit and Iperk sequences. Lithology and depositional facies are similar to equivalent sequences of Taglu C-42. Gas with a flow rate of 28.7 Mcf/d was recovered in the Reindeer Sequence at 8170 ft (2490 m). Sandstones between 8150 and 9800 ft (2484-2987 m) were tested for gas (Bowerman and Coffman, 1975). Twelve core samples were available at variable depths from 3120 to 9271 ft (951-2826 m) that cover

the Kugmallit, Richards and Reindeer sequences. Noticeable mineralogical differences between sequences were not observed.

In Taglu G-33, all I/S is randomly mixed-layered. Compositions range from 27 to 65 %I. There is little depth-related change in composition (Fig. IV-5). However, below 6817 ft (2078 m), I-contents become less variable and average about 45 %I. After K-saturation, these samples give similar compositions of about 65 %I. In terms of layer-charge development, these samples were fully illitized because 65 %I is the maximum I-content for random I/S.

The I-content of I/S at depths comparable to Taglu C-42 is higher by about 20 % in Taglu G-33. The layer charge in random I/S of Taglu G-33 is similar to that in Taglu C-42 at depths about 3000 ft shallower than in Taglu C-42. Advanced illitization in Taglu G-33 is probably related to hydraulics and temperature (see Discussion). Taglu G-33 contains a geopressure zone, the top of which is located at 7600 ft (2317 m), 1200 ft higher than in Taglu C-42. In addition, geothermal gradients in the eastern part of the Taglu field are generally higher than in the western part (see Fig. I-9). The contour of the 30°C/km gradient runs between Taglu C-42 and G-33.

#### **Wells in the vicinity of Reindeer and Taglu**

Several wells in the vicinity of the Reindeer and Taglu fields have core samples covering a wide range of depths. These wells provide the database to appraise the lateral variation of I/S diagenesis and its relationship to other geologic variables in the area. The wells include Kumak E-58, Niglintgak M-19, Garry P-04, Adgo C-15, Mallik A-06, Ivik J-26,

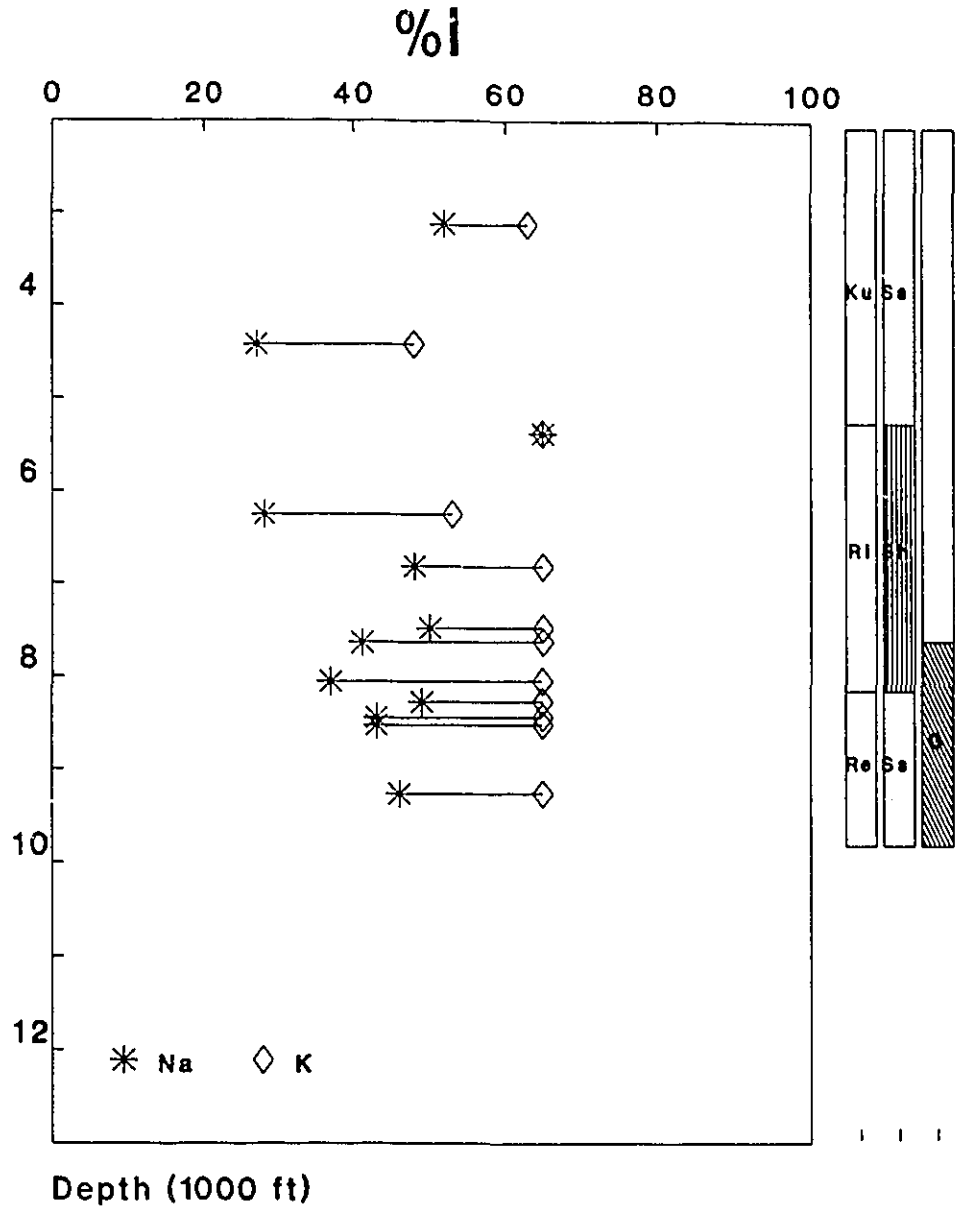


Figure IV-5. Plot of I-content (%I) in Na- and K-saturated I/S with depth, stratigraphy, lithology and geopressure for Taglu G-33. Ri - Richards, Ku - Kugmallit; for other abbreviations, see Fig. IV-1.

and Unark L-24 (see Fig. I-11). The Kumak, Niglintgak, Garry and Adgo wells are located on diapir-cored anticlines. They are stratigraphically similar to Reindeer D-27 (Fig. IV-6). The stratigraphy of Mallik A-06 is comparable to the Taglu wells. The Ivik and Unark wells contain younger sequences than those of the other wells. All wells are hydrocarbon-bearing or, at least, display some shows. Most of them are geopressured at variable subsurface depths (Hitchon et al., 1990).

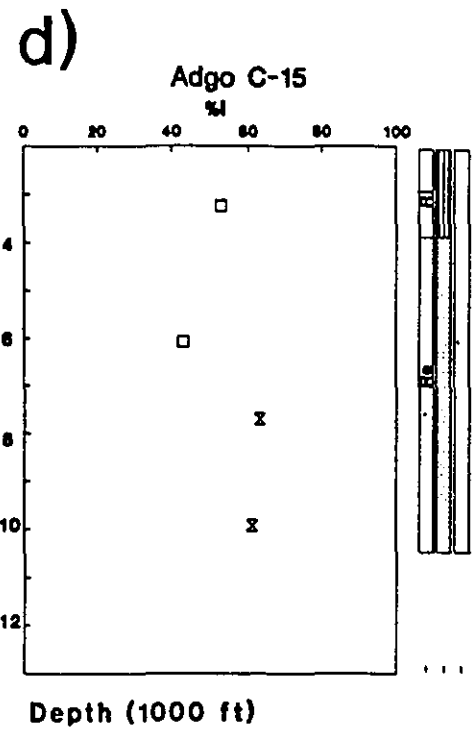
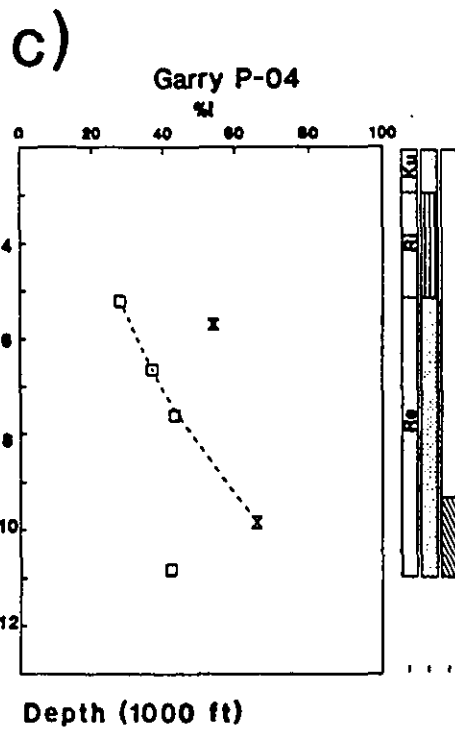
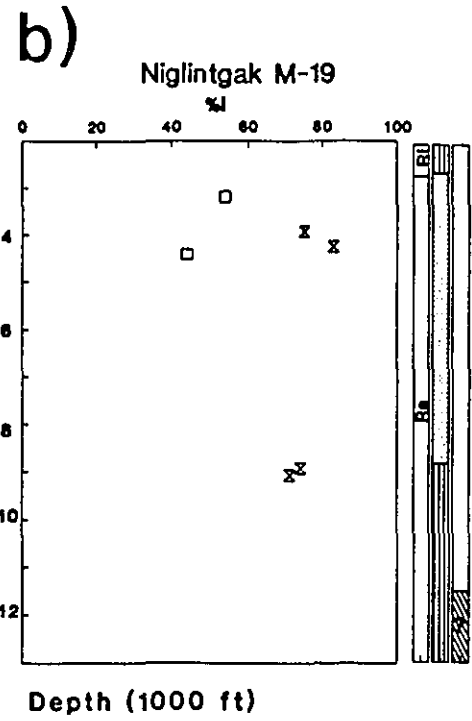
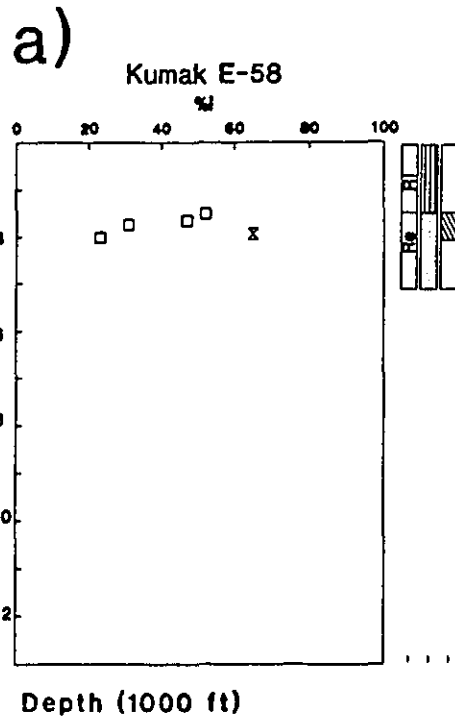
**Kumak E-58** is located about 30 km north of Reindeer D-27 (T.D. 5100 ft; 1543 m). I/S mixed-layers show variable compositions from 23 to 65 %I in a relatively short depth interval between 3517 and 4028 ft (1072-1228 m). The well contains a narrow geopressure zone which is located at the top of the Reindeer Sequence (which spans the depth range from 3451 to 4052 ft; 1052-1235 m).

**Niglintgak M-19** is characterized by the presence of I/S with high I-layer contents at shallow depths. R>1-ordered I/S occurs at 4254 ft (1297 m). The present temperature at this depth is about 30°C which is too low for the given I/S compositions. Similar to Reindeer D-27, most illitization may have occurred at greater burial depths before the pre-Perk erosional events removed considerable portions of the section.

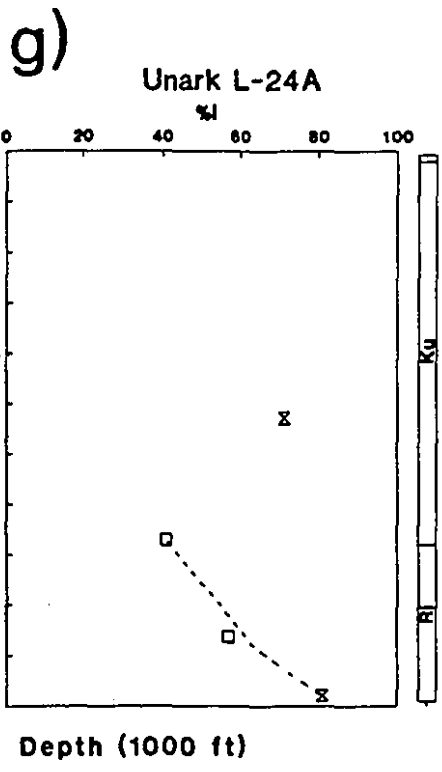
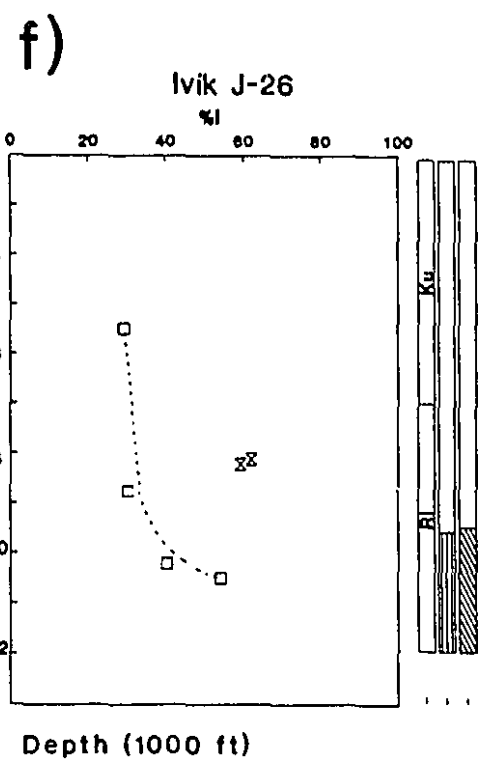
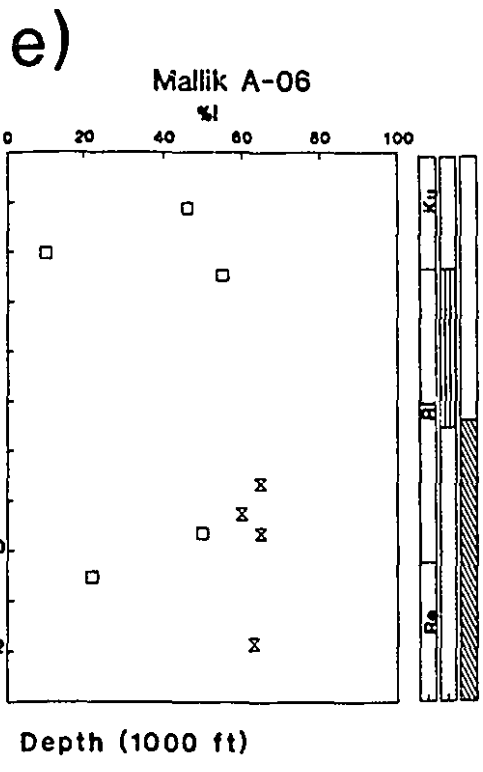
**Garry P-04** shows a more or less well-defined I/S trend with a gradient of .8 %I/100 ft. The proportion of I-layers increased from 28 %I to 66 %I in the interval from 5211 to 9852 ft (1588-3003 m). There may be a reversal in composition and ordering at 10833 ft (3302 m) where random I/S with 42 %I occurs.

**Adgo C-15** contains random I/S and a mixture of random and ordered I/S. Though it is not possible to establish a systematic I/S trend from the data available, R1-ordered

Figure IV-6. Plots of I-content (%I) versus depth, stratigraphy, lithology and geopressure for wells in the vicinity of Reindeer and Taglu. □ - random I/S, X - mixture of random and ordered I/S or  $R \geq 1$ -ordered I/S. For other symbols, see previous figures. For data, see Appendix I-3.



1



I/S appears as part of the mixture of random and ordered I/S at 7704 ft (2348 m), about 2000 ft shallower than in Garry P-04. The interval of the transition from random to ordered I/S may extend over more than 2200 ft (7704-9926 ft; 2348-3025 m). Vertical offset by a growth fault between the Adgo and Garry blocks is estimated to be about 1500 ft. This growth fault may account for most of the compositional differences between the Adgo and Garry wells at similar depths. In other words, the present compositions may have been acquired before movement on the fault.

**Mallik A-06** is located about 20 km northeast of the Taglu field. Mallik A-06 displayed ordered I/S at 8656 ft (2638 m), about 3000 ft shallower than in Taglu C-42. Unlike Taglu C-42, in Mallik A-06 the sandy facies that characterize the Reindeer Sequence continue upwards in the Richards Sequence to about 7500 ft (2286 m). The top of the geopressure zone is also raised to 7345 ft (2239 m) (Hitchon et al., 1990). Reversals in composition and ordering occur at 9660 (2944 m) and 10530 ft (3210 m) (random I/S with 50 and 22 %I, respectively).

**Ivik J-26** penetrated thick successions of the Kugmallit and Richards sequences. Alluvial and deltaic sandstones dominate the stratigraphic section above 8500 ft (2591 m), while shale is the principal lithology in the section below. A more or less systematic trend of I/S diagenesis is found in the shaly section (1.2 %I/100 ft). Proportions of I-layers increase from 30 to 54 %I in an interval between 8755 and 10494 ft (2669-3199 m). A mixture of random and ordered I/S with about 60 %I occurs in a sandy interval at about 8200 ft (2499 m).

**Unark L-24** shows a trend similar to Ivik J-26. I-layer contents increase parabolically

from 41 to 81 %I in an interval from 9696 to 12778 ft (2955-3895 m) [1.2 %I/100 ft]. As Ivik J-26, this well also shows a relatively high I-content of I/S in the sandy interval at relatively shallow subsurface depth (7280 ft; 2219 m).

### **Offshore Wells**

The study of offshore wells is limited by the scarcity of cores and the poor quality of drill-cutting samples. Most drill-cutting samples show signs of contamination by drilling mud. Thus, the data for offshore wells are based on available cores. Eleven wells, from which 1 to 8 core samples were obtained, include Netserk B-44, Netserk F-40, Kadluk O-07, Nipterk L-19, Tarsiut N-44, Pitsiulak A-05, Issungnak 2O-61, Alerk P-23, Itiyok I-27, Amerk O-09, and Koakoak O-22. In addition, Kenalooak J-94 was included because its location may provide information on the frontier area of the basin, although no core samples were available.

Offshore wells are characterized by younger stratigraphic sequences compared to onshore wells (Appendix III; see also Fig. I-5). The Iperk and Kugmallit sequences together are about 2 to 4 km thick. The Mackenzie Bay-Akpak Sequence is usually less than 500 m thick. The Richards and Reindeer sequences are present in wells from the western part of the basin (e.g. Tarsiut, Nipterk). In general, shale is predominant but, in the Kugmallit Sequence, deltaic and/or turbiditic sandstones constitute a considerable thickness. Geothermal gradients are unusually high ( $>30^{\circ}\text{C}/\text{km}$ ) for a basin embodying thick successions of Tertiary sediments. Major oil and several gas discoveries were made in the Kugmallit Sequence associated with growth faults and diapir-cored anticline

structures. Most wells are geopressured at variable depths (Hemingson and Carew, 1984; Hitchon et al., 1990). X-ray diffraction patterns of the  $<.1 \mu$  fractions are similar to those of onshore samples. I/S, illite, kaolinite and, seldomly, chlorite are present. I/S and illite constitute more than 90 % of the fine fractions, and kaolinite and/or chlorite make up the rest.

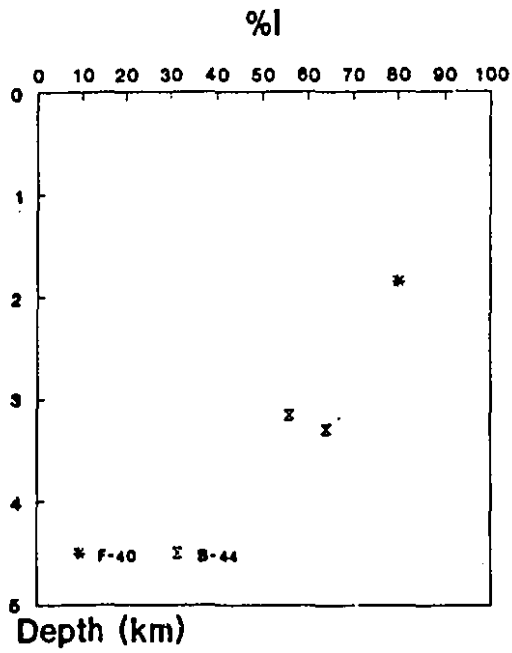
**Netserk B-44** is the well nearest to onshore wells. It is located about 18 km north of Adgo C-15 and at about the same latitude as Ivik J-26. Two samples were available from 10391 and 10845 ft (3167 and 3306 m) [Fig. IV-7]. I/S of both samples is a mixture of random and ordered I/S. Random I/S is dominant at 10391 ft (3167 m), whereas ordered I/S is predominant at 10845 ft (3306 m). **Netserk F-40**, which is located about 12 km north of B-44, contains a highly illitized I/S (80 %I) at 6080 ft (1853 m).

The Kadluk, Nipterk, Tarsiut and Pitsiulak wells represent the western portion of the mid-shelf where numerous diapirs are encountered in addition to growth faults. For **Kadluk O-07**, four samples were available from 981 to 2402 m. The interval comprises the Mackenzie Bay and Kugmallit sequences. It contains random, but highly illitized I/S (56-65 %I). The maximum I-content for random I/S (65 %I) is acquired at 1483 m, below which depth little change in composition is observed.

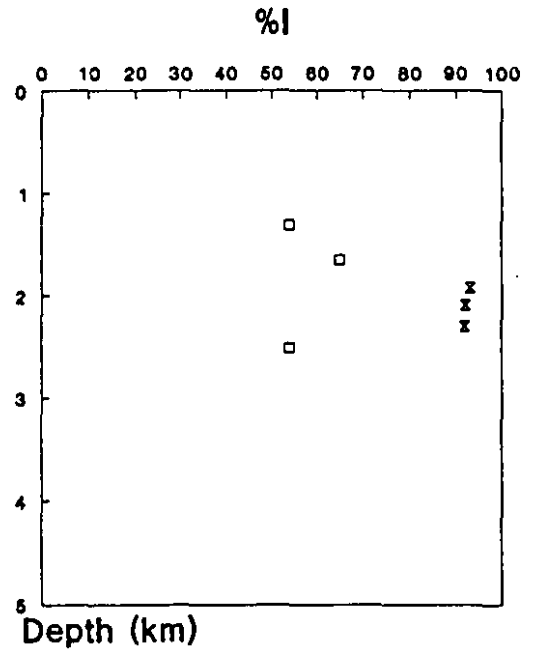
**Nipterk L-19** contains various types of I/S in an interval between 1306 and 2511 m including random, R1-, and R>1-ordered, for which compositions range from 54 to 93 %I. Random I/S reaches the maximum I-content (~ 60 %I) at 1650 m. I/S in the interval between 1923 and 2303 m is ordered with the maximum degree of ordering occurring at 2094 m. There is a reversal in composition and ordering at 2511 m (random I/S with 54

Figure IV-7. Plots of I-content (%I) versus depth for offshore wells. □ - random I/S, X - mixture of random and ordered I/S or  $R \geq 1$ -ordered I/S. For data, see Appendix I-4.

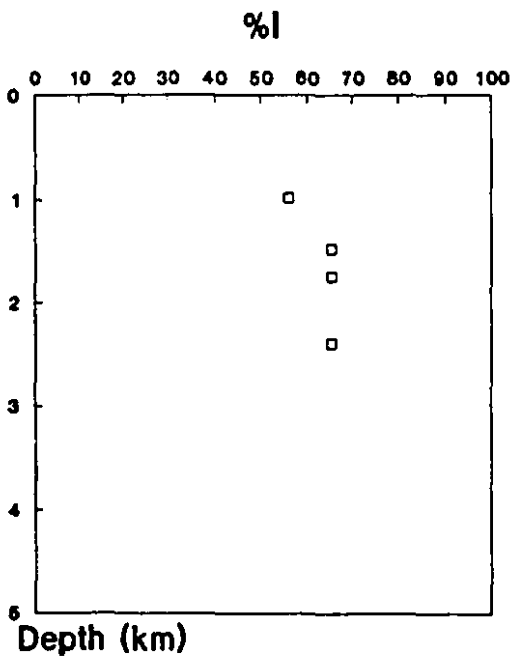
a) Netserk



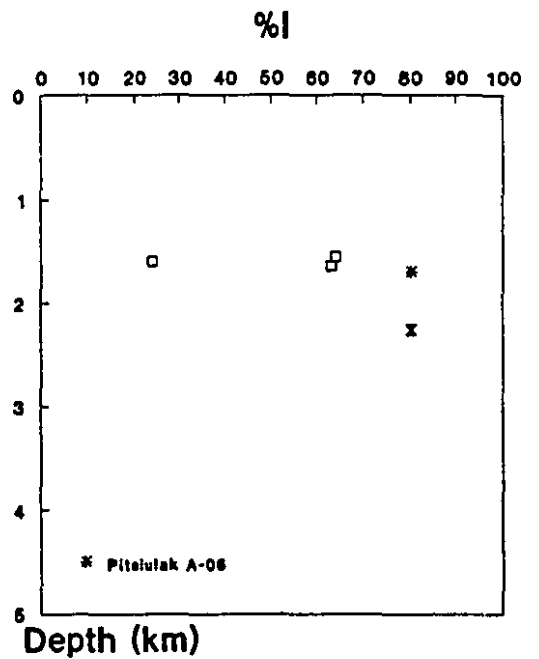
b) Nipterk L-19



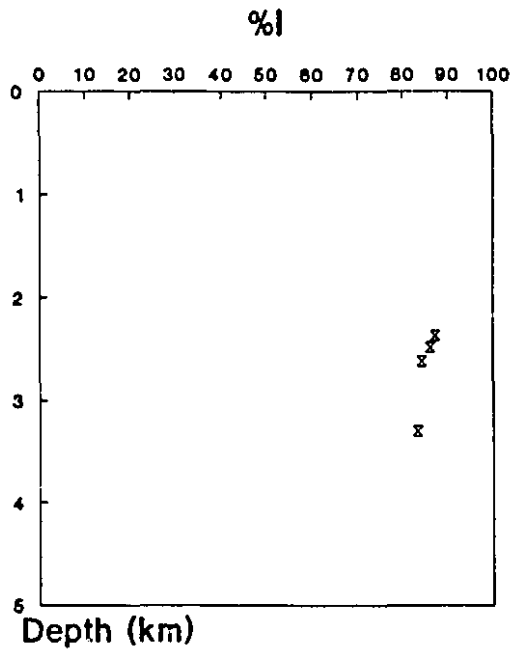
c) Kadluk O-07



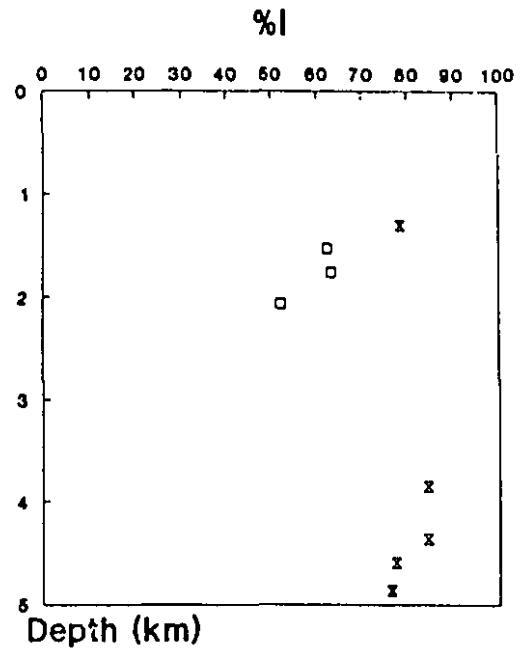
d) Tarsiut N-44



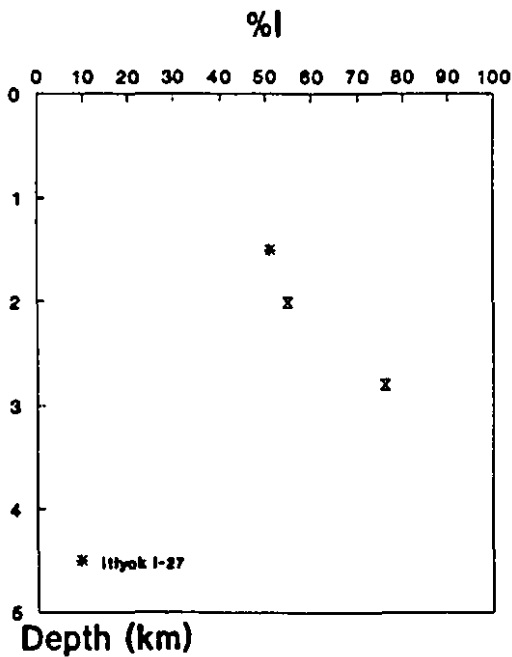
e) Issungnak 2O-61



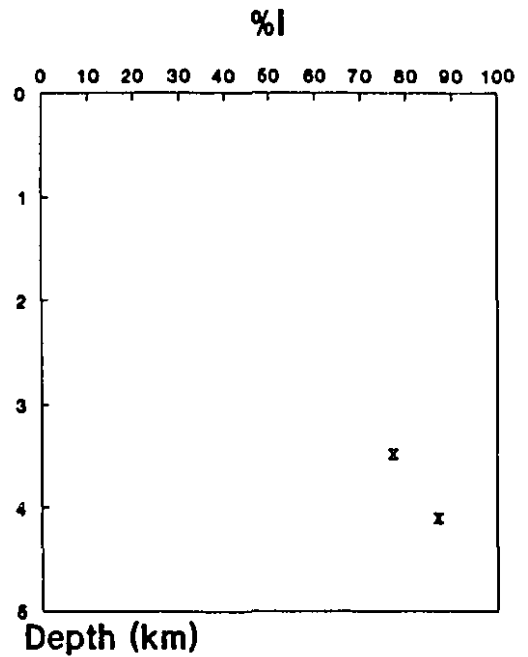
f) Amerk O-09



g) Alerk P-23



h) Koakoak O-22



%I).

**Tarsiut N-44** contains I/S with the lowest I-layer content among offshore samples (24 %I, 1596 m). Random I/S from 1558 and 1647 m are highly illitized (63 and 64 %I, respectively). I/S from 2266 m is R1-ordered. **Pitsiulak A-05** which is located about 20 km west of Tarsiut N-44 shows a mixture of random and ordered I/S at 1701 m.

The **Issungnak, Itiyok, Amerk and Alerk** wells represent the eastern part of the mid-shelf. Diapir fields that prevail in the west do not appear to extend to the area. Most wells did not penetrate older sequences such as the Richards that is usually encountered at about 2-2.5 km subsurface depth in the west. The area saw continuous sedimentation throughout the Tertiary so that the present depths may equal maximum burial depths. The cumulative thickness of Tertiary sediments exceeds 11 km near the Issungnak field. Samples were available for depths ranging from 1313 to 4866 m. Various types of I/S were present, for which compositions range from 51 to 87 %I. In general, random I/S was predominant above about 2000 m; below I/S became ordered. In **Issungnak 20-61**, samples were available from 2374 to 3306 m. I/S mixed-layers are all ordered (Appendix I-4). I/S from 1507 m in **Itiyok I-27** is random. Two samples from **Alerk P-23** include a mixture of random and ordered I/S at 2019 m and R1-ordered I/S at 2799 m. In **Amerk O-09**, random I/S is present to 2069 m, while below 3861 m I/S is ordered. (Note that samples were not available between the depths mentioned.)

The **Koakoak and Kenalooak** wells are located further offshore. Although shallow samples are not available, the depth intervals for the occurrence of random or ordered I/S are probably not very different from those for the mid-shelf. Drill-cutting samples

obtained from below 2700 m indicate that I/S was already ordered at this depth, despite the fact that these samples show signs of contamination by drilling mud. This sample depth is by no means the minimum depth for the first appearance of ordered I/S.

## DISCUSSION

### Mixture of Random and Ordered I/S

A mixture of random and ordered I/S is identified in a transitional interval between random and R1-ordered I/S, 1650 ft thick in Reindeer D-27 and probably 1000 ft thick in Taglu C-42. The widespread occurrence of mixtures of random and ordered I/S in the Beaufort-Mackenzie Basin suggests that it may have been overlooked in studies of other basins.

The thickness of the interval in which the mixture occurs may be a relative measure of the reaction rate for the structural transition from random to R1-ordered I/S, i.e. ordering. For Reindeer D-27, the average burial rate was about 900 ft/Ma during deposition of the 7806 ft-thick Reindeer Sequence (Thanetian-Ypresian; Dixon, 1986), and thus the thickness of 1650 ft would correspond to a time span of about 1.8 Ma. This value should be taken as an approximation only, because tectonics involving the Cordillera and the Arctic Ocean had complicated the burial history of the basin. Though ordering is a relatively sluggish reaction, it does not appear to slow the overall illitization reaction, i.e. the increase in I-contents of I/S. The proportion of I-layers increases from 53 to 65 %I in the interval of the mixture of random and ordered I/S in Reindeer D-27 (Fig. IV-1).

## Basinal Trends

Proportions of I-layers in Beaufort-Mackenzie I/S generally increased with depth, while the dominant type changed from random to  $R > 1$ -ordered I/S. In the interval of random I/S, the increase of I-layers was fast and assumed a parabolic trend with respect to depth, where a trend could be established (e.g. Taglu C-42, Ivik J-26, Unark L-24, Garry P-04). In Reindeer D-27, Taglu G-33, and some other wells, no apparent trend was observed. However, K-saturation indicates that most of the I/S mixed-layers were fully illitized for random I/S below a certain depth, e.g. 4800 ft (1463 m) in Reindeer D-27, 6817 ft (2078 m) in Taglu G-33. A relatively fast rate of illitization in the interval of random I/S (.8-2.9 %I/100 ft) is probably due to chemical and structural instabilities, i.e. high free energy, characteristic of random I/S. Random I/S appears to contain excess cations unfit for di-octahedral sites (see Chapter V).

Once ordering has started, the rate slows down to .2-1.15 %I/100 ft (Reindeer D-27, Taglu C-42). The slow rate of conversion in the composition range of ordered I/S has been noticed in many studies of I/S diagenesis (e.g. Perry and Hower, 1970). F and Franks (1979) attributed the retardation of illitization to the depletion of potassium. However, hydrothermal experiments in a system, which presumably contained sufficient potassium, also indicated slower reaction rates for ordered I/S (Whitney and Northrop, 1988). The slow rates are probably related to chemical and structural stability of expandable layers acquired following the ordering reaction.

In the Beaufort-Mackenzie Basin, the transition in the composition range of ordered I/S appeared to be smooth. I-layers increased linearly from a mixture of random and

ordered I/S to R1-ordered I/S to R>1-ordered I/S (e.g. Reindeer D-27, Taglu C-42). The absence of a break in compositional trends suggests that the transitions may be gradual, first-order reactions. Upon simple K-saturation, higher-order I/S as well as illite developed from R1-ordered I/S by transforming high-charge expandable-layers into I-layers (see Fig. III-6). This suggests that all ordered I/S and probably also illite may share a common structure. In other words, the R1-structure acquired from ordering of random I/S could be used as a base for the transition from R1-ordered through R>1-ordered I/S to illite.

Several wells in the Beaufort-Mackenzie Basin showed reversals in I/S composition and ordering. Random I/S appeared at considerable subsurface depths below a thick section of ordered I/S (e.g. Mallik A-06, Garry P-04, Nipterk L-19). The mineralogical compositions and lithology of deep samples containing random I/S were not significantly different, i.e., these samples are probably not bentonitic. The reversal is probably due to non-reaction or retarded-reaction rather than retro-diagenesis. This reversal should be related to diagenetic factors of the local environment. However, it was not possible from the data available to identify specific causes.

#### **Effects of Geopressure and Lithology on I/S Diagenesis**

Illitization of Beaufort-Mackenzie I/S appeared to be faster and more advanced in geopressured zones and sandy intervals than in normally pressured zones and shaly intervals, respectively. In Reindeer D-27, the interval with relatively low I-content and compositional gradient between 9800 and 10800 ft (2987-3292 m) lies within the

normally pressured zone. I/S in Taglu G-33 acquired most layer charge for random I/S at a depth about 3000 ft shallower than in Taglu C-42 that is only 6 km apart from G-33 (Fig. IV-8). The top of the geopressure zone in Taglu G-33 is located about 1200 ft higher than that in Taglu C-42. Mallik A-06 which is stratigraphically similar to Taglu C-42 displayed ordered I/S at a depth about 3000 ft shallower than in Taglu C-42. In Mallik A-06, delta front/delta plain sandstones are present to a depth about 2000 ft higher in the stratigraphic section than in Taglu C-42. The top of the geopressure zone is also raised by about 2500 ft. In Ivik J-26 and Unark L-24, samples from the sandy interval showed higher I-content than those from the shaly section, even though they are from shallower depths.

Apparently, geopressure and a high sandstone/shale ratio accelerated illitization of I/S in the Beaufort-Mackenzie Basin. In particular, the role of geopressure appears to contradict Colten-Bradley's (1987) conclusion based on thermodynamic arguments that geopressure will inhibit the dehydration of smectite. However, dehydration of smectite in diagenetic environments is, in fact, the result of chemical reactions involving layer-charge increase and absorption of cations with low dehydration energy (see Chapter II). I/S in geopressured environments may have a higher probability of reacting with pore water solutes owing to the higher water/particle ratios than under normally pressured conditions (cf. Whitney, 1990). The same reasoning applies to sandy sections because of their greater porosity and permeability and, therefore, higher chance of encounters between I/S and pore water solutes. It should be noted that geopressure distribution in the Beaufort-Mackenzie Basin is facies-controlled (see Fig. I-10) [Hemingson and Carew,

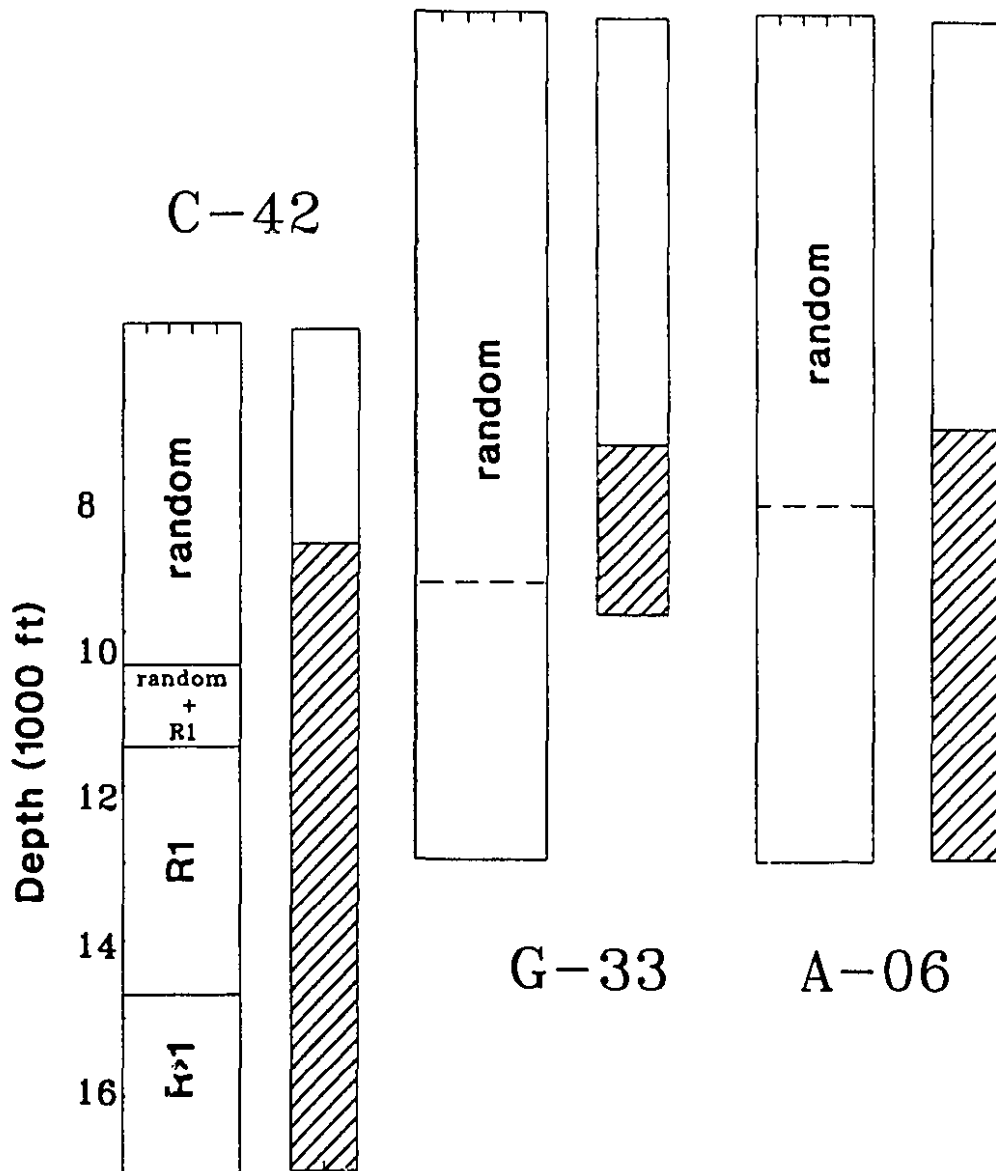


Figure IV-8. Diagram showing the effect of geopressure on I/S diagenesis. Geopressed sections are hatched. Dashed line represents the base of a random I/S interval.

1984; Hitchon et al., 1990]. I/S diagenesis is probably of secondary importance for geopressure development in the basin compared to stratigraphic and structural controls. Rapid I/S diagenesis may be the consequence of geopressure rather than the cause.

### **Temperature and I/S Diagenesis**

Illitization of I/S in offshore wells is, in general, more advanced compared to onshore samples from comparable depths. The maximum I-content for random I/S (~65 %I) appeared to be acquired at depths about 1-1.5 km shallower than onshore. The same I/S composition that was attained at about 1.5-2 km subsurface depth offshore was found at a depth of about 3 km onshore (e.g. Taglu C-42). Higher I-contents at shallow depths onshore are related to uplifted structures (e.g. Reindeer D-27, Niglintgak M-19). The initial composition of I/S in offshore wells was probably not very different from onshore I/S. I/S at shallow subsurface depths offshore and those less evolved I/S from equivalent stratigraphic units onshore showed compositions of about 20-30 %I.

Higher I-contents of I/S in offshore wells than onshore at comparable depths are probably temperature-related. Geothermal gradients offshore are about 5-10°C/km higher than onshore (see Fig. I-9). Most wells would reach a temperature of about 60°C at 2 km subsurface depth offshore, which appears to be a threshold temperature for active illitization of I/S in the basin (e.g. Taglu C-42). Temperature is probably the ultimate control for activation of the illitization reaction. Geopressure, lithology, and chemistry of the starting material may contribute substantially to local variations in I/S compositions.

## Hydrocarbons and I/S Diagenesis

Many aspects of petroleum geology and geochemistry of the Beaufort-Mackenzie Basin have been studied in detail. However, until now it was not clear why hydrocarbons are reservoired at specific depths in individual wells. For example, Hemingson and Carew (1984) tried to establish the relationship of hydrocarbon occurrence to geopressure, but concluded that no obvious direct relationship existed. In the Beaufort-Mackenzie Basin, hydrocarbons are found above, within and below geopressure zones.

Figure IV-9 compares positions of hydrocarbon occurrence with the depths for the occurrence of the various types of I/S identified in this study. For wells with no hydrocarbon shows (e.g. Reindeer D-27), the depth of hydrocarbon occurrences in adjacent wells in the same field was used.

In general, hydrocarbons appear to occur above and in the top part of the interval of random I/S. They rarely occur below the depth where ordered I/S begins to appear. Deep hydrocarbon reservoirs are found in wells where illitization begins at relatively great depth (e.g. Taglu, Mallik). For wells where the apparent depth of illitization is shallow due to uplift, caused either by growth faults, diapirs or tectonics, hydrocarbons also occur at shallow depths (e.g. Reindeer). In offshore wells where the depth of illitization is 1 to 1.5 km shallower than onshore, many hydrocarbon discoveries were made at depths of 1-2 km.

These observations indicate that there is a close relationship between hydrocarbon occurrence and I/S diagenesis in the Beaufort-Mackenzie Basin. Smectite-water derived from I/S diagenesis may have played an important role in the migration of hydrocarbons.

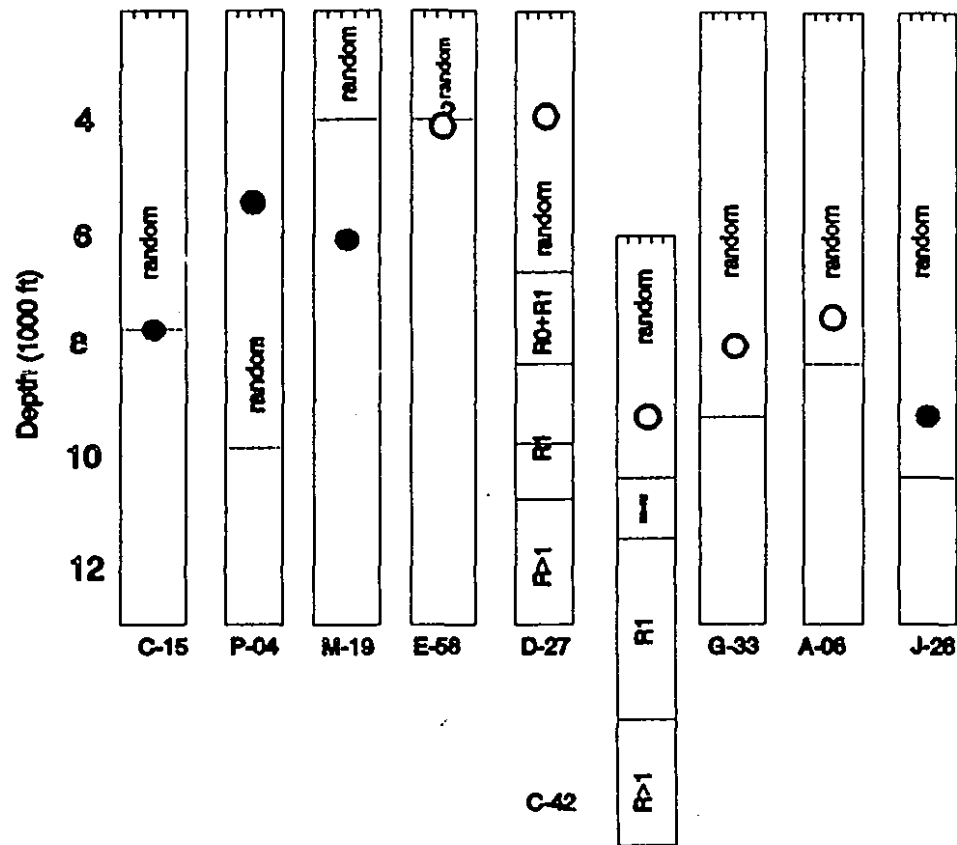


Figure IV-9. The relationship between positions of hydrocarbon occurrence and I/S diagenesis. Filled circle- oil-dominant, empty circle- gas-dominant.

Smectite-water moves upward as does compactional water. Other than the pressure effect which forces hydrocarbons out of shale pores, the catalytic effect of I/S while hydrocarbons are being generated, may influence hydrocarbon occurrence. The catalytic effect has been demonstrated in experimental studies which showed that I/S clays acted as acid catalysts to reduce the activation energy of kerogen decomposition (Johns and Shimoyama, 1972; Johns, 1979; Goldstein, 1983). It has also been noted that in the presence of I/S clays as mineral matrices, the yield of light-weight hydrocarbons was increased compared to heavier molecular products (Espitalie et al., 1980; Johns, 1981).

## CHAPTER V. GEOCHEMISTRY AND OXYGEN ISOTOPES

In the previous chapters, I/S diagenesis in the Beaufort-Mackenzie Basin has been discussed on the basis of mineralogy. This chapter discusses the geochemistry and O-isotope compositions of I/S in relation to mineralogical changes which appeared to be sensitive to depth-related variables, i.e. temperature and local diagenetic factors such as fluid pressure, lithology and probably many others. The Reindeer D-27 well is chosen for further discussions for the following reasons: Samples that display, as mentioned, a wide range of I-contents and structures are available from a depth range of about 3 km. The stratigraphic section below 6000 ft, where drill-cutting samples of good quality were obtained in addition to core samples, consists of relatively homogeneous mudrocks, and thus lithology is not a variable that needs to be considered.

### EXPERIMENTAL METHODS

Samples for geochemical and isotope analyses were prepared without the chemical treatments that were applied in the mineralogical studies (see Chapter I). Preliminary analyses of the mineralogical samples indicated a high degree of contamination by sodium metaphosphate that was used as dispersant, despite of up to three days of dialysis. Therefore, untreated samples were size-fractionated from the same or similar subsurface depth, in cases where previous sample preparation had consumed all material. Only soluble salts were removed by dialysis until chloride was no longer detected with  $\text{AgNO}_3$  solution. The  $<1 \mu$  fractions were collected by centrifugation and freeze-dried.

Major, minor, trace and rare earth element analyses were carried out by induction-

coupled plasma atomic emission spectrometry through the services of the Centre de Recherches Petrographiques et Geochimiques, Centre National de la Recherche Scientifique, Vandoeuvre, France (for accuracy and precision, see Appendix IV).

O-isotope analyses were conducted in collaboration with the Isotopic Laboratory in the Department of Geology, University of Western Ontario under the supervision of F.J. Longstaffe. Samples were pretreated at 200°C for 2 hours to remove adsorbed and interlayer water. Oxygen was extracted by fluorination according to Clayton and Mayeda (1963), and converted to CO<sub>2</sub> for which the isotopic composition was measured. Accuracy of the analyses was checked by monitoring the δ<sup>18</sup>O of standard NBS-28 (9.64 ‰ relative to SMOW) analyzed in cycle with the samples. The mean δ<sup>18</sup>O value of the NBS-28 standard was 9.72 ‰.

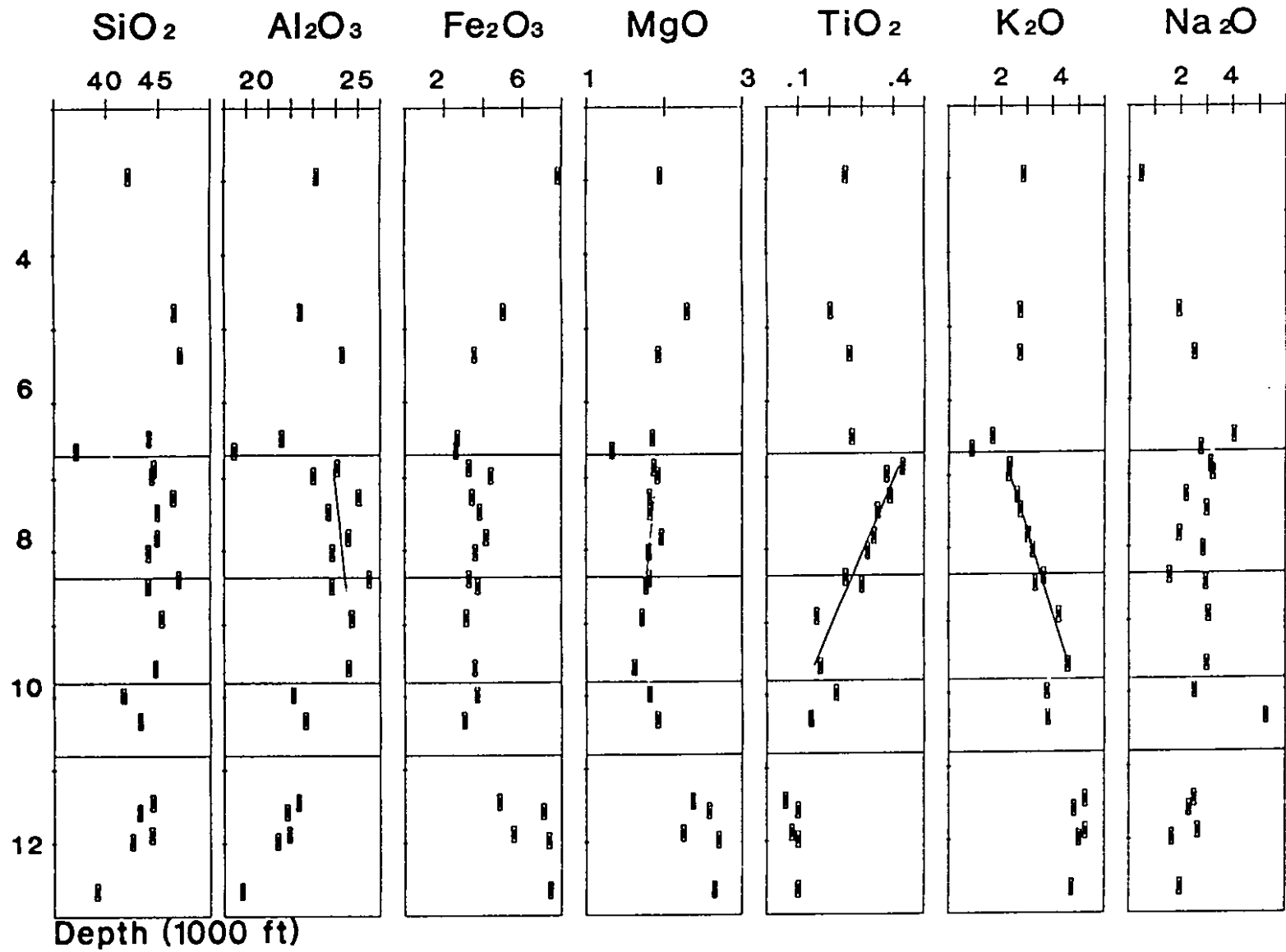
## RESULTS

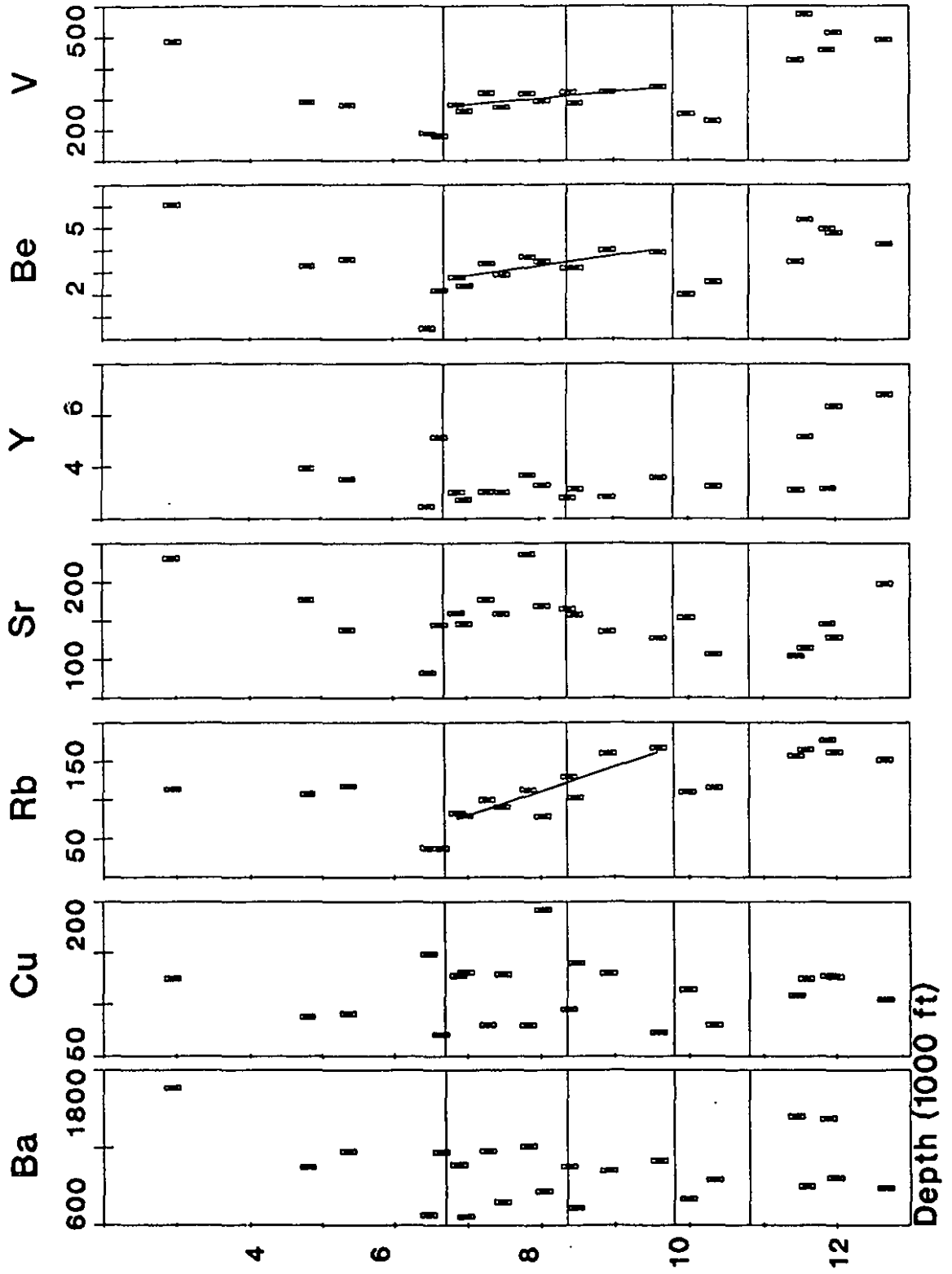
### Geochemistry

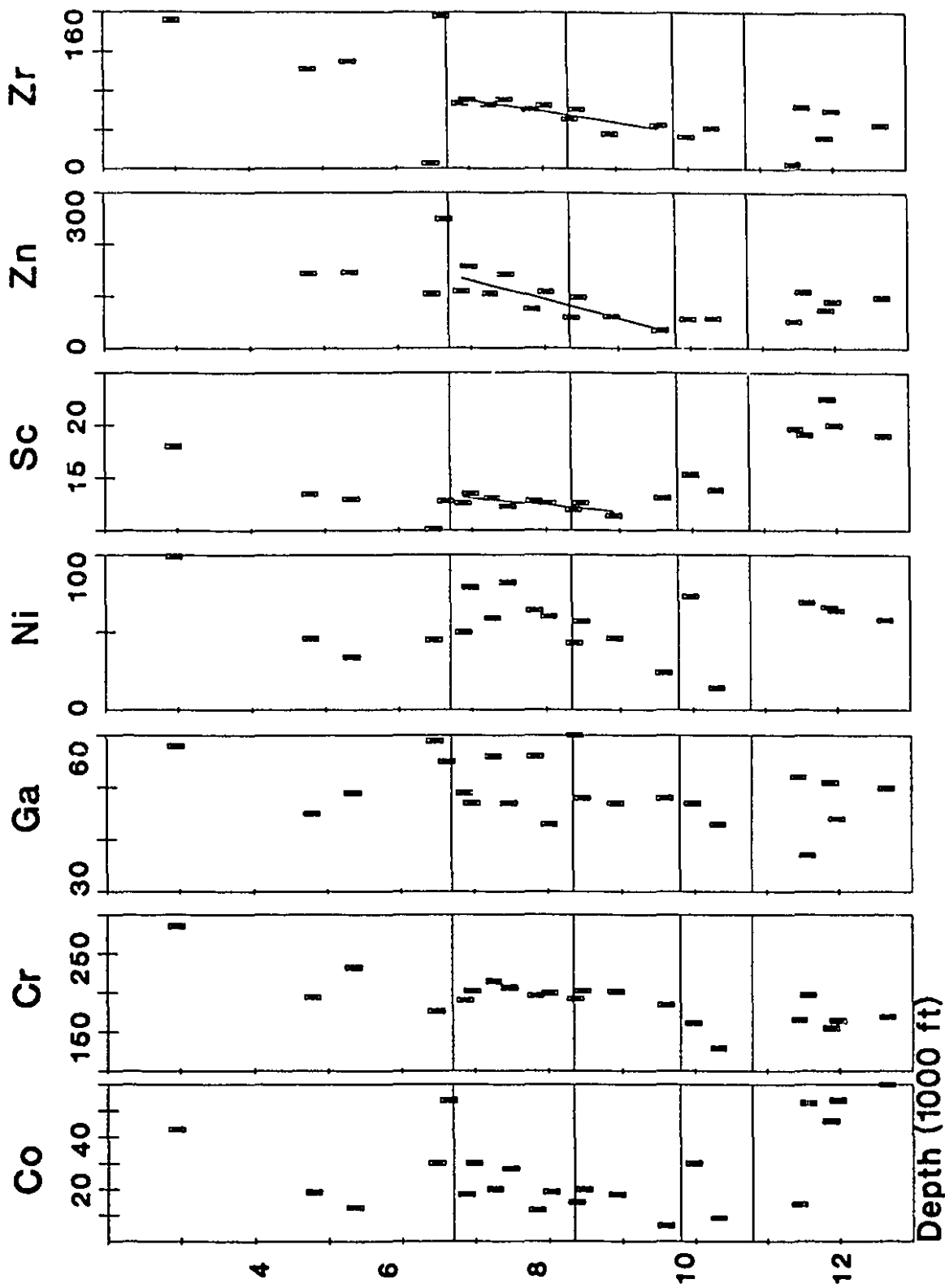
Concentrations of major, minor and trace elements are plotted with respect to depth and mineralogy in Figure V-1 (for data, see Appendix V). Figure V-2 shows the results of principal component analysis (PCA) for major, minor and trace elements and the scatter diagram of the data with respect to the first two principal components.

PCA is efficient, as a starting point, for differentiating samples in a multivariate data set, and identifying the most effective variables, i.e. elements that could be used to characterize samples. Elements having a positive correlation plot close together (e.g. Rb-K<sub>2</sub>O, Al<sub>2</sub>O<sub>3</sub>-SiO<sub>2</sub>), whereas elements having a negative correlation plot at great distance

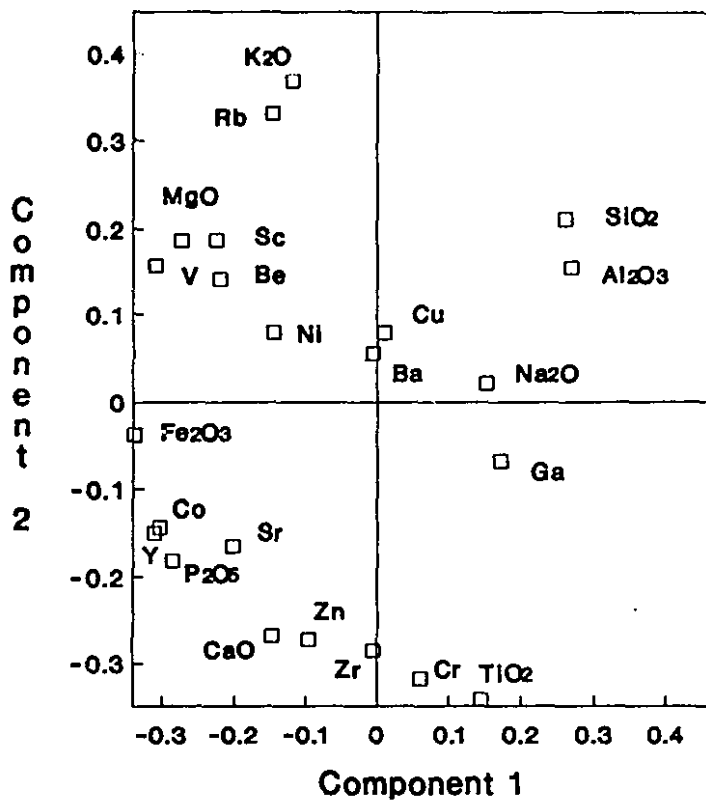
Figure V-1. Major and trace element concentrations in  $<.1 \mu$  fractions of the Reindeer D-27 well with respect to depth. For major elements, the unit is wt. %; for trace elements, ppm. Horizontal lines divide the intervals based on I/S mineralogy and composition:  $< 6700$  - random I/S; 6700-8350 - mixture of random and ordered I/S; 8350-10800 - R1-ordered I/S; 9800-10800 - lowered I-content;  $>10800$  ft - R $>1$ -ordered I/S (Cretaceous).







a)



b)

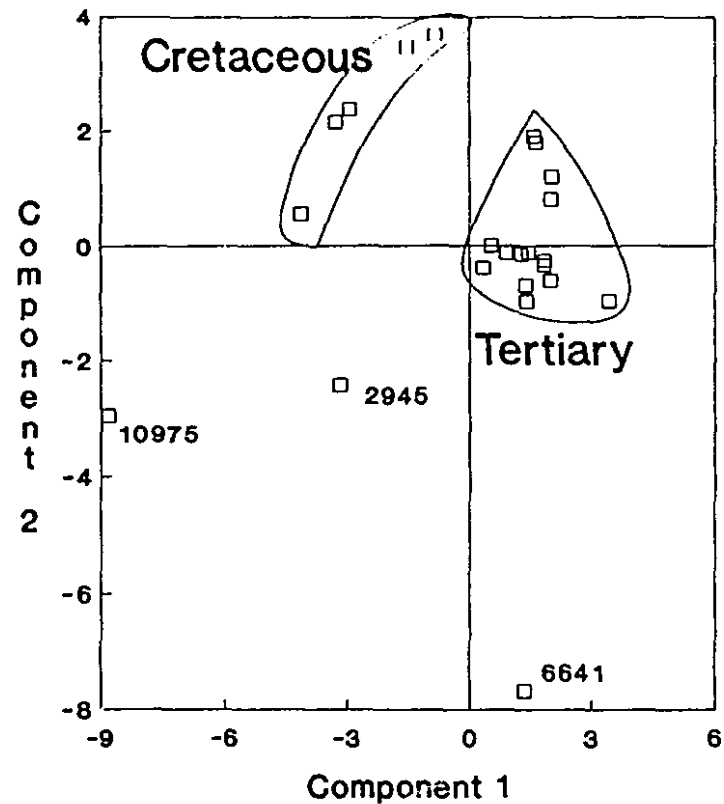


Figure V-2. Plots of principal component analysis. a) Principal components. b) Scatter diagram.

in the diagram (e.g.  $K_2O-TiO_2$ ). Elements showing least inter-sample variability plot close to the origin (e.g. Ba, Cu). As speculated on the basis of mineralogical data (see Chapter IV), the results show that Cretaceous samples are markedly different from Tertiary samples and plot in a separate field (Fig. V-2b). Three samples from the depths of 2945, 6641, and 10975 ft plot in isolation. Sample 2945 showed an unusually high I-content (92 %I) for the shallow burial depth where I/S is random. Sample 6641 is probably bentonitic. Sample 10975 contains a considerable amount of chlorite. These samples were excluded in further data analysis and interpretation.

### *Major elements*

Potassium and titanium display systematic antithetic trends with depth in the interval where ordered I/S appears (6700-9800 ft): concentrations of potassium increase, whereas those of titanium decrease (Fig. V-1). However, both elements do not show trends in the interval of random I/S. Concentrations of these elements are relatively uniform in the Cretaceous interval. A lower  $K_2O$  concentration is observed in the interval just above the Cretaceous section, for which mineralogical analyses indicated lowered I-contents of I/S.

Major structural, i.e. tetrahedral and octahedral, elements such as Si, Al, Fe and Mg do not display clear depth-trends, however, their behavior and/or concentrations are significantly different in intervals delineated on the basis of I/S mineralogy and composition (Fig. V-1). In the interval of random I/S, the data points for most elements are scattered, but some  $SiO_2$  concentrations are higher than in other intervals. In the interval where R1-ordered I/S appears, concentrations of  $Al_2O_3$  seem to increase with

depth, while concentrations of MgO decrease. In this interval, SiO<sub>2</sub> and Fe<sub>2</sub>O<sub>3</sub> concentrations are more or less uniform at about 44.95 % and 3.57 %, respectively. The Cretaceous interval is characterized by relatively low concentrations of SiO<sub>2</sub> and Al<sub>2</sub>O<sub>3</sub> and higher concentrations of Fe<sub>2</sub>O<sub>3</sub> and MgO compared to the Tertiary samples. This may be partly due to the presence of chlorite. However, core samples (11443, 12462 ft) that do not contain appreciable amounts of chlorite (see Chapter IV) also show different concentrations for these elements from the Tertiary. Therefore, the different chemical composition of the Cretaceous samples may also be due to the effect of provenance.

Interlayer cations other than K<sup>+</sup>, i.e. Na<sup>+</sup> and Ca<sup>2+</sup>, do not show systematic depth-trends. Nonetheless, these cations are negatively correlated with SiO<sub>2</sub> and Al<sub>2</sub>O<sub>3</sub> which are positively correlated with each other (Appendix VI). The apparent positive correlation between Al<sub>2</sub>O<sub>3</sub> and SiO<sub>2</sub> (Fig. V-3) is due to the presence of kaolinite in the samples. The molar ratios of Al<sub>2</sub>O<sub>3</sub> and SiO<sub>2</sub> in kaolinite do not vary significantly compared to I/S minerals. Variations in the abundance of kaolinite relative to I/S would modify the relative concentrations of Al<sub>2</sub>O<sub>3</sub> and SiO<sub>2</sub> with respect to other elements, and result in collinearity between Al<sub>2</sub>O<sub>3</sub> and SiO<sub>2</sub>. Concentrations of Na<sub>2</sub>O and CaO that occur exclusively in I/S of the fine clay fractions, decrease as the proportions of kaolinite increase, and vice versa.

### ***Trace elements***

Trace elements can be grouped into 4 categories based on ionic size, coordination, valency and behavior: interlayer, tetrahedral, octahedral, and adsorbed elements.

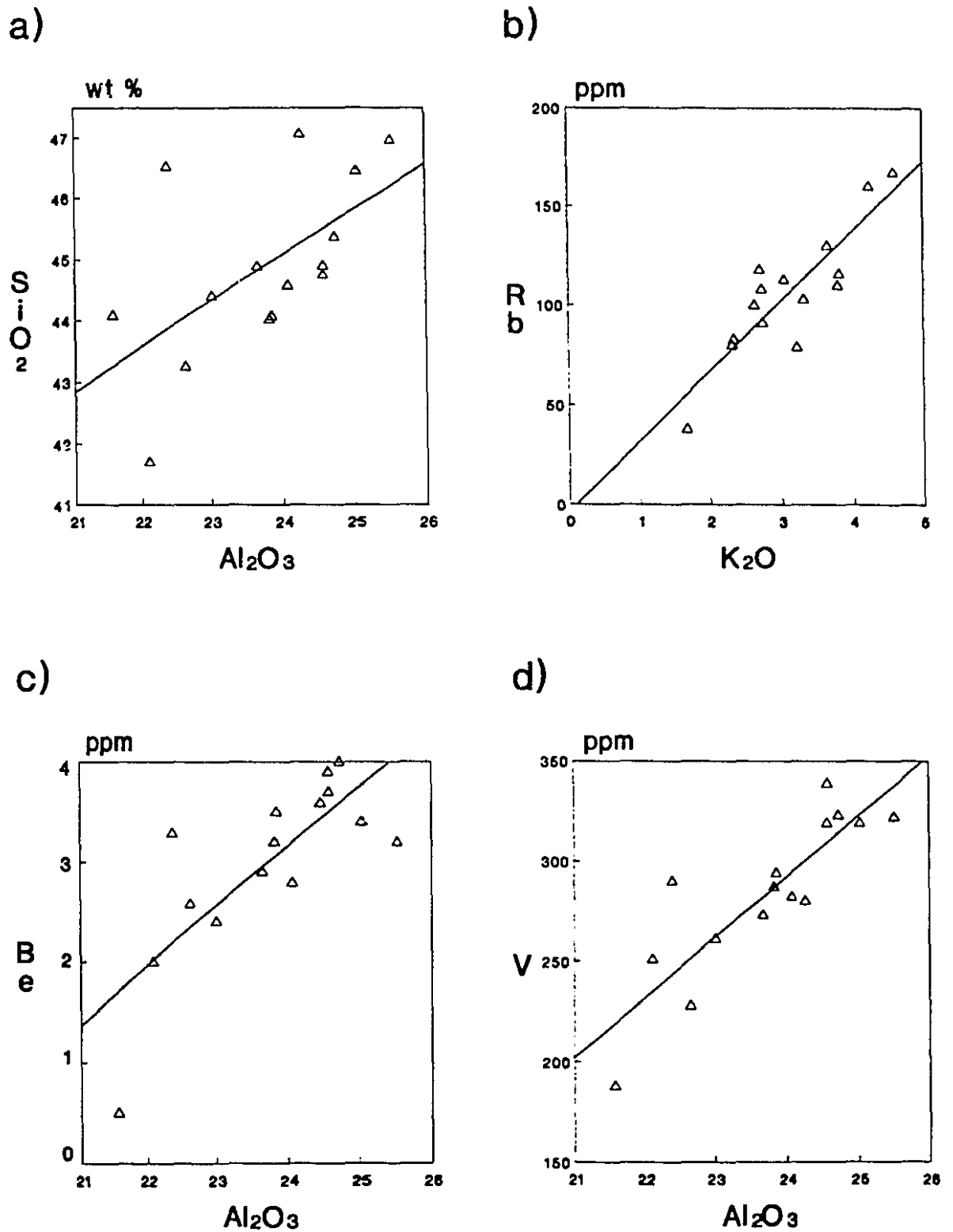


Figure V-3. Scatter plots of positively correlated elements. Cretaceous samples are not included. A.  $\text{Al}_2\text{O}_3$ - $\text{SiO}_2$ . B.  $\text{K}_2\text{O}$ -Rb. C.  $\text{Al}_2\text{O}_3$ -Be. D.  $\text{Al}_2\text{O}_3$ -V. For correlation coefficients, see Appendix VI.

Interlayer elements include Ba, Cu, Rb, Sr and Y. These elements are characterized by large ionic radii ( $>.8 \text{ \AA}$ ) and cubic coordination. Concentrations of Rb increase more or less linearly with depth (Fig. V-1), and show a positive correlation with  $\text{K}_2\text{O}$  (Fig. V-3). Concentrations of Ba, Cu, Sr and Y are variable.

Be and V, because of their relatively small ionic size, are candidates for tetrahedral occupancy. Concentrations of both elements increase with depth (Fig. V-1), and show positive correlations with  $\text{Al}_2\text{O}_3$  (Fig. V-3). Octahedral elements may include Co, Cr, Ga, Ni, Sc, Zn and Zr. These elements show a large difference in concentrations between Cretaceous and Tertiary intervals. The Cretaceous interval is characterized by higher Co, Sc, V, and lower Cr concentrations compared to the Tertiary interval. Concentrations of Sc, Zn and Zr decrease with depth in the Tertiary interval (Fig. V-1).

Nb and Th do not show a significant relationship to depth, stratigraphy or other elements (for data, see Appendix IV-2). This and very low concentrations ( $<5 \text{ ppm}$ ) suggest that these elements are probably not structurally bound, and may belong to the group of adsorbed elements.

#### ***Rare earth elements***

Concentrations of rare earth elements (REE) are considerably lower than North American shale composition (NASC) and clay minerals previously studied (Cullers et al., 1975; Chaudhuri and Cullers, 1979; Clauer et al., 1990) (Fig. V-4). However, the relative distribution of REE is similar to NASC, being enriched in light REE relative to heavy REE. La/Yb, La/Sm, Gd/Yb, and Sm/Eu ratios range between 11-38, 3-13, 2-4, 4-8, and

# REE Distribution

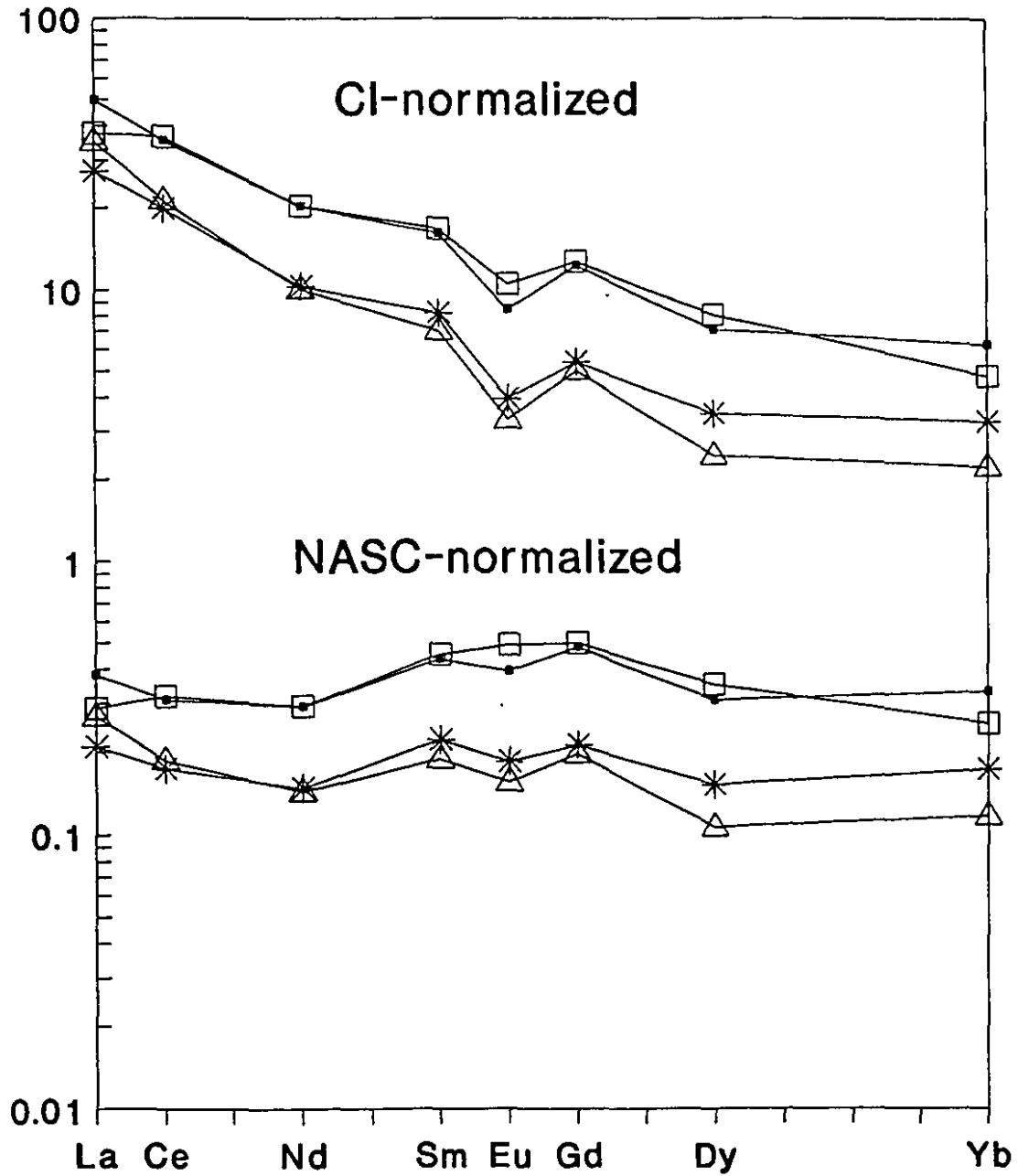


Figure V-4. Distribution of rare earth elements. CI - Chondrite I, NASC - North American Shale Composition.  $\Delta$  - Tertiary sample average, \* - Cretaceous sample average,  $\blacksquare$  - Sample 2945,  $\square$  - Sample 10975. For data, see Appendix V-3.

average 18.5, 6.7, 2.6 and 5.3, respectively.

Concentrations of light REE, especially La and Ce, increase with depth in the main interval of the Tertiary section (Fig. V-5). Both elements show strong positive correlations to  $Al_2O_3$ , Be and V (Fig. V-6). Correlations with  $K_2O$  and Rb, for which REE are supposed to substitute because of their large ionic size, though less obvious, are positive. No definite correlations with Y and Sc were detected, despite the chemical affinity of the REE to these elements.

Cretaceous samples are relatively depleted in light REE and enriched in heavy REE compared to Tertiary samples. Two samples, 2945 and 10975, which were significantly different in geochemistry and mineralogy from others, show a relatively high REE content.

### ***Structural formulae***

Several elements showed systematic trends in the depth range from about 6700 to 9800 ft. Structural formulae were calculated for I/S from that interval. It was assumed (i) that the total cationic-charge equals the total layer-charge  $q_T$ , (ii) that the octahedral charge  $q_o$  equals (No. of  $Mg^{2+}$  - No. of  $Ti^{4+}$  in the formula unit) and (iii) that the tetrahedral charge equals  $(q_T - q_o)$  (Table V-1). The excess and/or shortage of up to |.16| and |.26| for Si and Al, respectively, in the structural formula-unit were noted. These aberrations might be due to the presence of kaolinite, discrete illite (?) and probably amorphous phases (Foscolos and Powell, 1982). However, systematic corrections could not be made because of the small amounts of these impurities (e.g. <5 % for kaolinite).

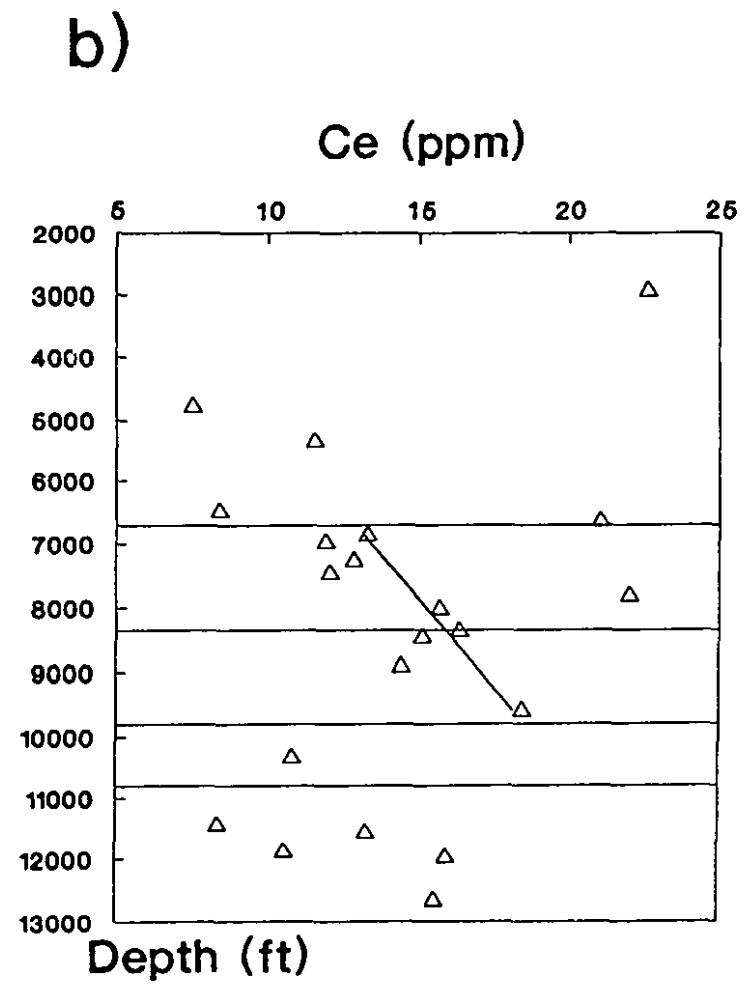
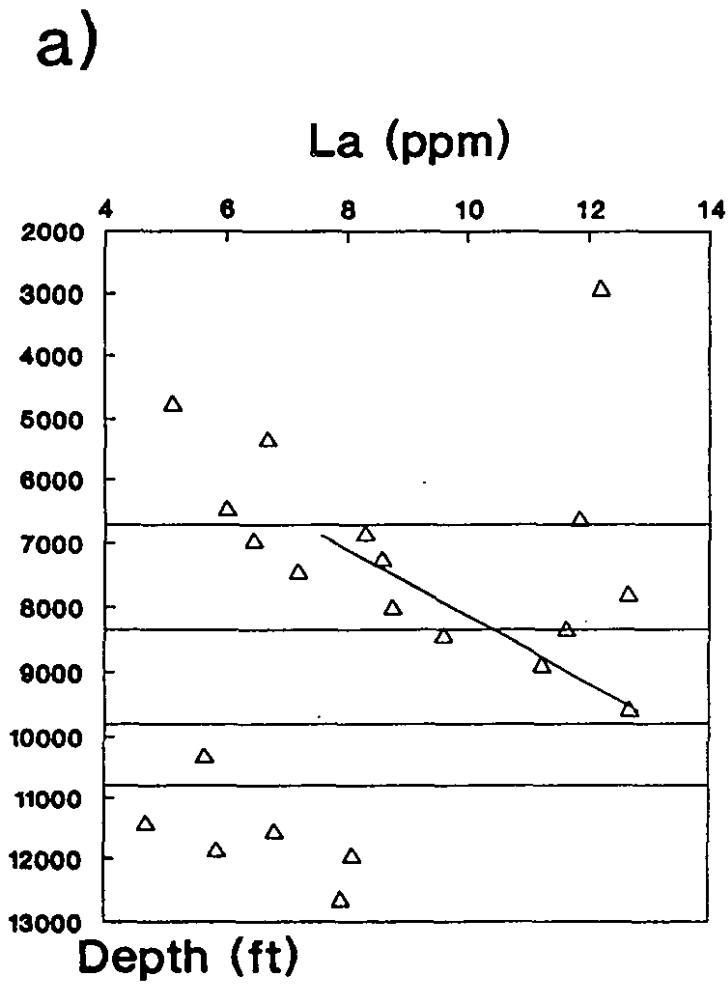


Figure V-5. (a) La and (b) Ce concentrations as function of depth. Horizontal lines delineate the same I/S divisions as in Figure V-1.

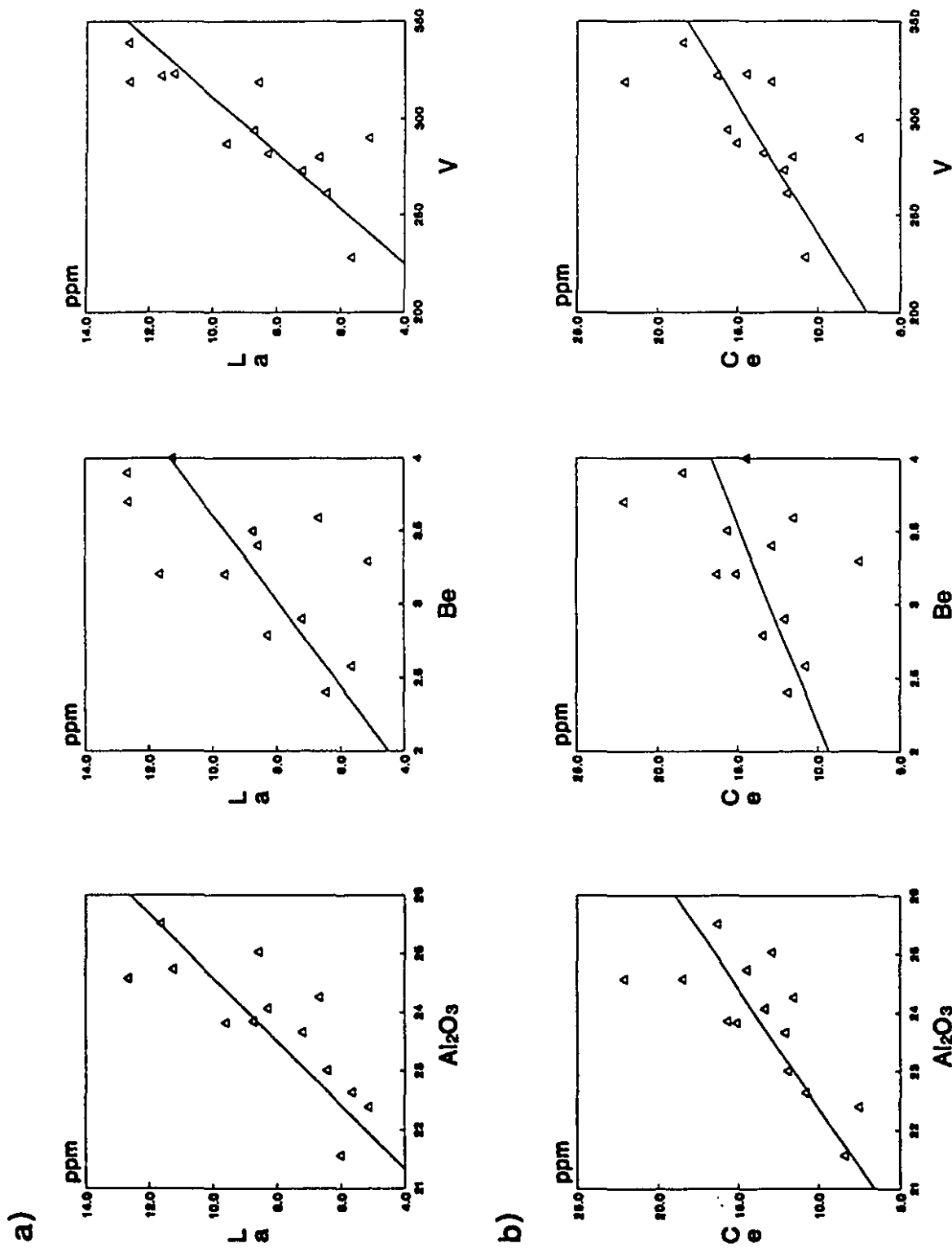


Figure V-6. Scatter plots of (a) La and (b) Ce concentrations with respect to  $Al_2O_3$ , Be, and V.

Semi-quantitative analysis by X-ray diffraction methods has a precision  $>\pm 5\%$  which is too large an error margin compared to the relatively small differences between samples. Discrete illite cannot be distinguished from elementary illite particles that were originally stacked in crystallites of I/S, but dissociate and contribute the intensity to peaks of discrete illite (see Chapter III). An exceptionally good alignment of  $K_2O$  data points for samples between 6475 and 9597 ft (correlation coefficient: .9858) suggests that most illite was originally part of I/S. Otherwise, the concentration of potassium would vary depending on the relative abundance of discrete illite present in the samples.

### Oxygen Isotopes

$\delta^{18}O$  values range from 2.91 to 15.72 ‰ (relative to SMOW), which are considerably lower than the Gulf Coast results of Yeh and Savin (1977).  $\delta^{18}O$  values generally increase with depth. This trend is opposite to that in the Gulf Coast where  $\delta^{18}O$  values decrease with depth.  $\delta^{18}O$  values increase linearly and relatively rapidly in the interval of random I/S (0.20 ‰/100 ft) (Fig. V-7). Between 6700 and 10028 ft the increase slows down, and the gradient flattens to about 0.03 ‰/100 ft. At 10329 ft, the value abruptly falls to 11.41 ‰. Low values of this magnitude continue down to 11443 ft. At 11575 ft, the  $\delta^{18}O$  returns to a high value of 14.54 ‰, below which depth little change was observed. At about the same depth (11600 ft), geophysical logs indicate the onset of geopressure in the Cretaceous section (Hitchon et al., 1990).

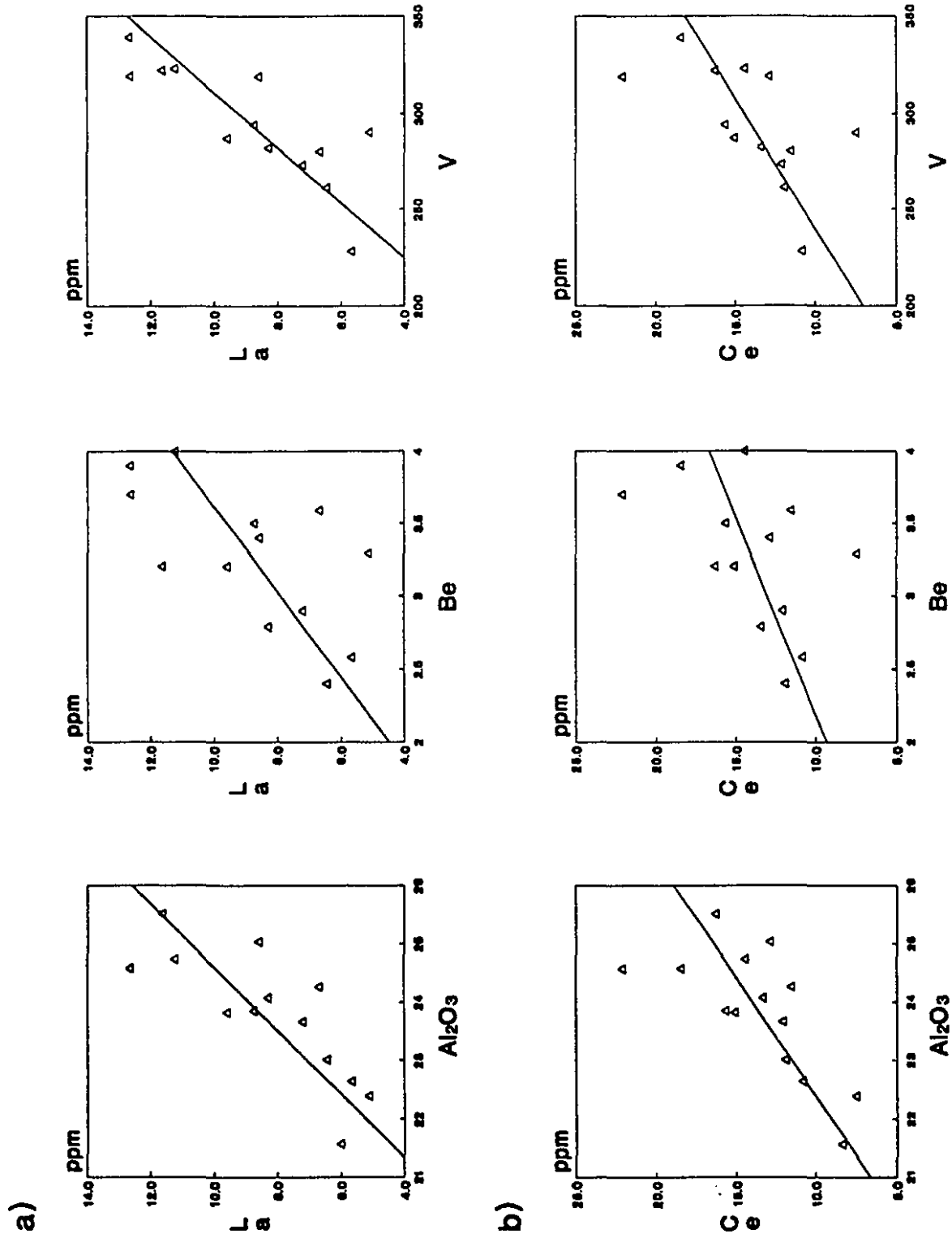


Figure V-6. Scatter plots of (a) La and (b) Ce concentrations with respect to Al<sub>2</sub>O<sub>3</sub>, Be, and V.

Table V-1. Structural formulae of I/S. Reindeer D-27.

Sample depth	Structural formulae
6475	$K_{1.17}Na_{0.62}Ca_{0.03}(Al_{1.63}Mg_{0.22}Fe_{0.16}Ti_{0.02})(Si_{3.35}Al_{0.65})O_{10}(OH)_2$
6872*	$K_{2.23}Na_{0.47}Ca_{0.04}(Al_{1.62}Mg_{0.21}Fe_{0.19}Ti_{0.03})(Si_{3.42}Al_{0.58})O_{10}(OH)_2$
6975	$K_{2.23}Na_{0.48}Ca_{0.05}(Al_{1.55}Mg_{0.22}Fe_{0.25}Ti_{0.02})(Si_{3.39}Al_{0.62})O_{10}(OH)_2$
7270*	$K_{2.25}Na_{0.32}Ca_{0.03}(Al_{1.63}Mg_{0.20}Fe_{0.19}Ti_{0.02})(Si_{3.56}Al_{0.44})O_{10}(OH)_2$
7475	$K_{2.27}Na_{0.44}Ca_{0.06}(Al_{1.60}Mg_{0.21}Fe_{0.22}Ti_{0.02})(Si_{3.36}Al_{0.64})O_{10}(OH)_2$
7825*	$K_{2.29}Na_{0.29}Ca_{0.05}(Al_{1.56}Mg_{0.22}Fe_{0.24}Ti_{0.02})(Si_{3.53}Al_{0.47})O_{10}(OH)_2$
8025	$K_{3.32}Na_{0.43}Ca_{0.06}(Al_{1.60}Mg_{0.21}Fe_{0.21}Ti_{0.02})(Si_{3.33}Al_{0.67})O_{10}(OH)_2$
8375*	$K_{3.34}Na_{0.23}Ca_{0.04}(Al_{1.64}Mg_{0.20}Fe_{0.18}Ti_{0.01})(Si_{3.55}Al_{0.45})O_{10}(OH)_2$
8475	$K_{3.33}Na_{0.44}Ca_{0.06}(Al_{1.60}Mg_{0.20}Fe_{0.22}Ti_{0.02})(Si_{3.30}Al_{0.70})O_{10}(OH)_2$
8915*	$K_{4.41}Na_{0.45}Ca_{0.02}(Al_{1.64}Mg_{0.19}Fe_{0.18}Ti_{0.01})(Si_{3.30}Al_{0.70})O_{10}(OH)_2$
9597*	$K_{4.44}Na_{0.44}Ca_{0.02}(Al_{1.62}Mg_{0.18}Fe_{0.20}Ti_{0.01})(Si_{3.26}Al_{0.74})O_{10}(OH)_2$

Sample depth- median depth for drill-cutting samples. \* - cores.

Semi-quantitative analysis by X-ray diffraction methods has a precision  $>\pm 5\%$  which is too large an error margin compared to the relatively small differences between samples. Discrete illite cannot be distinguished from elementary illite particles that were originally stacked in crystallites of I/S, but dissociate and contribute the intensity to peaks of discrete illite (see Chapter III). An exceptionally good alignment of  $K_2O$  data points for samples between 6475 and 9597 ft (correlation coefficient: .9858) suggests that most illite was originally part of I/S. Otherwise, the concentration of potassium would vary depending on the relative abundance of discrete illite present in the samples.

### Oxygen Isotopes

$\delta^{18}O$  values range from 2.91 to 15.72 ‰ (relative to SMOW), which are considerably lower than the Gulf Coast results of Yeh and Savin (1977).  $\delta^{18}O$  values generally increase with depth. This trend is opposite to that in the Gulf Coast where  $\delta^{18}O$  values decrease with depth.  $\delta^{18}O$  values increase linearly and relatively rapidly in the interval of random I/S (0.20 ‰/100 ft) (Fig. V-7). Between 6700 and 10028 ft the increase slows down, and the gradient flattens to about 0.03 ‰/100 ft. At 10329 ft, the value abruptly falls to 11.41 ‰. Low values of this magnitude continue down to 11443 ft. At 11575 ft, the  $\delta^{18}O$  returns to a high value of 14.54 ‰, below which depth little change was observed. At about the same depth (11600 ft), geophysical logs indicate the onset of geopressure in the Cretaceous section (Hitchon et al., 1990).

Figure V-7. Depth plot of  $\delta^{18}\text{O}$  values of I/S and calculated isotopic compositions of pore water according to Savin and Lee (1988). All values in SMOW. For I/S: \* - cores,  $\Delta$  - drill cuttings; pore water: +. Solid lines represent discontinuities in oxygen isotope trends. Dashed lines represent the same mineralogical divisions as in Figure V-1 (Note that a 8350 ft line is not shown). For data, see Table V-2.



## INTERPRETATION AND DISCUSSION

### Geochemistry

The difference in chemical composition, especially concentrations of several structural elements and probably REE, between Cretaceous and Tertiary samples indicates that they may not share a common provenance. Though the general source for both Cretaceous and Tertiary sediments is the Cordilleran orogen, the mode of deposition was significantly different. Flyschoid and molassoid sedimentation in the foreland basin of the rising Cordillera dominated the Cretaceous (Albian) depositional system. As the basin became mature, the fluvio-deltaic system with its depocentre in the Beaufort-Mackenzie Basin was established in the latest Cretaceous to Early Tertiary. Although the exact provenance of the I/S mixed-layer clays is not known, higher concentrations of MgO, Fe<sub>2</sub>O<sub>3</sub>, most octahedral and tetrahedral trace elements, and heavy REE in the Cretaceous samples suggest less silicic parental rocks.

Several elements showed systematic trends with respect to depth. Concentrations of octahedral elements generally decrease, while concentrations of tetrahedral elements increase with depth. Concentrations of interlayer elements other than K, Rb and REE do not show a definite trend. Among the elements assigned to various sites, Cu, Ga, Sc, Y, Zn, Zr and REE require some consideration. Cu was assigned to an interlayer position, because it did not show a trend or correlation with depth and other elements. Ga was dispensed as an octahedral element because of its chemical affinity to Al, though it did not show a relationship to depth, stratigraphy and other elements. Sc, Zn and Zr can be distributed either in interlayer or octahedral sites. However, octahedral sites were chosen,

because concentrations of these elements, as for other structural elements, were significantly different between Tertiary and Cretaceous intervals and/or changed systematically with depth. The decrease of Sc, Zn and Zr with depth is probably related to diagenesis, i.e. illitization of I/S (see further discussion below).

REE are expected to occupy interlayer sites because of their large ionic size. Concentrations of REE, especially light REE, increase with depth. They show relatively strong correlations to Be and V which may substitute for tetrahedral Al. The covariance of REE with Be and V is probably due to the valency increase caused by  $V^{5+}$  which could be partly counter-balanced by  $Be^{2+}$  and, in turn, the local valency deficiency caused by Be could be compensated by high-charge interlayer cations such as REE (+3). Therefore, the increase in concentrations of REE with depth is probably real, although they are considered extremely immobile. In the Gulf Coast, a similar increase in REE concentrations was observed (Chaudhuri and Cullers, 1979); however, it was interpreted as a provenance effect. In the Beaufort-Mackenzie Basin, the increase in REE concentrations is gradual over a depth range of 1 km (Fig. V-5), corresponding to the interval for which mineralogical analysis also established a linear increase in I-content of I/S from 55 to 78 %I. Therefore, the depth trend for the REE is attributed convincingly to diagenesis, rather than to provenance.

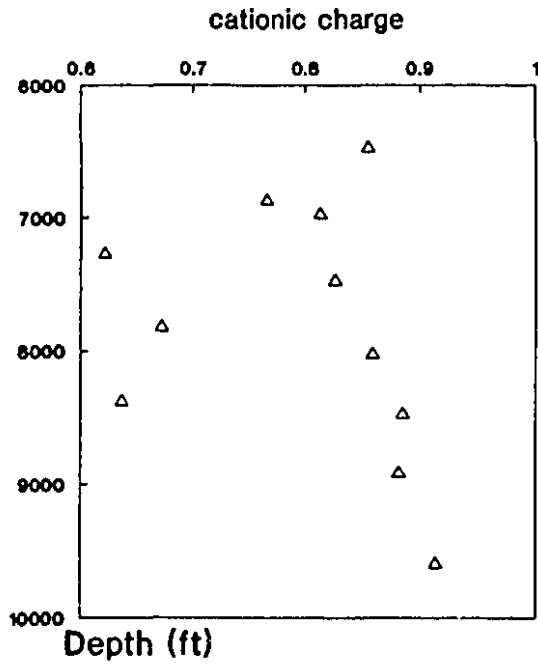
The behavior of structural elements is related to layer-charge development. It appears that octahedral sheets release elements such as Mg, Ti, Sc, Zn and Zr that differ in valency and/or ionic size from Al. The release of octahedral elements would decrease the overall layer-charge (see Fig. V-8). Fe and transition elements belonging to Groups VI

and VIII (Cr, Co and Ni) do not show a statistically significant variation with depth. These elements are di- and trivalent in six-fold coordination. They may better fit in octahedral sites than other elements in terms of valency and ionic size. The increase in Be, V and  $Al_2O_3$  is related to layer-charge development in tetrahedral sheets. To counter the charge increase caused by addition of these tetrahedral elements, Si should be released. However, the trend is obscured by the presence of kaolinite.

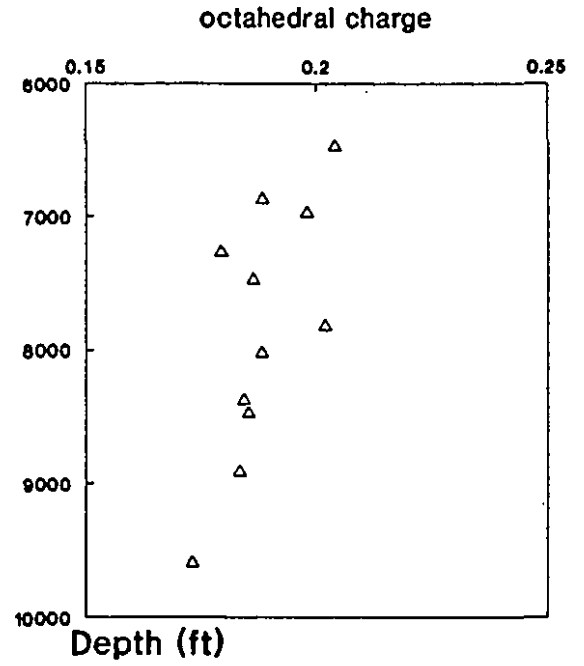
The curves for  $K_2O$  and Rb show a close correspondence to the mineralogical trends based on I/S varieties (for a detailed discussion of I/S burial trends, see Chapter III). Concentrations of  $K_2O$  increase linearly between 6700 and 9800 ft (.1 %/1000 ft) where the increase in the proportion of I-layers is also linear (~10 %I/1000 ft). The lack of regularity in the interval of random I/S is probably due to the occurrence of K and Rb in exchangeable interlayer positions. The depth interval of lower  $K_2O$  and Rb concentrations coincides with that of lower I-contents between 9800 and 10800 ft. Concentrations of  $K_2O$  and Rb are relatively uniform at about 5 % and 160 ppm, respectively, in the Cretaceous section where I-contents stay at about 86 %I.

The cationic charge of I/S increases with depth while the tetrahedral charge increases and the octahedral charge decreases (Fig. V-8). The overall changes in geochemistry and layer charges are related to illitization of I/S. If a stochastic model applies to I/S minerals, then the layer formulae would be obtained by extrapolating formula composition (Table V-1) to 0 and 100 %I, respectively (Fig. V-9), and the sum of [%I•(I-layer formula)] and [%S•(S-layer formula)] would approximate the individual structural formulae, and thus chemistry. The smectite-layers would have the formula

a)



b)



c)

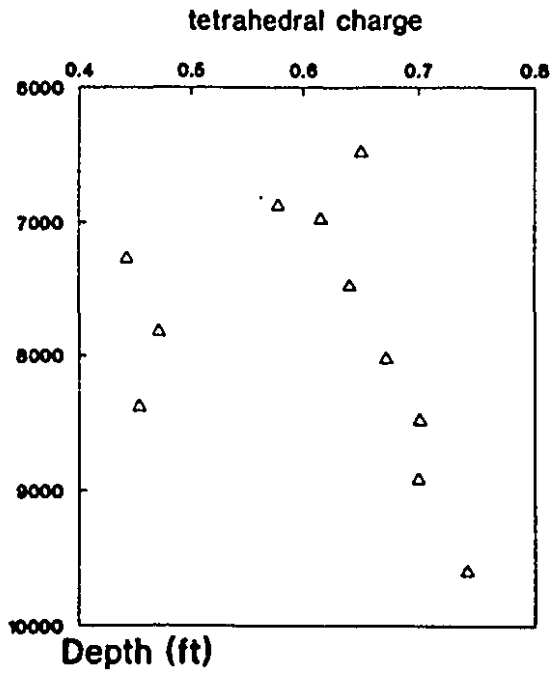


Figure V-8. Plots of cationic, octahedral, and tetrahedral charges with depth. For data, see Table V-1.

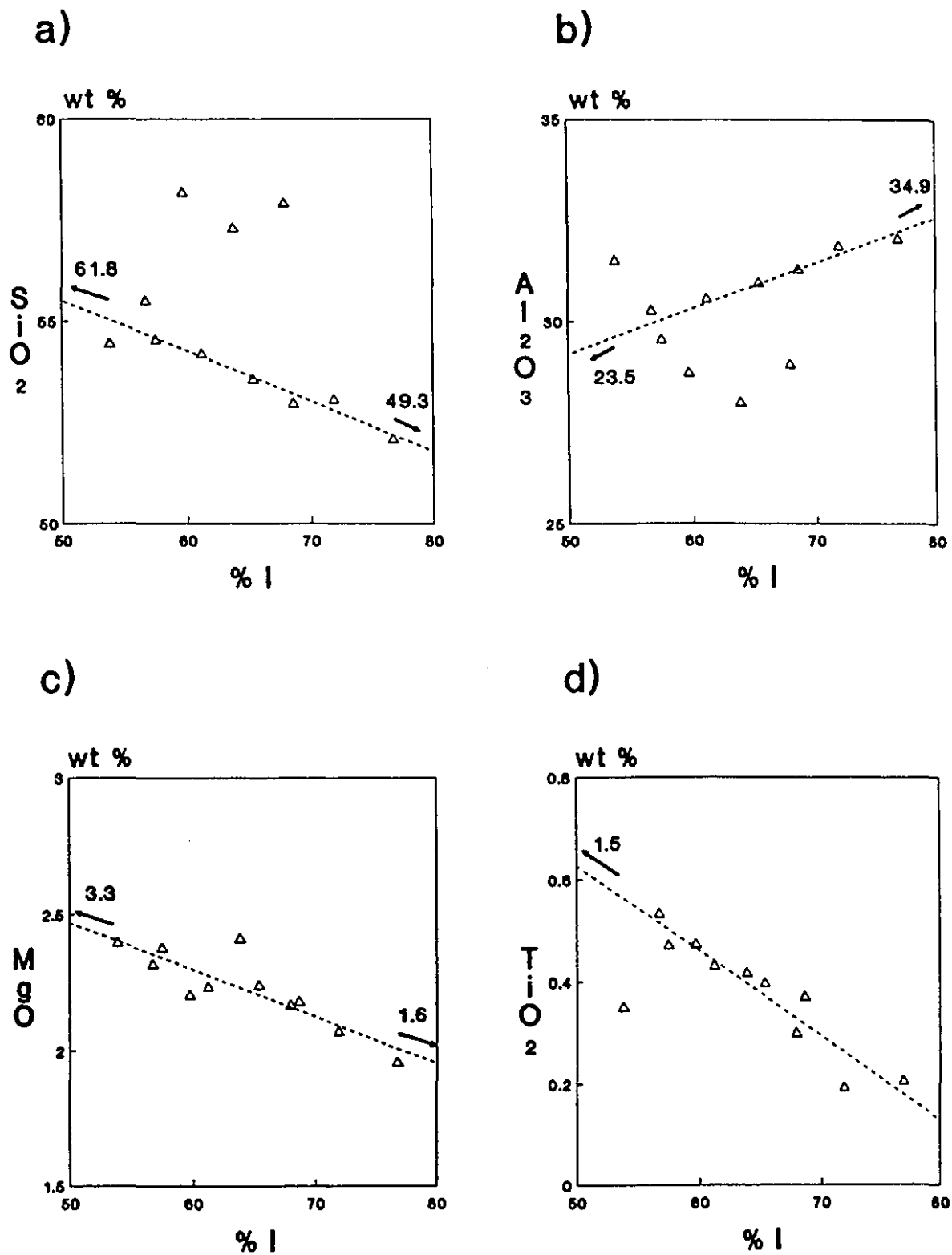


Figure V-9. Plots of SiO<sub>2</sub>, Al<sub>2</sub>O<sub>3</sub>, MgO and TiO<sub>2</sub> concentrations in a formula unit with respect to I-contents. Concentrations of these elements were calculated from the structural formulae in Table V-1 and normalized to 100 %. Numbers represent extrapolated values to 0 and 100 %I.

$[Al_{1.57}Fe_{.19}Mg_{.31}Ti_{.07}][Si_{3.84}Al_{.16}]O_{10}(OH)_2$ , and the illite-layers  $[Al_{1.84}Mg_{.16}][Si_{3.33}Al_{.67}]O_{10}(OH)_2$ . The resulting layer-formulae are similar to structural formulae for natural smectite and illite minerals.

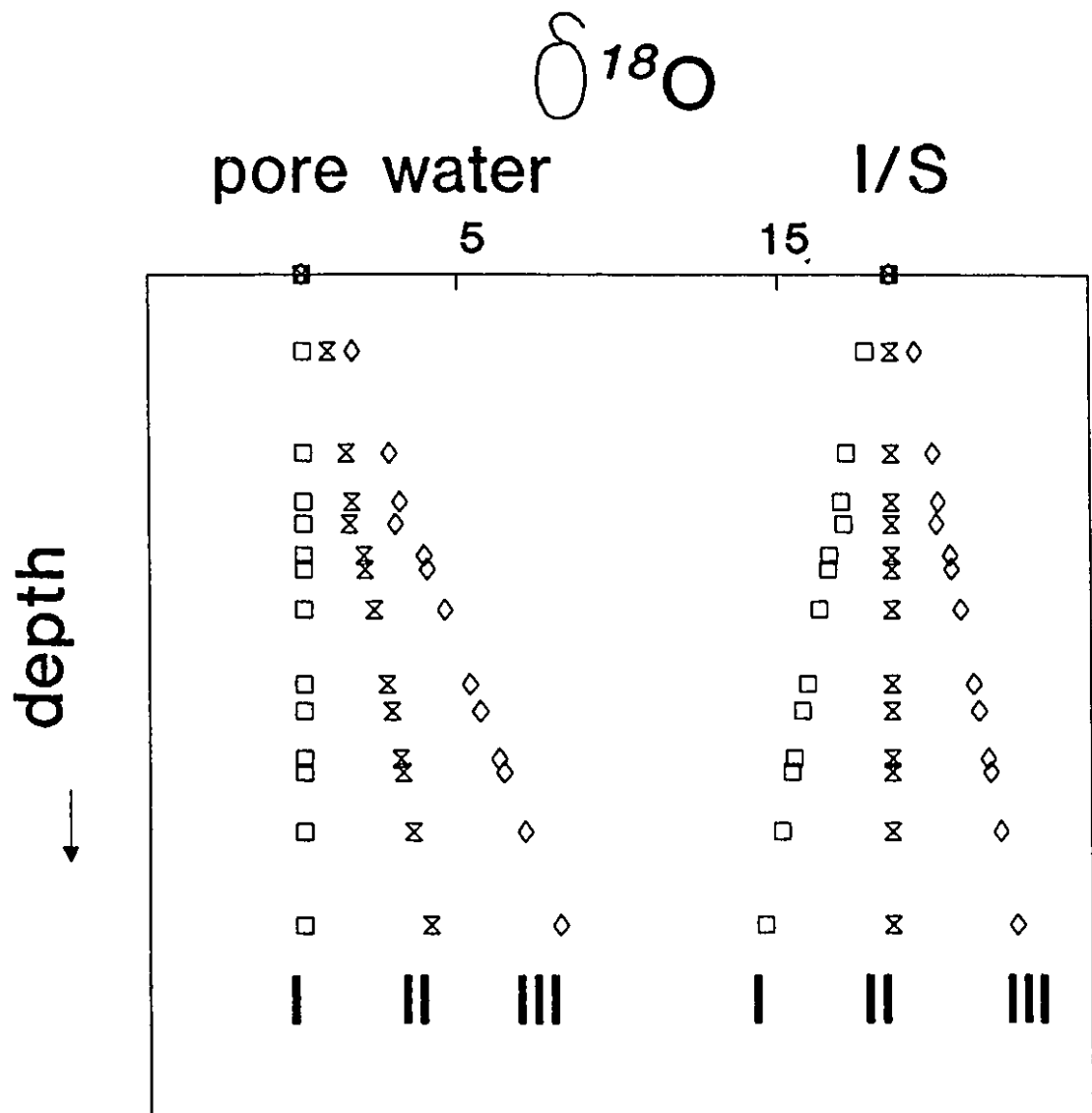
### Oxygen Isotopes

The relatively low  $\delta^{18}O$  values are due to sub-zero temperatures in the high latitudes where water/rock interaction at the surface is probably negligible; and also to  $^{18}O$ -depleted surface water resulting from the global fractionation of atmospheric, and thus meteoric waters ("Rayleigh effect").

The increase in  $\delta^{18}O$  values with depth is very unusual, because the burial increase in temperature and I-contents of I/S would shift the isotopic composition of I/S towards the lower values of pore waters. In the Gulf Coast and elsewhere,  $\delta^{18}O$  values of I/S decrease with depth (e.g. Yeh and Savin, 1977). Mathematical models predict that the  $\delta^{18}O$  of I/S in isotopic equilibrium with pore water would decrease with increasing burial depth (Suchecky and Land, 1983). However, if the variations in  $\delta^{18}O$  values of pore water ( $d\delta^{18}O_{\text{pore water}}$ ) exceed those due to thermal fractionation ( $d\Delta_{I/S\text{-water}}$ ), different profiles of  $\delta^{18}O$  for I/S would result (Fig. V-10). If  $d\delta^{18}O_{\text{pore water}} = -d\Delta_{I/S\text{-water}}$ ,  $\delta^{18}O_{I/S}$  will be constant. If  $d\delta^{18}O_{\text{pore water}} < -d\Delta_{I/S\text{-water}}$ ,  $\delta^{18}O_{I/S}$  will decrease with depth. If  $d\delta^{18}O_{\text{pore water}} > -d\Delta_{I/S\text{-water}}$ ,  $\delta^{18}O_{I/S}$  will increase with depth.

The isotopic composition of pore water (see Fig. V-1) was calculated according to Savin and Lee (1988):

$$1000 \ln \alpha_{I/S\text{-water}} = (2.58 - 0.19 \times I) \times 10^6 T^{-2} - 4.19$$



- I.  $\delta^{18}\text{O}_{\text{pore water}} = 0$
- II.  $d\delta^{18}\text{O}_{\text{pore water}} = -d \Delta_{\text{I/S-water}}$
- III.  $d\delta^{18}\text{O}_{\text{pore water}} > -d \Delta_{\text{I/S-water}}$

Figure V-10. Models depicting variable oxygen isotopic trends of I/S resulting from variations in  $\delta^{18}\text{O}$  of pore water. The relative depth and  $\Delta_{\text{I/S-water}}$  values are taken from Reindeer D-27 data.

where  $I$  = fraction of illite-layers which varies between 0.0 and 1.0 (Table V-2). The current geothermal gradient (.6°C/100 ft; Geotech Engineering, 1983) was assumed to correspond to the downhole temperature gradient. About 60°C was assumed to be the threshold temperature of active illitization (for rationale, see Chapter IV). This required that the observed I/S compositions were obtained at temperatures about 30°C higher than, or at depth about 5000 ft deeper than at present, which appear to be reasonable estimates conforming to the stratigraphy and the burial history based on basinal trends of I/S diagenesis (see Chapter IV).

The isotopic trends of the pore water suggest that at least two, but possibly as many as four water-masses, each having different isotopic evolution paths, might have existed (Fig. V-11a). A single curve could accommodate isotopic compositions other than those between 10329 and 11443 ft, i.e. pore waters might have evolved from water having an original O-isotopic composition of about -30 ‰ (Fig. V-11b). The value suggests that the original water was probably meteoric water (<-20 ‰ in the region at present). A discontinuity may exist at about 6700 ft (Fig. V-11a) where the increase in  $\delta^{18}\text{O}$  of I/S as well as pore water has slowed. Pore water below 6700 ft might have evolved from water having an original isotopic composition higher than that of the water above. However, at this depth no significant change in stratigraphy and facies is observed. The depth corresponds to the top of the interval where ordering of I/S takes place. Note that the extrapolation of  $\delta^{18}\text{O}$  values for ordered I/S and pore water, in general, does not produce the starting isotopic compositions (e.g. Whitney and Northrop, 1988, Fig. 8). Ordering probably involves a full-scale dissolution of I/S (for detailed discussion, see

Table V-2. Oxygen isotopic composition of I/S and calculated  $\delta^{18}\text{O}$  of pore water using I/S-water fractionation factors according to Savin and Lee (1988). \* - cores. \*\* - projected %I for samples without mineralogical data on the I/S trend curve (see Fig. IV-1).

Sample depth	$\delta^{18}\text{O}$ I/S	$\delta^{18}\text{O}$ water	Temperature, K	%I	$\Delta_{\text{I/S-water}}$
3700*	3.10	-	325.35	45	19.38
4782*	9.86	-8.67	331.84	40	18.55
5355*	10.89	-6.86	335.28	60	17.75
6113*	12.36	-4.80	339.83	60	17.16
6475	13.12	-3.87	342.00	54**	16.99
6641*	13.17	-3.89	343.00	42	17.06
6872*	14.44	-2.16	344.38	60	16.60
6975	13.57	-2.99	345.00	58**	16.56
7270*	14.96	-1.31	346.77	63	16.27
7825	14.84	-1.03	350.10	62**	15.87
8025	15.25	-0.46	351.30	65	15.71
8375*	15.72	0.29	353.40	79	15.43
8475	14.94	-0.41	354.00	69**	15.35
8915*	15.19	0.17	356.64	84	15.02
9597*	15.46	0.99	360.73	80	14.47
9975	14.98	0.64	363.00	73**	14.34
10028*	14.25	-0.04	363.32	74	14.29
10329*	11.41	-2.67	365.12	76	14.08
10475	10.86	-3.13	366.00	76**	13.99
10867*	10.36	-3.26	368.35	86**	13.62
10975	11.56	-2.00	369.00	86**	13.56
11443*	11.27	-2.05	371.81	84	13.32
11575	14.54	1.32	372.60	86**	13.22
11884*	14.33	1.26	374.45	84	13.07
11975	14.99	2.00	375.00	86**	12.99
12462*	14.75	1.99	377.92	86	12.76
12655	14.36	1.73	379.08	86	12.63

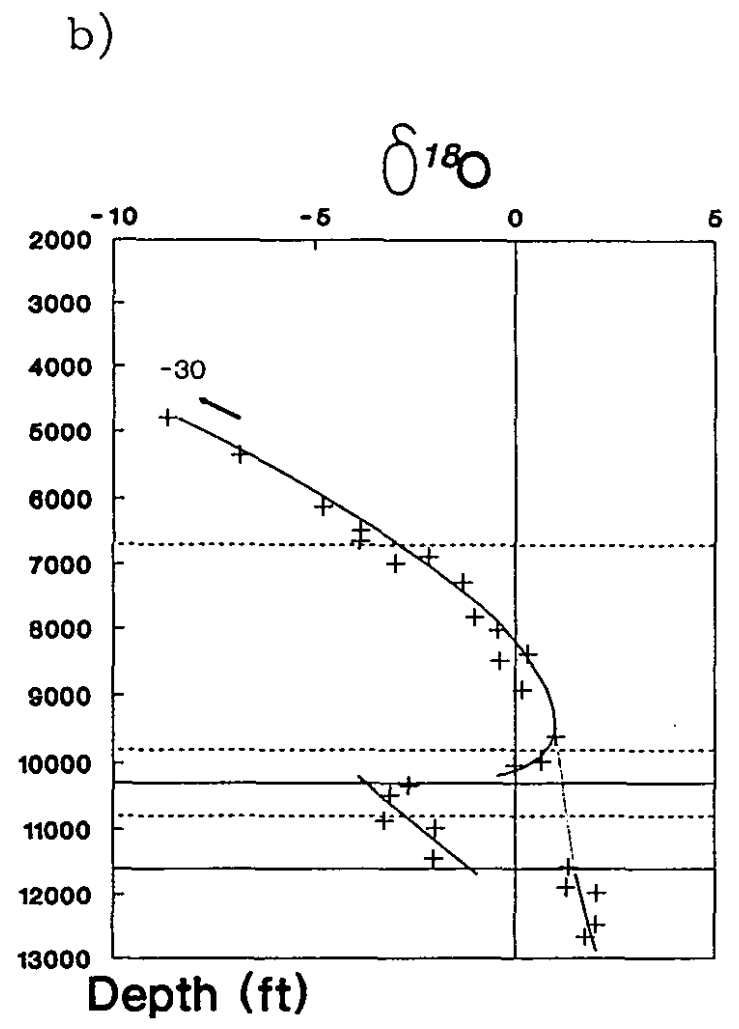
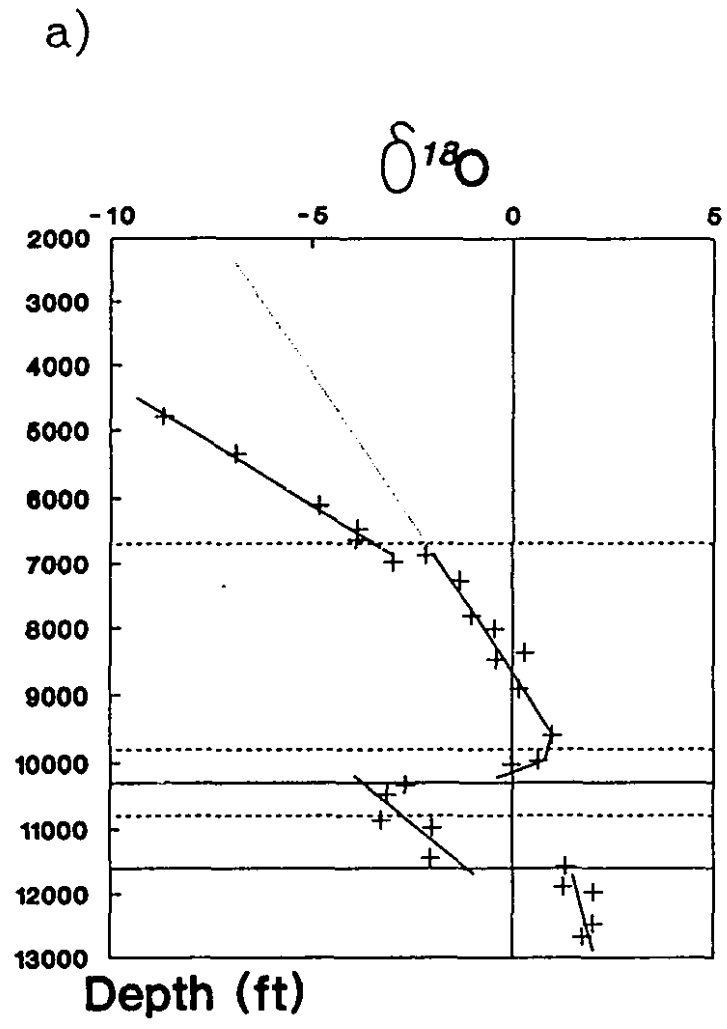


Figure V-11. Interpretation of the isotopic composition of pore water. a) Individual trends. b) Single curve with a low band of  $\delta^{18}O$ . Inflection at about 10000 ft is probably due to mixing.

previous chapters) and, therefore, a 100 % exchange of oxygen with pore water, compared to partial exchange in reactions of random I/S (up to 65 %; Whitney and Northrop, 1988). Thus, ordering might result in isotopic resetting of I/S. The subsequent isotopic trend could be related to  $\delta^{18}\text{O}$  values of I/S and pore water at the time of resetting, however, not to the original composition. The gentler slope is probably due to the slowness of the reaction compared to that of random I/S (see Chapter IV).

The low  $\delta^{18}\text{O}$  values between 10329 and 11443 ft are puzzling. The depth range overlaps, however, does not coincide with the interval of low I-contents and corresponding geochemical compositions (9800-10800 ft), implying that the rearrangement of structural oxygen may have taken place independently of chemical and mineralogical changes. The coincidence of the base of this interval with the top of the geopressure zone (11600 ft) suggests that the isotopic composition is related to the hydraulic regime. The inflection of  $\delta^{18}\text{O}$  to lower values at about 10000 ft indicates that mixing of water, probably upwards, may take place. However, the narrowness of the mixing zone suggests that the water in a compartment 1500 ft thick was effectively isolated from the waters above and below. If this is so, the geopressured Cretaceous water-mass below 11600 ft probably had no connection with the major Tertiary water, though the isotopic trend appears to continue after the gap of the anomalous zone in the Tertiary above.

The relative timing of emplacement, origin and nature of the isotopically light water-mass in the stratigraphic section encompassing the Tertiary and the Cretaceous (Albian) could be related to mineralogy and geochemistry of I/S in the interval. Cretaceous I/S from the interval does not show significant differences in composition and chemistry from

that below, whereas I/S from the Tertiary section is characterized by relatively low I-content and  $K_2O$  concentrations compared to that above. The water chemistry may have caused retarded illitization in the Tertiary section and, if so, I/S in the Cretaceous section had been illitized prior to the emplacement of this isotopically and chemically different water. The water might have a composition which inhibits the illitization process, or the relatively closed system hampers the efficient supply of ions essential for the reaction progress. Cannibalization of the internal source was probably insufficient to keep up the pace with the open system above.

## CHAPTER VI. CONCLUSIONS, CONTRIBUTIONS TO KNOWLEDGE, AND SUGGESTIONS FOR FUTURE RESEARCH

The burial diagenetic trends of I/S mixed-layer clays in the Beaufort-Mackenzie Basin have been scrutinized on the basis of mineralogical, geochemical, and isotopic analyses of core and drill-cutting samples from onshore and offshore wells.

Illitization in the Beaufort-Mackenzie Basin is characterized by the following four types of I/S: random, a mixture of random and ordered, R1-ordered, and R>1-ordered I/S. A mixture of random and ordered I/S is identified in a transitional, but separate interval from random to R1-ordered I/S. The widespread occurrence of the mixture suggests that mixed-layering in I/S may not be an artifact of interparticle diffraction between the fundamental particles. The fundamental particle hypothesis predicts that the mixture of smectite and R1-ordered I/S would produce X-ray diffraction patterns characteristic of random I/S (Nadeau et al., 1984a). X-ray diffraction patterns consisting of both random and ordered I/S support an alternative hypothesis that the natural I/S clays occur as Markovian crystallites in which illite- and smectite-layers are stacked together and neighbor each other.

K-saturation experiments provide a key insight into the mechanisms of the illitization reaction. Simple K-saturation alters the composition and/or the degree of ordering in I/S, suggesting that the illitization reaction in nature can be transformational. Ostwald ripening which assumes a unit- or about <5 cell size for I/S particles cannot explain the results of K-saturation.

Neoformation probably occurs at the transition from random to R1-ordered I/S.

Ordering requires large-scale mass transfer, because it involves re-sequencing of randomly arranged I- and S-layers into an orderly form. Therefore, dissolution of the whole crystallite might take place at this stage. The major changes in slope of mineralogical, geochemical, and isotopic trends occur in coincidence with the boundary where ordered I/S begins to appear. The mixture of random and ordered I/S may represent a metastable state in the ordering reaction. Dissolution under diagenetic conditions is usually very sluggish. Therefore, the metastable co-existence of reactants and products is not unusual. The thickness of the interval where mixtures of random and ordered I/S occur hints at the rate of the ordering reaction (e.g. 1650 ft in Reindeer D-27 that correspond to a time span of about 1.8 Ma). However, ordering does not appear to slow the illitization of I/S, since the I-content keeps increasing in the interval of a mixture of random and ordered I/S.

The proportion of I-layers in I/S mixed-layer clays increases with depth, while the dominant type of I/S changes from random I/S to a mixture of random and ordered I/S to R1-ordered I/S to R>1-ordered I/S. A temperature of about 60°C is probably the threshold temperature for activation of the illitization reaction. The increase in I-content is fast and shows a parabolic trend with respect to depth in the interval of random I/S, whereas it is slow and linear in the range of ordered I/S. For random I/S, potassium availability may be the rate-limiting factor. Below a certain depth, most random I/S acquired layer-charges high enough to form I/S of about 65 %I. However, illitization may not have progressed due to the lack of potassium. This may have been the cause for the absence of a systematic compositional trend in the interval of random I/S (e.g. Reindeer D-27, Taglu G-33).

The increase of I-contents in ordered I/S is gradual and continuous, suggesting that the reaction kinetics of ordered I/S may be first-order, regardless of the degree of ordering. Upon simple K-saturation, higher-ordered I/S and illite developed from R1-ordered I/S by transformation of high-charge expandable layers into I-layers through potassium fixation. Similarly, long-range ordered I/S and illite may develop from the R1-structure during burial diagenesis.

Geopressure in the Beaufort-Mackenzie Basin is facies-controlled (Hemingson and Carew, 1984; Hitchon et al., 1990). I/S diagenesis is probably of secondary importance in geopressure development. Illitization appears to be faster and more advanced in geopressured zones. The I/S reaction in geopressured environments may have been enhanced owing to the higher water/particle ratio compared to normally pressured conditions (cf. Whitney, 1990). Illitization in sandy intervals is also faster and more advanced than in shales for similar reasons. Higher porosity and permeability in sandy sediment increase the chances of encounters between I/S and pore water solutes.

The distribution of hydrocarbons in the Beaufort-Mackenzie Basin is closely related to I/S diagenesis. Hydrocarbons generally occur above and in the top part of the random I/S interval, but rarely below the depth where ordered I/S occurs. Deep hydrocarbon reservoirs are found in wells where illitization begins at relatively great depth (e.g. Taglu, Mallik). Where the apparent depth of illitization is shallow due to uplift, caused either by growth faults, diapirs or tectonics, hydrocarbons also occur at shallow depths (e.g. Reindeer). In offshore wells where the depth of illitization is 1 to 1.5 km shallower than onshore, many hydrocarbon discoveries were made at depths of 1-2 km.

Elemental geochemistry and oxygen isotopes provide a lilliputian view into the behavior of atoms in I/S, i.e. interlayer and structural cations and anions, respectively, during illitization. The behavior and concentrations of elements can be related to I/S composition that varies systematically with depth.

I/S in the Beaufort-Mackenzie Basin appears to consist of layers having the formulae of  $[Al_{1.57}Fe_{.19}Mg_{.31}Ti_{.07}][Si_{3.84}Al_{.16}]O_{10}(OH)_2$  and  $[Al_{1.84}Mg_{.16}][Si_{2.33}Al_{.67}]O_{10}(OH)_2$  for smectite- and illite-layers, respectively. The increase in concentrations of  $K_2O$ , Rb and REE, the decrease in concentrations of octahedral elements such as Mg, Ti, Sc, Zn and Zr, and the increase in concentrations of tetrahedral elements such as Be and V are attributed to the conversion of S-layers to I-layers with increasing depth. The conversion appears to involve the release of octahedral elements other than Al and probably Fe, Co, Cr and Ni. The presence or excess of ions which do not fit into di-octahedral sites of S-layers probably triggers their conversion to I-layers.

The increase in cationic contents of I/S, especially potassium and Rb, is counter-balanced by the increase in layer charge. The selective sorption of ions with low dehydration energy by high-charge layers would result in the formation of I-layers, and thus cause the increase in  $K_2O$  and Rb with depth compared to other interlayer elements (e.g.  $Na^+$ ,  $Ca^{2+}$ ) that do not show a systematic trend. The total layer-charge increases while the octahedral charge decreases and the tetrahedral charge increases. In other words, the layer-charge development reaction involves both octahedral and tetrahedral sheets.

The mobilization of REE appears to occur during illitization. Concentrations of REE,

especially La and Ce, increase with depth. This is probably linked to incorporation of ions with high valency (e.g.  $V^{5+}$ ) in tetrahedral sites. The excess valency due to V is partly counter-balanced by ions with low valency (e.g.  $Be^{2+}$ ) and, in turn, the local valency deficiency caused by Be could be compensated by high-charge interlayer cations such as REE (+3).

The behavior of the anion, i.e. oxygen, suggests that pore water may play an important role in illitization.  $\delta^{18}O$  values of I/S increase with depth, which contrasts with decreasing trends observed in the Gulf Coast and elsewhere. The isotopic composition of I/S depends on temperature, I-contents and the isotopic composition of pore water in equilibrium with the clays. The increase in  $\delta^{18}O$  of I/S is only possible, if the increase in  $\delta^{18}O$  of pore water was greater than the decrease in fractionation values resulting from increased temperature and I-contents with increasing burial depth.

Calculated  $\delta^{18}O$  values of pore water in equilibrium with I/S for the Reindeer D-27 well suggest that the original water was probably meteoric water with a composition of about -30 ‰. The stratification of pore water was postulated from the presence of the isotopically light interval, about 1500 ft thick. The depth range of the isotopically light zone overlaps, however, does not coincide with that of low I-contents and corresponding geochemical compositions, suggesting the isotopic re-equilibration.

### **Contributions to Knowledge**

The present knowledge of I/S diagenesis relies heavily on observations made in the U.S. Gulf Coast. This study provides a new basin-scale database on mineralogy,

geochemistry and oxygen isotopes of I/S mixed-layer clays in the Beaufort-Mackenzie Basin, which in some respects is comparable to the Gulf Coast in size and geology. The major contributions of this study are:

1. A widespread occurrence of a mixture of random and ordered I/S in natural environments has been reported for the first time in this study. The co-occurrence of random and ordered I/S signifies that I/S may not consist of "fundamental particles". The rate of the ordering reaction is estimated from the thickness of a transitional interval from random to R1-ordered I/S where the mixture occurs.
2. K-saturation experiments provide insight into the identity of I/S and the constituents in I/S. I/S consists of, at least, three components: illite, low-charge, and high-charge expandable layers. Changes in composition and the degree of ordering after K-saturation suggest that these components occur together as stacked layers in crystallites.
3. The relationship between fluid pressure and I/S diagenesis is first shown in field studies. Advanced illitization in geopressured zones supports Whitney's (1990) view that high water/particle ratios may promote dewatering of I/S, which involves chemical reactions such as layer-charge development and K-fixation.
4. Hydrocarbon occurrence shows an apparent relation to I/S diagenesis. This relationship between the two found in this study may apply to future exploration in the Beaufort-Mackenzie and adjacent basins.
5. The mobilization of REE during I/S diagenesis is convincingly demonstrated in this study. The increase in REE concentrations is related to the layer-charge development reaction in tetrahedral sheets, while the proportion of I-layers increases with depth.

6. Oxygen isotopes show the increase in  $\delta^{18}\text{O}$  values with depth, which is opposite to the trends observed in the Gulf Coast and elsewhere. To explain this unusual trend, a new model is devised.

### Suggestions for Future Research

Despite extensive knowledge and available databases for the illitization of smectitic material, too many conflicting ideas have been developed and left unresolved for the last 10 years. The present thesis attempts to clarify some of the controversial aspects on the basis of theoretical considerations, experimental and analytical data for I/S mixed-layer clays from the Beaufort-Mackenzie Basin. The following studies should be carried out after this investigation:

1. In order to obtain a better understanding of the unusual oxygen isotope trend in Reindeer D-27, 3 or 4 parallel investigations should be carried out using other stable and radioactive isotopes and other minerals such as hydrogen isotopes, K/Ar and the oxygen-isotope zonation in fine-grained quartz that may contain authigenic overgrowths. One such study (Rb/Sr of I/S) is presently under way at the Department of Geological Sciences at McGill (M.Sc. thesis of K. Sears, in progress), but this must be augmented by the other forementioned methods in order to elucidate the sources of the elements involved in the reactions and to evaluate the extent of the reactions occurring at different burial levels and times.
2. More detailed insight into layer-charge development and distribution could be obtained by applying the alkylammonium method in XRD studies rather than simple cation-

saturation. This method would be particularly efficient, if alkylammonium treatment was used in conjunction with TEM studies as shown by Vali et al. (1991).

3. Thermodynamic studies based on hydrothermal experiments should consider the colloidal nature of I/S mixed-layer clays. I/S in dispersions may behave very differently from that in rocks.

4. In addition, formation-water chemistry and chlorite evolution are subjects of further studies.

## REFERENCES

- Aagaard, P. and Helgeson, H.C., 1983. Activity/composition relations among silicates and solutions. II. Chemical and thermodynamic consequences of ideal mixing of atoms among energetically equivalent sites in montmorillonites, illites, and mixed layer clays: *Clays Clay Minerals*, v. 31, 207-217.
- Aja, S.U., Rosenberg, P.E., and Kittrick, J.A., 1991. Illite equilibria in solutions: I. Phase relationships in the system  $K_2O-Al_2O_3-SiO_2-H_2O$  between 25 and 250 °C: *Geochim. Cosmochim. Acta*, v. 55, 1353-1364.
- Altaner, S.P. and Bethke, C.M., 1988. Interlayer order in illite/smectite: *Am. Mineralogist*, v. 73, 766-774.
- Aronson, J.L. and Hower, J., 1976. Mechanism of burial metamorphism of argillaceous sediment. 2. Radiogenic argon evidence: *G.S.A. Bull.*, v. 87, 738-744.
- Baronnet, A., 1984. Growth kinetics of the silicates. A review of basic concepts: *Fortschr. Miner.*, v. 62, 187-232.
- Bell, T.E., 1986. Microstructure in mixed-layer illite/smectite and its relationship to the reaction of smectite to illite: *Clays Clay Minerals*, v. 34, 146-154.
- Bethke, C.M., Vergo, N. and Altaner, S.P., 1986. Pathways of smectite illitization: *Clays Clay Minerals*, v. 34, 125-135.
- Boles, J.R. and Franks, S.G., 1979. Clay diagenesis in Wilcox sandstones of southwest Texas: Implications of smectite diagenesis on sandstone cementation: *Jour. Sediment. Petrol.*, v. 49, 55-70.
- Bowerman, J.N. and Coffman, R.C., 1975. The geology of the Taglu gas field in the

- Beaufort Basin, Northwest Territories: in C.J. Yorath, E.R. Parker and D.J. Glass, eds., *Canada's Continental Margins*, Can. Soc. Petrol. Geol., Memoir 4, 649-662.
- Brindley, G.W., 1966. Ethylene glycol and glycerol complexes of smectites and vermiculite: *Clay Miner.*, v.6, 237-259.
- Bruce, C.H., 1984. Smectite dehydration-its relation to structural development and hydrocarbon accumulation in northern Gulf of Mexico basin: *A.A.P.G. Bull.*, v.68, 673-683.
- Burke, W.H., Denison, R.E., Hetherington, R.B., Koepnick, R.B., Nelson, H.F., and Otto, J.B., 1982. Variations of sea water  $^{87}\text{Sr}/^{86}\text{Sr}$  throughout Phanerozoic time: *Geology*, v. 10, 516-519.
- Burst, J.F., 1969. Diagenesis of Gulf Coast clayey sediments and possible relation to petroleum migration: *G.S.A.Bull.*, v. 53, 73-93.
- Chamney, T. P., 1973. Tuktoyaktuk Peninsula Tertiary and Mesozoic biostratigraphic correlations: *Geological Survey of Canada, Paper 73-1, pt. B*, 171-178.
- Chaudhuri, S. and Cullers, R.L., 1979. The distribution of rare-earth elements in deeply buried Gulf Coast sediments: *Chem. Geol.*, v. 24, 327-338.
- Clauer, N., O'Neil, J.R., Bonnot-Courtois, C., and Holtzapffel, T., 1990. Morphological, chemical, and isotopic evidence for an early diagenetic evolution of detrital smectite in marine sediments: *Clays Clay Minerals*, v. 38, 33-46.
- Clayton, R.N. and Mayeda, T.K., 1963. The use of bromine pentafluoride in the extraction of oxygen from oxides and silicates for isotopic analysis: *Geochim. Cosmochim. Acta.*, v. 27, 43-52.

- Colten-Bradley, V.A., 1987. Role of pressure in smectite dehydration-effects on geopressure and smectite-to-illite transformation: *A.A.P.G.Bull.*, v. 71, 1414-1427.
- Crowell, J.C., 1974. Origin of Late Cenozoic basins in southern California: in W.R. Dickinson, ed., *Soc. Econ. Paleon. Mineral., Spec. Publ.*, No. 22, 190-204.
- Cullers, R.L., Chaudhuri, S., Arnold, B., Lee, M., and Wolf, C.W.Jr., 1975. Rare-earth distributions in clay minerals and in the clay-sized fraction of the Lower Permian Havensville and Eskridge shales of Kansas and Oklahoma: *Geochim. Cosmochim. Acta.*, v. 39, 1691-1703.
- Daily, G.C., 1976. A possible mechanism relating progradation, growth faulting, clay diapirism and overthrusting in a regressive sequence of sediments: *Can. Petrol. Geol. Bull.*, v. 24, 92-116.
- Dickinson, W.R. and Suczek, C.A., 1979. Plate tectonics and sandstone composition: *A.A.P.G.Bull.*, v. 63, 2164-2181.
- Dietrich, J.R., Dixon, J. and McNeil, D.H., 1985. Sequence analysis and nomenclature of Upper Cretaceous to Holocene strata in the Beaufort-Mackenzie Basin: *Geological Survey of Canada, Paper 85-1A*, 613-628.
- Dixon, J., 1986. Cretaceous to Pleistocene stratigraphy and paleogeography, northern Yukon and northwestern District of Mackenzie: *Bull. Can. Petrol. Geol.*, v. 34, 49-70.
- Dixon, J. and Dietrich, J.R., 1990. Canadian Beaufort Sea and adjacent land areas: in A. Grantz, L. Johnson, and J.F. Sweeney, eds., *The Arctic Ocean Region: The Decade of North American Geology, The Geology of North America, Volume L*,

G.S.A., 239-256.

Dixon, J., Dietrich, J.R., McNeill, D.H., McIntyre, D.J., Snowdon, L.R. and Brooks, P., 1985. Geology, Biostratigraphy and Organic Geochemistry of Jurassic to Pleistocene Strata, Beaufort-Mackenzie Area, Northwest Canada: Can. Soc. Petrol. Geol., Course Notes.

Dixon, J., Morrell, G.R., Dietrich, J.R., Proctor, R.M., and Taylor, G.C., 1988. Petroleum Resources of the Mackenzie Delta-Beaufort Sea: Geological Survey of Canada, Open file, 1926, 74p.

Drever, J.J., 1973. The preparation of oriented clay mineral specimens for X-ray diffraction analysis by a filter-membrane peel technique: Am. Mineralogist, v. 58, 553-554.

Eberl, D.D. and Hower, J., 1976. Kinetics of illite formation: G.S.A. Bull., v. 87, 1326-1330.

Eberl, D.D. and Srodon, J., 1988. Ostwald ripening and interparticle diffraction effects for illite crystals: Am. Mineralogist, v. 78, p. 1335-1345.

Eberl, D.D., Srodon, J., Kralik, M. Taylor, B.E. and Peterman, Z.E., 1990. Ostwald ripening of clays and metamorphic minerals: Science, v. 248, 474-477.

Eberl, D.D., Srodon, J., Lee, M., Nadeau, P.H. and Northrop, H.R., 1987. Sericite from the Silverton caldera, Colorado: Correlation among structure, composition, origin, and particle thickness: Am. Mineralogist, v. 72, 913-934.

Eslinger, E. and Pevear, D., 1988. Clay Minerals for Petroleum Geologists and Engineers: SEPM Short Course Notes, v. 22.

- Espitalie, J. Madec, M. and Tissot, B., 1980. The role of mineral matrix in kerogen pyrolysis: Influence on petroleum generation and migration: A.A.P.G.Bull., v. 64, 59-66.
- Foscolos, A.E. and Kodama, H., 1974. Diagenesis of clay minerals from Lower Cretaceous shales of northeastern British Columbia: Clays Clay Minerals, v. 22, 319-335.
- Foscolos, A.E. and Powell, T.G., 1982. Mineralogical and geochemical transformation of clays during catagenesis and their relation to oil generation: in A.D. Miall, ed., Facts and Principles of World Petroleum Occurrence, Can. Soc. Petrol. Geol., Memoir 6, 153-172.
- Garrels, R.M., 1984. Montmorillonite/illite stability diagrams: Clays Clay Minerals, v. 32, 161-166.
- Geotech Engineering, 1983. Subsurface temperature data from Arctic wells: Earth Physics Branch, Energy, Mines and Resources, Ottawa, Open File 83-11.
- Goldstein, T.P., 1983. Geocatalytic reactions in formation and maturation of petroleum: A.A.P.G.Bull., v. 41, 152-159.
- Hawkings, T.J. and Hatlelid, W.G., 1975. The regional setting of the Taglu gas field: in C.J. Yorath, E.R. Parker and D.J. Glass, eds., Canada's Continental Margins. Can. Soc. Petrol. Geol., Memoir 4, 633-648.
- Hemingson, P. and Carew, W., 1984. Hydrocarbons & geopressures in the Beaufort-Mackenzie Basin: National Conference on Earth Sciences, Geopressures and hydrocarbon Occurrences, November 5-8, 1984, Banff, Alberta, Canada.

- Hitchon, B., Underschultz, J.R., Bachu, S., and Sauveplane, C.M., 1990. Hydrogeology, geopressure and hydrocarbon occurrences, Beaufort-Mackenzie Basin: *Bull. Can. Petrol. Geol.*, v. 38, 215-235.
- Howard, J.J., 1981. Lithium and potassium saturation of illite/smectite clays from interlaminated shales and sandstones: *Clays Clay Minerals*, v. 29, 136-142.
- Howard, J.J. and Roy, D.M., 1985. Development of layer charge and kinetics of experimental smectite alteration: *Clays Clay Minerals*, v. 33, 81-88.
- Hower, J., 1981. X-ray diffraction identification of mixed-layer clay minerals: in F.J. Longstaffe, ed., *Clays and Resource Geologist*, Mineral. Assoc. Canada, Short Course Handbook 7, 39-59.
- Hower, J., Eslinger, E.V., Hower, M.E., and Perry, E.A., 1976. Mechanism of burial metamorphism of argillaceous sediment: 1. Mineralogical and chemical evidence: *G.S.A. Bull.*, v. 87, 725-737.
- Hower, J. and Mowatt, T.C., 1966. The mineralogy of illites and mixed-layer illite/montmorillonite: *Am. Mineralogist*, v. 51, 825-854.
- Inoue, A., Bouchet, A., Velde, B. and Meunier, A., 1989. Convenient technique for estimating smectite layer percentage in randomly interstratified illite/smectite minerals: *Clays Clay Minerals*, v. 37, 227-234.
- Inoue, A., Kohyama, N., Kitagawa, R., and Watanabe, T., 1987. Chemical and morphological evidence for the conversion of smectite to illite: *Clays Clay Minerals*, v. 35, 111-120.
- Inoue, A., Velde, B., Meunier, A. and Touchard, G., 1988. Mechanism of illite formation

during smectite-to-illite conversion series by scanning and transmission electron microscopes: *Am. Mineralogist*, v.73, 1325-1334.

Jackson, M.L., 1969. *Soil Chemical Analysis-Advanced Course: 2nd Ed.*, Published by the author, Madison, Wisconsin, 895p.

Johns, W.D., 1979. Clay mineral catalysis and petroleum generation: *Ann. Rev. Earth Planet. Sci.*, v. 7, 183-198.

Johns, W.D., 1981. The role of the clay mineral matrix in petroleum generation during burial diagenesis: in H. van Olphen and F. Veniale, eds., *Developments in Sedimentology*, Vol. 35: *Proc. Int. Clay Conf.*, 655-644.

Johns, W.D. and Shimoyama, A., 1972. Clay minerals and petroleum forming reactions during burial diagenesis: *A.A.P.G.Bull.*, v. 56, 2160-2167.

Judge, A. and Bawden, W., 1987. Geothermal gradients: in *Marine Science Atlas of the Beaufort Sea: Geology and Geophysics*, Geological Survey of Canada, Misc. Report 40, p.7.

Lagaly, G., 1979. The "Layer Charge" of regular interstratified 2:1 clay minerals: *Clays Clay Minerals*, v. 27, 1-10.

Lagaly, G. and Weiss, A., 1975, The layer charge of smectitic layer silicates: *Proc. Int. Clay Conf. Mexico City*, v. 1, 157-172.

Lasaga, A.C., 1981. Rate laws of chemical reactions: in *Mineral. Soc. Amer., Reviews in Mineralogy*, Vol. 8, *Kinetics of Geochemical Processes*, A.C. Lasaga and R.J. Kirkpatrick, eds., 1-68.

Lee, J.H., Ahn, J.H., and Peacor, D.R., 1985. Textures in layered silicates: *Progressive*

- changes through diagenesis and low temperature metamorphism: *Jour. Sediment. Petrol.*, v. 55, 532-540.
- Mack, L.E., Awwiller, D.N., Erwin, M.E., and Long, L.E., 1990. Exchangeable Sr in mudrocks: Its utility in diagenetic studies: in G.S.A., 1990 Annual Meeting, *Abstr. with Prog.*, v. 22, p.A52.
- MacEwan, D.H.C., 1956. Fourier transform methods for studying scattering from lamellar systems. I. A direct method for analyzing interstitial mixtures: *Kolloid-Z.*, v. 149, 96-108.
- Magara, K., 1975. Reevaluation of montmorillonite dehydration as cause of abnormal pressure and hydrocarbon migration: *A.A.P.G. Bull.*, v. 59, 292-302
- Magara, K., 1976. Water expulsion from clastic sediments during compaction- directions and volumes: *A.A.P.G. Bull.*, v.60, 543-553.
- McNeil, D.H., 1985. Tertiary foraminiferal biostratigraphy of the Beaufort-Mackenzie Basin: in Dixon, J., Dietrich, J.R., McNeil, D.H., McIntyre, D.J., Snowdon, L.R. and Brooks, P., *Geology, Biostratigraphy and Organic Geochemistry of Jurassic to Pleistocene Strata, Beaufort-Mackenzie Area, Northwest Canada*, *Can. Soc. Petrol. Geol., Course Notes*, 32-38.
- Meunier, A. and Velde, B., 1989. Solid solutions in illite/smectite mixed layer minerals and illite: *Am. Mineralogist*, v. 74, 1106-1112.
- Moore, D.M. and Reynolds, R.C.Jr., 1989. *X-Ray Diffraction and the Identification and Analysis of Clay Minerals*: Oxford University Press, New York, 332p.
- Morton, R.A. and Land., L.S., 1988. Regional variations in formation water chemistry,

- Frio Formation (Oligocene), Texas Gulf Coast: A.A.P.G. Bull., v. 71, 191-206.
- Morton, J.P., 1985, Rb-Sr evidence for punctuated illite/smectite diagenesis in the Oligocene Frio Formation, Texas Gulf Coast: G.S.A. Bull., v. 96, 114-122.
- Nadeau, P.H. and Reynolds, R.C.Jr., 1981. Burial and contact metamorphism in the Mancos Shale: *Clays Clay Minerals*, v. 29, 249- 259.
- Nadeau, P.H., Tait, J.M., McHardy, W.J. and Wilson, M.J., 1984a. Interstratified XRD characteristics of physical mixtures of elementary clay particles: *Clay Miner.*, v. 19, 67-76.
- Nadeau, P.H., Wilson, M.J., McHardy, W.J., and Tait, J.M., 1984b. Interstratified clays as fundamental particles: *Science*, v. 225, 923-925.
- Nadeau, P.H., Wilson, M.J., McHardy, W.J., and Tait, J.M., 1984c. Interparticle diffraction: A new concept for interstratified clays: *Clay Miner.*, v. 19, 757-769.
- Nakano, T., Kajwara, Y., and Farrell, C.W., 1989. Strontium isotope constraint on the genesis of crude oils, oil-field brines, and Kuroko ore deposits from the Green Tuff region of northeastern Japan: *Geochim. Cosmochim. Acta*, v. 53, 2683-2688.
- Norris, D.K. and Yorath, C.J., 1981. The North American Plate from the Arctic Archipelago to the Romanzoff Mountains: in A.E.M. Nairns, M. Churkin, Jr. and F.G. Stehli, eds., *The Oceans, Basins and Margins*, v. 5, The Arctic Ocean, 37-103, Plenum Press.
- Norrish, K. and Ransell-Colom, J.A., 1963. Low angle X-ray diffraction studies of the swelling of montmorillonite and vermiculite: *Clays Clay Minerals*, v. 10, 123-149.
- Ohr, M., Halliday, A.N., and Peacor, D.R., 1991. Sr and Nd isotopic evidence for

- punctuated clay diagenesis, Texas Gulf Coast: *Earth Planet. Sci. Lett.*, v. 105, 110-126.
- Palmer, M.R. and Edmond, J.M., 1989. The strontium isotope budget of the modern ocean: *Earth Planet. Sci. Lett.*, v. 92, 11-26.
- Perry, E.A. and Hower, J., 1970. Burial diagenesis in the Gulf Coast pelitic sediments: *Clays Clay Minerals*, v. 18, 165-177.
- Pytte, A.M. and Reynolds, R.C.Jr., 1989. The thermal transformation of smectite to illite: in *Thermal History of Sedimentary Basins*, N.D. Naeser and T.H. McCulloh, eds., Springer-Verlag, New York, 133-140.
- Rettke, R.C., 1981. Probable burial diagenesis and provenance effects on Dakota Group clay mineralogy, Denver basin: *Jour. Sediment. Petrol.*, v. 51, 541-551.
- Reynolds, R.C.Jr., 1980. Interstratified clay minerals: in G.W. Brindley and G. Brown, eds., *Crystal Structures of Clay Minerals and their X-ray Identification*, Mineral. Soc. London, 249-304.
- Reynolds, R.C.Jr., 1985. NEWMOD<sup>®</sup>, a Computer Program for the Calculation of One-Dimensional Diffraction Patterns of Mixed-Layered Clays: R.C Reynolds, Jr., Dartmouth College, Hanover, New Hampshire.
- Reynolds, R.C.Jr., 1989. Diffraction by small and disordered crystals: in *Modern Powder Diffraction: Reviews in Mineralogy* vol. 20, *Miner. Soc. Am.*, 145-182.
- Reynolds, R.C.Jr. and Hower, J., 1970. The nature of interlayering in mixed-layer illite-montmorillonites: *Clays Clay Minerals*, v. 18, 25-36.
- Roberson, H.E. and Lahann, R.W., 1981. Smectite to illite conversion rates: Effects of

I  
solution chemistry: *Clays Clay Minerals*, v. 29, 129-135.

Russell, C.W., Cowart, J.B., and Russell, G.S., 1988. Strontium isotopes in brines and associated rocks from Cretaceous strata in the Mississippi salt dome basin (southeastern Mississippi, U.S.A.): *Chem. Geology*, v. 74, 153-171.

Sass, B.M., Rosenberg, P.E., and Kittrick, J.A., 1987. The stability of illite/smectite during diagenesis: An experimental study: *Geochim. Cosmochim. Acta*, v. 51, 2103-2115.

Savin, S.M. and Lee, M., 1988. Isotopic studies of phyllosilicates: in S.W. Bailey, ed., *Hydrous Phyllosilicates (exclusive of micas)*, *Reviews in Mineralogy*, vol. 19, 189-223.

Sawhney, B.L., 1966. Kinetics of cesium sorption by clay minerals: *Soil Sci. Soc. Amer. Proc.*, v. 32, 565-569.

Sawhney, B.L., 1972. Selective sorption and fixation of cations by clay minerals: A review: *Clays Clay Minerals*, v. 20, 93-100.

Schmidt, V., 1987. Petrological/diagenetic study of Upper Cretaceous and Tertiary strata, Beaufort-Mackenzie Basin: Geological Survey of Canada, Open file

Schultz, J.L., Boles, J.R., and Tilton, G.R., 1989. Tracking calcium in the San Joaquin basin, California: A strontium isotopic study of carbonate cements at North Coles Levee: *Geochim. Cosmochim. Acta*, v. 53, 1991-1999.

Snowdon, L.R. and Brooks, P., 1985. Organic geochemistry: in Dixon, J., Dietrich, J.R., McNeil, D.H., McIntyre, D.J., Snowdon, L.R. and Brooks, P., *Geology, Biostratigraphy and Organic Geochemistry of Jurassic to Pleistocene Strata*,

- Beaufort-Mackenzie Area, Northwest Canada, Can. Soc. Petrol. Geol., Course Notes, 51-65.
- Srodon, J., 1980. Precise identification of illite/smectite interstratification by X-ray powder diffraction: *Clays Clay Minerals*, v. 28, 401-411.
- Srodon, J., 1984. X-ray powder diffraction identification of illitic materials: *Clays Clay Minerals*, v. 32, 337-349.
- Stanley, K.O. and Benson, L.V., 1979. Early diagenesis of High Plains Tertiary vitric and arkosic sandstone, Wyoming and Nebraska: in P.A. Scholle and P.R. Schluger, eds., *Aspects of Diagenesis*, SEPM Spec. Publ., v. 26, 401-423.
- Starinsky, A., Bielski, M, Lazar, B., Wakshal, E., and Steinitz, G., 1980. Marine  $^{87}\text{Sr}/^{86}\text{Sr}$  ratios from the Jurassic to Pleistocene: Evidence from groundwaters in Israel: *Earth Planet. Sci. Lett.*, v. 47, 75-80.
- Stueber, A.M., Baldwin, A.D., Curtis, J.B.Jr., Pushkar, P., and Steele, J.D., 1975. Geochemistry of strontium in the Scioto River drainage basin, Ohio: *G.S.A. Bull.*, v. 86, 892-896.
- Stueber, A.M., Pushkar, P., and Hetherington, E.A., 1984. A strontium isotopic study of Smackover brines and associated solids, southern Arkansas: *Geochim. Cosmochim. Acta*, v. 48, 1637-1649.
- SucHECKI, R.K. and Land, L.S., 1983. Isotope geochemistry of burial metamorphosed volcanogenic sediments, Great Valley sequence, northern California: *Geochim. Cosmochim. Acta*, v. 47, 1487-1499.
- Vali, H. and Bachmann, L., 1988. Ultrastructure and flow behavior of colloidal smectite

dispersions: *J. Colloid Interface Sci.*, v. 126, 278-291.

Vali, H. and Hesse, R., 1990. Alkylammonium treatment of clay minerals in ultrathin section: A new method for HRTEM examination of expandable layers: *Am. Mineralogist*, v. 75, 1445-1449.

Vali, H., Hesse, R., and Kohler, E., 1991. Combined freeze-etched replicas and HRTEM images as tools to study fundamental particles and multiphase nature of 2:1 layer silicates: *Am. Mineralogist*, v. 76, 1973-1985.

Vali, H. and Köster, H.M., 1986. Expanding behaviour, structural disorder, regular and random irregular interstratification of 2:1 layer-silicates studied by high-resolution images of transmission electron microscopy: *Clay Miner.*, v. 21, 827-859.

Van Olphen, H., 1977. *An Introduction to Clay Colloid Chemistry*: Wiley, New York, 318p.

Velde, B. and Brusewitz, A.M., 1986. Compositional variation in component layers in natural illite/smectite: *Clays Clay Minerals*, v. 34, 651-657.

Warren, B.E. and Averbach, B.L., 1950. The effect of cold-work distortion on X-ray patterns: *Jour. Appl. Physics*, v.21, 595-599.

Watanabe, T., 1981. Identification of illite/montmorillonite interstratifications by X-ray powder diffraction: *Jour. Miner. Soc. Japan, Spec. Issue 15*, 32-41.

Whitney, G., 1990. Role of water in the smectite-to-illite reaction: *Clays Clay Minerals*, v. 38, 343-350.

Whitney, G. and Northrop, H.R., 1988. Experimental investigation of the smectite to illite reaction: Dual reaction mechanisms and oxygen-isotope systematics: *Am.*

Mineralogist, v. 73, 77-90.

Willumsen, P.S. and Cote, R.P., 1982. Tertiary sedimentation in the southern Beaufort Sea, Canada: in A.F. Embry and H.R. Balkwill, eds., Arctic Geology and Geophysics, Can. Soc. Petrol. Geol., Memoir 8, 43-54.

Yeh, H.W., 1980. D/H ratios and late stage dehydration of shales during burial: Geochim. Cosmochim. Acta, v. 44, 341-352.

Yeh, H-W. and Savin, S.M., 1977. Mechanism of burial metamorphism of argillaceous sediments: 3. O-isotope evidence: G.S.A.Bull., v. 88, 1321-1330.

Young, F.G., Myhr, D.W. and Yorath, C.J., 1976. Geology of the Beaufort-Mackenzie Basin: Geological Survey of Canada, Bull. 336, 63p.

Yorath, C.J. and Norris, D.K., 1975. The tectonic development of the southern Beaufort Sea and its relationship to the origin of the Arctic Ocean Basin: in C.J. Yorath, E.R. Parker and D.J. Glass, eds., Canada's Continental Margins, Can. Soc. Petrol. Geol., Memoir 4, 589-612.

Zen, E-An, 1962. Problem of the thermodynamic status of the mixed-layer minerals: Geochim. Cosmochim. Acta, v. 26, 1055-1067.

Zheng, Y.F., 1989. Influences of the nature of the initial Rb-Sr system on isochron validity: Chem. Geol., v. 80, 1-16

## **APPENDICES**

- I. Sample wells, depths and I/S composition.
- II. Changes in I/S composition upon K-saturation.
- III. Stratigraphic data available for offshore wells.
- IV. Accuracy and precision of geochemical analysis.
- V. Geochemical data- major, trace and rare earth element concentrations.
- VI. Correlation chart for 24 major, minor, trace and rare earth elements.

Appendix I. Sample wells, depths and I/S composition.

1) Reindeer D-27

Sample depth	saddle/ peak ratio	air-dried 003 <sub>1</sub> /004 <sub>s</sub> f.w.h.m. peak	Reich- weite	%I	Remarks	
2945	-	1.55	27.04	R>1	92	core
3700	.56	2.53	27.37	R0	45	core
4800	.46	2.69	27.62	R0	40	core
5330	.90	2.18	27.38	R0	60	core
6100	.90	2.38	27.50	R0	60	core
6000-6150	.81	2.59	27.50	R0	60	
6200-6250	.90	2.73	27.53	R0+R1	57	
6300-6350	.92	2.07	27.21	R0+R1	59	
6400-6450	.67	3.04	27.84	R0	47	
6500-6550	.28	2.60	28.17	R0	27	
6600-6650	.72	2.90	27.61	R0	52	
6641	.50	2.43	28.22	R0	42	core
6700-6750	.83	2.81	27.64	R0+R1	53	
6800-6850	.83	2.66	27.52	R0+R1	57	
6866	.90	2.67	27.54	R0	60	core
6900-6950	.86	2.67	27.58	R0+R1	56	
7000-7050	.53	2.82	27.70	R0	43	
7100-7150	.77	3.03	27.60	R0+R1	52	
7200-7250	.88	2.46	27.47	R0+R1	57	
7277	.96	2.25	27.41	R0	63	core
7300-7350	.90	2.43	27.46	R0+R1	58	
7400-7450	-	2.06	27.37	R0+R1	69	
7500-7550	.60	2.70	27.57	R0	46	
7600-7650	.93	2.33	27.45	R0+R1	59	
7800-7850	.94	2.37	27.45	R0+R1	62	
7855	-	2.04	27.32	R0+R1	75	core
7900-7950	-	2.12	27.38	R0+R1	63	

8000-8050	1	2.23	27.36	R0+R1	65	
8100-8150	1	1.95	27.31	R0+R1	65	
8200-8250	1	1.93	27.31	R0+R1	65	
8300-8350	-	1.88	27.33	R0+R1	70	
8375	-	1.78	27.31	R1	79	core
8400-8450	-	1.95	27.30	R1	69	
8500-8550	.98	2.16	27.35	R0+R1	64	
8600-8650	-	1.98	27.36	R1	69	
8700-8750	-	2.02	27.37	R1	71	
8800-8850	.84	2.95	27.64	R0+R1	57	
8915	-	1.53	27.22	R>1	84	core
8900-8950	-	1.84	27.31	R1	72	
9000-9050	-	1.84	27.25	R1	76	
9100-9150	-	1.81	27.28	R1	76	
9200-9250	-	1.72	27.31	R1	75	
9300-9350	-	1.68	27.28	R1	76	
9400-9450	-	1.78	27.30	R1	73	
9500-9550	-	1.73	27.23	R1	83	
9574	-	1.49	27.23	R>1	80	core
9600-9650	-	1.58	27.25	R>1	82	
9700-9750	-	1.69	27.28	R>1	80	
9800-9850	-	1.81	27.31	R1	75	
9900-9950	-	2.01	27.43	R1	71	
10000-10050	-	1.99	27.45	R1	73	
10028	-	1.66	27.44	R1	74	core
10100-10150	-	2.09	27.47	R1	70	
10200-10250	-	1.83	27.43	R1	74	
10300-10350	-	1.88	27.35	R1	77	
10329	-	1.70	27.41	R1	76	core
10400-10450	-	1.84	27.40	R1	76	
10500-10550	-	1.90	27.38	R1	77	

10600-10650	-	1.66	27.41	R1	76	
10700-10750	-	1.63	27.28	R1	76	
10800-10850	-	1.51	27.21	R>1	84	CHL
10867	-	1.73	26.95	R>1	94	core, CHL
10900-10950	-	1.43	27.10	R>1	88	CHL
11000-11050	-	1.46	27.00	R>1	92	CHL
11100-11150	-	1.38	27.10	R>1	88	CHL
11200-11250	-	1.38	27.13	R>1	87	CHL
11300-11350	-	1.46	27.17	R>1	85	chl
11400-11450	-	1.42	27.22	R>1	84	chl
11443	-	1.37	27.21	R>1	84	core
11500-11550	-	1.63	27.20	R>1	84	chl
11600-11650	-	1.37	27.21	R>1	84	chl
11700-11750	-	1.40	27.19	R>1	84	chl
11800-11850	-	1.41	27.22	R>1	83	chl
11884	-	1.34	27.21	R>1	84	core
11900-11950	-	1.36	27.20	R>1	84	chl
12000-12050	-	1.49	27.00	R>1	92	chl
12100-12150	-	1.30	27.16	R>1	86	chl
12200-12250	-	1.32	27.16	R>1	86	chl
12300-12350	-	1.39	27.13	R>1	87	chl
12400-12450	-	1.31	27.20	R>1	84	chl
12462	-	1.42	27.15	R>1	86	core
12500-12550	-	1.50	27.01	R>1	92	chl
12600-12650	-	1.32	27.20	R>1	84	chl
12650-12660	-	1.47	27.14	R>1	86	chl

1. Sample depth in feet.
2. Saddle/peak ratio of  $(001)_{10}/(001)_{17}$  for glycolated I/S.
3. f.w.h.m.- full width at half-maximum intensity in  $2\theta$  based on deconvolution of diffraction curves with a two peak model in the 3.3 Å region.  
peak- peak position in  $2\theta$ .
4. CHL- a large amount of chlorite present (10-50 %).  
chl- a small amount of chlorite present (usually <5 %).

2) Taglu C-42

Sample depth	saddle/ peak ratio	air-dried 003 <sub>1</sub> /004 <sub>s</sub> f.w.h.m. peak	Reich- weite	%I	Remarks	
8468	.11	N.A.	N.A.	R0	13	core
9436	.23	N.A.	N.A.	R0	24	core
9738	.40	N.A.	N.A.	R0	35	core
10000-10100	.28	N.A.	N.A.	R0	28	
10430	.98	1.97	27.47	R0+R1	64	core
10400-10500	.61	N.A.	N.A.	R0	46	
10508	-	2.06	27.42	R0+R1	71	core
10700-10800	.42	N.A.	N.A.	R0	37	
10900-11000	.66	N.A.	N.A.	R0	48	
11100-11100	.33	N.A.	N.A.	R0	30	
11200-12300	.46	N.A.	N.A.	R0	38	
11300-11400	.98	N.A.	N.A.	R0	63	
11500-11600	-	1.86	27.31	R1	77	
11600-11700	-	1.66	27.22	R1	78	
12100-12200	-	1.81	27.27	R1	68	
12400-12500	-	1.63	27.20	R1	70	
12700-12800	-	1.69	27.29	R1	71	
12900-13000	-	1.63	27.24	R1	77	
13500-13600	-	1.60	27.24	R1	75	
13700-13800	-	1.44	27.17	R1	68	
13800-13900	-	1.58	27.22	R1	80	
14500-14600	-	1.66	27.25	R1	78	
14700-14800	-	1.48	27.19	R≥1	82	
14900-15000	-	1.48	27.24	R≥1	80	
15200-15300	-	1.43	27.28	R≥1	80	
15400-15500	-	1.42	27.19	R>1	82	
15700-15800	-	1.47	27.33	R>1	79	
15900-16000	-	1.40	27.19	R>1	85	
16000-16060	-	1.50	27.25	R>1	82	

3) Wells in the vicinity of Reindeer and Taglu

a) Taglu G-33

Sample depth	Reichweite	%I
3124	R0	52
4427	R0	27
5376	R0	65
6254	R0	28
6817	R0	48
7489	R0	50
7637	R0	41
8058	R0	37
8279	R0	49
8443	R0	43
8525	R0	43
9271	R0	46

b) Kumak E-58

Sample depth	Reichweite	%I
3517	R0	52
3656	R0	47
3751	R0	31
3953	R0+R1	65
4028	R0	23

c) Niglintgak M-19

Sample depth	Reichweite	%I
3181	R0	54
3915	R0+R1	75
4254	R>1	83
4426	R0	44
8910	R1	74
9062	R1	71

d) Garry P-04

Sample depth	Reichweite	%I
5211	R0	28
5693	R0+R1	54
6644	R0	37
7617	R0	43
9852	R0+R1	66
10833	R0	42

e) Adgo C-15

Sample depth	Reichweite	%I
3238	R0	53
6086	R0	43
7704	R0+R1	63
9926	R1	61

f) Mallik A-06

Sample depth	Reichweite	%I
3128	R0	46
4040	R0	10
4470	R0	55
8656	R0+R1	65
9266	R0+R1	60
9655	R0+R1	65
9660	R0	50
10530	R0	22
11852	R0+R1	63

g) Ivik J-26

Sample depth	Reichweite	%I
5494	R0	29
8118	R0+R1	62
8219	R0+R1	59
8755	R0	30
10213	R0	40
10494	R0	54

h) Unark L-24A

Sample depth	Reichweite	%I
7280	R1	71
9696	R0	41
11624	R0	57
12778	R>1	81

4) Offshore wells

Sample well and depth	Reichweite	%I	
Netserk B-44	10391 ft	R0+R1	56
	10845 ft	R0+R1	64
Netserk F-40	6080 ft	R>1	80
Kadluk O-07	981 m	R0	56
	1483 m	R0	65
	1752 m	R0	65
	2402 m	R0	65
Nipterk L-19	1306 m	R0	54
	1650 m	R0	65
	1923 m	R>1	93
	2094 m	R>1	92
	2303 m	R≥1	92
	2511 m	R0	54
Tarsiut N-44	1558 m	R0	64
	1596 m	R0	24
	1647 m	R0	63
	2266 m	R≥1	80
Pitsiulak A-05	1701 m	R0+R1	80
Issungnak 20-61	2374 m	R1	87
	2494 m	R1	86
	2624 m	R1	84
	3306 m	R>1	83
Itiyok I-27	1507 m	R0	51
Alerk P-23	2019 m	R0+R1	55
	2799 m	R1	76

Amerk O-09	1313 m	R1	78
	1534 m	R0	62
	1765 m	R0	63
	2069 m	R0	52
	3861 m	R1	84
	4370 m	R>1	84
	4602 m	R≥1	77
	4866 m	R>1	76
Koakoak O-22	3486 m	R1	77
	4106 m	R>1	87
	>2700 m	R1	*
Kenalooak J-94	>2700 m	R1	*

\* drill-cutting samples contaminated by drilling mud.

Appendix II. Changes in I/S composition upon K-saturation.

1) Reindeer D-27

Sample depth	%I	
	Na	K
3700	45	47
4800	40	62
5330	60	65
6100	60	65
6100-6150	55	65
6500-6550	27	55
6641	42	64
6866	60	65
7277	63	65
7500-7550	46	65
7855	75	74
8000-8050	65	65
8375	79	86
8500-8550	64	75
8915	84	91
9000-9050	76	82
9500-9550	83	81*
9574	80	82
10000-10050	73	72*
10329	76	84
10500-10550	77	77
11443	84	89**
11500-11550	84	84**
11884	84	88**
12000-12050	92	88**
12462	86	89**
12500-12550	92	89**
12650-12660	86	91**

2) Taglu C-42

Sample depth	%I	
	Na	K
8468	13	33
9436	24	47
9738	35	62
10400-15000	46	63
10900-11000	48	65

3) Taglu G-33

Sample depth	%I	
	Na	K
3124	52	63
4427	27	48
5376	65	65
6254	28	53
6817	48	65
7489	50	65
7637	41	65
8058	37	65
8279	49	65
8443	43	65
8525	43	65
9271	46	65

\* - The apparent decrease is due to different methods used in estimating composition.

\*\* - X-ray diffraction patterns did not show differences upon K-saturation except for the increase in intensities of (001)<sub>illite</sub>.

**Appendix III.** Stratigraphic data available for offshore wells (based on formation-top determinations filed at the Institute of Sedimentary and Petroleum Geology, Calgary; courtesy of J. Dixon, 1988).

Well Name	Iperk	Akpak-Mackenzie Bay	Kugmallit	Richards	Reindeer
Netserk B-44	10	395	941	1951	2719
Netserk F-40	20	719	1423	2426	3773
Kadluk O-07	30	676	1126	2584	-
Tarsiut N-44	40	749	1325	2270	3143
Pitsiulak A-05	49	797	1392	-	-
Issungnak 20-61	11	1178	2240	-	-
Itiyok I-27	31	1185	1460	-	-
Alerk P-23	11	865	1033	-	-
Koakoak O-22	59	2814	3053	3595	-
Kenalooak J-94	80	missing	3625	?	4476

**Appendix IV.** Accuracy and precision of geochemical analysis (based on a brochure by the Centre Nationale de la Recherche Scientifique, Vandoeuvre, France).

1) Major, minor and trace element in standard DR-N (diorite).

Major and minor elements (wt %)  
(46 analyses)

Trace elements (ppm)  
(20 analyses)

	$\bar{x}$	s	RV
SiO <sub>2</sub>	52.65	0.19	52.85
Al <sub>2</sub> O <sub>3</sub>	17.59	0.07	17.52
ΣFe <sub>2</sub> O <sub>3</sub>	9.68	0.05	9.70
MnO	0.21	0.004	0.22
MgO	4.36	0.03	4.40
CaO	7.0	0.06	7.05
Na <sub>2</sub> O	2.92	0.02	2.99
K <sub>2</sub> O	1.71	0.02	1.70
TiO <sub>2</sub>	1.03	0.01	1.09
P <sub>2</sub> O <sub>5</sub>	0.28	0.01	0.25

	$\bar{x}$	s	RV	DL
Ba	370	13	386	5
Be	1.6	0.25	1.8	0.5
Co	33	2.7	35	5
Cr	39	4	42	5
Cu	55	4	50	5
Nb	7.6	1.1	6	5
Ni	22	4	16	5
Rb	65	1.6	70	5
Sc	30	0.3	28	1
Sr	385	3.6	400	5
V	219	12	225	5
Y	26.8	0.3	30	1
Zn	136	4.8	145	5
Zr	127	4.3	125	5
Ga	20		22	10
Th	6		5	

$\bar{x}$  - mean; s - standard deviation; RV - recommended value (Geostandards Newsletter, 1982, Vol. 6, p. 91-159); DL - detection limit.

2) Rare earth elements (25 analyses; ppm)

	$\bar{x}$	s	C%	RV
La	81.93	3.30	4.03	82
Ce	149.38	5.72	3.83	151
Nd	64.15	3.12	4.86	65
Sm	11.85	0.53	4.50	12
Eu	3.66	0.18	4.91	3.7
Gd	9.87	0.51	5.17	9.5
Dy	6.31	0.31	4.90	6.2
Yb	1.81	0.10	5.62	1.9
Y	31.32	1.55	4.95	30

C% - relative standard deviation. RV - recommended value (Geostandards Newsletter, 1988, Vol. 12, p. 119-201).

Appendix V. Geochemical data- major, trace and rare earth element concentrations (Reindeer D-27). Sample depth for drill cuttings - median depth in feet. \* - core samples.

1) Major elements (wt %)

Sample Depth	SiO <sub>2</sub>	Al <sub>2</sub> O <sub>3</sub>	FerO <sub>3</sub>	MnO	MgO	CaO	Na <sub>2</sub> O	K <sub>2</sub> O	TiO <sub>2</sub>	P <sub>2</sub> O <sub>5</sub>	LOI	Total
2945*	42.15	23.13	7.80	0.07	1.95	0.86	0.48	2.87	0.25	0.32	19.58	99.46
4782*	46.53	22.39	5.00	0.06	2.29	0.81	1.91	2.72	0.20	0.20	17.74	99.85
5355*	47.07	24.46	3.54	tr.	1.92	0.24	2.50	2.70	0.26	0.16	16.89	99.74
6475	44.09	21.57	2.70	tr.	1.85	0.35	4.04	1.67	0.27	0.26	22.94	99.74
6641*	37.14	19.46	2.62	tr.	1.33	2.29	2.77	0.88	1.10	0.54	31.62	99.75
6872*	44.57	24.07	3.29	tr.	1.87	0.44	3.15	2.33	0.43	0.22	19.43	99.80
6975	44.40	23.01	4.41	0.02	1.92	0.64	3.24	2.31	0.38	0.24	18.61	99.18
7270*	46.45	25.03	3.45	tr.	1.82	0.34	2.22	2.62	0.39	0.20	17.13	99.65
7475	44.89	23.66	3.83	tr.	1.82	0.72	3.00	2.74	0.35	0.22	18.69	99.32
7825*	44.90	24.57	4.16	tr.	1.97	0.59	1.95	3.04	0.34	0.20	17.86	99.58
8025	44.07	23.85	3.62	tr.	1.81	0.70	2.87	3.22	0.32	0.20	18.98	99.64
8375*	46.97	25.51	3.27	tr.	1.81	0.45	1.58	3.65	0.25	0.17	15.87	99.53
8475	44.02	23.82	3.74	tr.	1.77	0.72	2.97	3.32	0.30	0.20	18.86	99.72
8915*	45.37	24.73	3.16	tr.	1.72	0.19	3.08	4.24	0.16	0.16	16.59	99.40
9597*	44.75	24.57	3.59	tr.	1.62	0.20	3.00	4.58	0.17	0.14	16.74	99.36
9975	41.70	22.10	3.70	0.02	1.82	1.92	2.54	3.79	0.22	0.15	22.11	100.07
10329*	43.26	22.64	3.04	0.02	1.92	0.60	5.24	3.82	0.14	0.17	18.06	98.91
10975	29.95	14.82	16.73	0.71	2.56	1.58	2.66	2.70	0.08	1.12	26.39	99.30
11443*	44.47	22.32	4.83	0.06	2.37	0.20	2.52	5.25	0.06	0.26	17.08	99.42
11575	43.21	21.81	7.08	0.30	2.58	0.64	2.33	4.83	0.10	0.30	16.47	99.65
11884*	44.17	21.91	5.55	0.39	2.25	0.29	2.66	5.25	0.08	0.17	16.65	99.57
11975	42.53	21.39	7.34	0.50	2.70	0.96	1.67	5.00	0.10	0.40	17.03	99.62
12655	39.14	19.81	7.44	0.72	2.65	1.70	1.97	4.73	0.10	0.69	20.13	99.08

2) Trace elements (ppm)

Sample Depth	Ba	Be	Co	Cr	Cu	Ga	Nb	Ni	Rb	Sc	Sr	Th	V	Zn	Zr
2945*	1664	6.08	43	205	125	58	<5	99	114	18	231	15	488	443	152
4782*	1051	3.29	19	194	88	45	<5	46	108	14	177	<5	290	144	102
5355*	1172	3.59	13	232	91	49	<5	34	118	13	138	<5	280	146	110
6475	682	0.50	30	176	149	59	10	45	38	10	83	<5	188	104	5
6641*	1168	2.20	54	386	71	55	12	33	38	13	145	<5	180	249	156
6872*	1069	2.79	18	190	128	49	<5	50	83	13	160	<5	282	109	67
6975	667	2.40	30	202	131	47	5	79	80	14	146	<5	261	157	71
7270*	1176	3.40	20	214	80	56	<5	59	100	13	177	<5	319	105	66
7475	780	2.90	28	206	129	47	5	82	91	12	159	<5	273	142	71
7825*	1216	3.70	12	196	80	56	<5	64	113	13	236	<5	319	75	61
8025	854	3.50	19	199	192	43	<5	60	79	13	169	<5	294	108	65
8375*	1055	3.20	15	192	95	60	<5	43	130	12	165	<5	322	59	51
8475	736	3.20	20	202	140	48	<5	57	103	13	158	<5	287	98	61
8915*	1023	4.00	18	201	130	47	<5	46	160	11	136	<5	323	61	36
9597*	1101	3.90	6	184	73	48	<5	24	167	13	128	<5	339	35	45
9975	803	2.00	30	161	114	47	5	73	110	15	154	<5	251	56	33
10329*	952	2.58	9	129	80	43	<5	14	116	14	107	<5	228	57	42
10975	648	4.00	167	154	96	34	<5	75	114	15	285	<5	550	161	44
11443*	1444	3.50	14	165	109	52	<5	41	157	20	105	<5	427	51	5
11575	904	5.40	53	197	125	37	<5	69	165	20	115	<5	574	109	64
11884*	1430	5.00	46	155	128	51	<5	66	178	23	147	<5	461	74	32
11975	968	4.80	54	164	127	44	<5	64	162	20	129	9	515	90	60
12655	889	4.30	60	169	105	50	<5	58	152	19	198	5	492	98	45

3) Rare earth elements (ppm)

Sample Depth	La	Ce	Nd	Sm	Eu	Gd	Dy	Yb	Y
2945	12.20	22.63	9.65	2.49	0.49	2.51	1.80	1.03	10.42
4782	5.11	7.50	3.41	0.74	0.17	0.87	0.65	0.42	3.95
5355	6.67	11.52	4.68	1.26	0.23	1.15	0.63	0.39	3.53
6475	6.01	8.39	4.75	1.13	0.26	0.80	0.79	0.26	2.48
6641	11.85	21.04	7.27	1.70	0.28	1.25	0.97	0.44	5.14
6872	8.29	13.38	4.80	1.20	0.20	1.10	0.64	0.35	3.02
6975	6.44	11.88	4.71	0.93	0.21	1.19	0.63	0.33	2.74
7270	8.59	12.84	5.10	0.97	0.18	0.93	0.61	0.36	3.02
7475	7.19	12.04	4.19	1.05	0.18	0.86	0.53	0.35	3.01
7825	12.66	22.03	6.60	1.25	0.22	1.45	0.65	0.46	3.68
8025	8.75	15.68	4.57	1.13	0.17	0.97	0.59	0.39	3.29
8375	11.63	16.33	4.54	1.05	0.18	0.80	0.58	0.31	2.81
8475	9.60	15.10	4.62	0.95	0.19	0.72	0.58	0.36	3.14
8915	11.23	14.41	3.77	0.90	0.15	1.00	0.48	0.33	2.84
9597	12.68	18.44	6.32	1.36	0.21	1.21	0.66	0.48	3.59
10320	5.66	10.82	4.12	1.20	0.15	1.32	0.67	0.35	3.24
10975	9.18	23.26	9.67	2.59	0.61	2.60	2.05	0.79	12.10
11443	4.69	8.35	3.87	1.48	0.19	1.06	0.74	0.47	3.12
11575	6.81	13.25	4.54	0.99	0.22	1.13	0.86	0.55	5.17
11884	5.86	10.58	4.39	1.13	0.16	0.98	0.63	0.45	3.19
11975	8.11	15.94	5.88	1.47	0.30	1.49	1.05	0.61	6.35
12655	7.91	15.55	5.72	1.24	0.28	0.86	1.14	0.61	6.82

**Appendix VI. Correlation chart for 24 major, minor, trace and rare earth elements.**

	SiO <sub>2</sub>	Al <sub>2</sub> O <sub>3</sub>	Fe <sub>2</sub> O <sub>3</sub>	MgO	CaO	Na <sub>2</sub> O
SiO <sub>2</sub>	1.0000					
Al <sub>2</sub> O <sub>3</sub>	0.6044	1.0000				
Fe <sub>2</sub> O <sub>3</sub>	0.1661	-0.1061	1.0000			
MgO	0.2541	-0.3993	0.6392	1.0000		
CaO	-0.6393	-0.5272	0.3203	0.1956	1.0000	
Na <sub>2</sub> O	-0.5496	-0.5009	-0.4966	-0.1897	-0.1605	1.0000
K <sub>2</sub> O	-0.1637	0.3467	-0.1067	-0.4625	0.0870	-0.0129
TiO <sub>2</sub>	0.0945	0.1878	0.1487	0.0343	-0.0439	-0.2443
Ba	0.5980	0.6493	0.0403	0.1265	-0.3988	-0.4429
Be	0.4863	0.7769	0.3059	-0.0995	-0.3231	-0.4429
Co	-0.3341	-0.5456	0.1041	0.0849	0.4850	0.0190
Cr	0.6737	0.5392	0.2937	-0.0026	-0.3794	-0.6197
Cu	-0.3585	-0.2625	-0.1626	-0.2096	0.1377	0.2005
Ga	0.3728	0.2933	-0.3195	-0.1160	-0.2889	-0.3616
Ni	-0.2022	-0.0967	0.4220	0.0482	0.4827	-0.3638
Rb	0.2417	0.5588	0.0473	-0.2922	-0.1726	-0.2379
Sc	-0.3275	-0.1544	0.4787	0.2275	0.6632	-0.1135
Sr	0.2505	0.4462	0.5966	0.3008	0.1914	-0.7379
V	0.5123	0.8536	0.2722	-0.2239	-0.2986	-0.6633
Y	0.1222	0.0417	0.5997	0.4454	0.2023	-0.3455
Zn	0.3242	-0.2177	0.4727	0.5355	-0.0578	-0.1154
Zr	0.5736	0.2669	0.6523	0.5362	-0.0930	-0.4525
La	0.1002	0.7620	-0.1276	-0.5806	-0.3713	-0.4271
Ce	-0.0604	0.6959	-0.0024	-0.4737	-0.1549	-0.3616

	K2O	TiO2	Ba	Be	Co	Cr
K2O	1.0000					
TiO2	-0.6763	1.0000				
Ba	0.2548	-0.0823	1.0000			
Be	0.5441	-0.0939	0.6665	1.0000		
Co	-0.5496	0.3870	-0.7480	-0.6616	1.0000	
Cr	-0.3092	0.4866	0.2416	0.4522	0.0828	1.0000
Cu	-0.2815	0.3050	-0.6795	-0.3049	0.5576	0.1219
Ga	-0.3092	0.2622	0.2189	-0.2409	0.0594	0.1898
Ni	-0.3738	0.6440	-0.4294	-0.1493	0.7561	0.3615
Rb	0.8701	-0.5907	0.5604	0.7356	-0.6643	0.0066
Sc	0.3066	-0.0945	0.1075	0.1738	-0.0739	-0.2587
Sr	-0.0018	0.4379	0.4469	0.5415	-0.1342	0.3919
V	0.5086	0.0306	0.6543	0.9009	-0.5333	0.4844
Y	0.2999	-0.2742	0.5290	0.5297	-0.5239	0.0332
Zn	-0.7743	0.5455	-0.2444	-0.1372	0.4690	0.5668
Zr	-0.2186	0.2734	0.3779	0.5258	-0.1974	0.6067
La	0.6227	-0.0623	0.4200	0.5748	-0.4810	0.1537
Ce	0.5197	0.1052	0.3877	0.5731	-0.5021	0.1218

	Cu	Ga	Ni	Rb	Sc	Sr
Cu	1.0000					
Ga	-0.2224	1.0000				
Ni	0.4278	0.0337	1.0000			
Rb	-0.5566	-0.1673	-0.4192	1.0000		
Sc	-0.3703	-0.4940	0.1182	0.2480	1.0000	
Sr	-0.1749	0.1208	0.4726	0.1250	0.2853	1.0000
V	-0.3173	0.0649	-0.0150	0.7059	0.0810	0.6095
Y	-0.4652	-0.3808	-0.2115	0.4039	0.5588	0.4744
Zn	0.2852	-0.1536	0.4417	-0.5771	-0.0623	0.4744
Zr	-0.2071	-0.3043	0.1006	0.0799	0.3309	0.4686
La	-0.1705	0.3313	-0.0262	0.6099	-0.1430	0.4112
Ce	-0.1351	0.2094	0.0832	0.4645	0.0170	0.5574

	V	Y	Zn	Zr	La	Ce
V	1.0000					
Y	0.3702	1.0000				
Zn	-0.2534	-0.0294	1.0000			
Zr	0.3417	0.5579	0.6585	1.0000		
La	0.7643	0.0854	-0.6966	-0.2662	1.0000	
Ce	0.6792	0.2119	-0.5689	-0.1245	0.9163	1.0000